

‘ONE-POT’ MANUFACTURING PROCESS YIELDING LOW-COST MAGNETIC SUPPORTS FOR BIOPROCESSING

By
Yu Yao

A thesis submitted to the University of Birmingham
for the degree of DOCTOR OF PHILOSOPHY

School of Chemical Engineering
College of Engineering and Physical Sciences
University of Birmingham
August 2011

UNIVERSITY OF
BIRMINGHAM

University of Birmingham Research Archive

e-theses repository

This unpublished thesis/dissertation is copyright of the author and/or third parties. The intellectual property rights of the author or third parties in respect of this work are as defined by The Copyright Designs and Patents Act 1988 or as modified by any successor legislation.

Any use made of information contained in this thesis/dissertation must be in accordance with that legislation and must be properly acknowledged. Further distribution or reproduction in any format is prohibited without the permission of the copyright holder.

Thesis abstract

One of the major drawbacks to the large scale application of magnetic support based separations in biotechnology is the astronomic price of large quantities of commercially available magnetic support materials. The aim of this work has been to develop a simple, fast and scalable 'one-pot' manufacturing route to cheap magnetic adsorbents to be used in High-Gradient Magnetic Fishing, Magnetically Enhanced Press Filtration and Magnetically Enhanced Centrifugation systems. An inverse liquid-liquid two phase polymerization technique employing low cost chemicals combined with the use of a rotor stator type high shear mixer was systematically investigated. When the 'ideal' manufacturing conditions were identified, nonporous superparamagnetic composite supports (3 μm average size; M_s : 34 A m² kg⁻¹; magnetic content: 44.3%) were successfully created. Following further optimization, the 'one-pot' manufacturing procedure was used to produce anion exchange magnetic adsorbents, and their binding capacity was determined using human serum albumin as a model species (Q_{max} =46.1 mg of protein per gram of adsorbent; K_d =2.52 μM). Further attempts to create cation exchange magnetic supports were unsuccessful mainly due to chemical incompatibility issues between the reaction chemicals and the ferrofluid used.

Acknowledgements

Obtaining a Doctor's degree is not only the biggest academic achievement to date, but also a milestone in my life. It is my honor to successfully graduate from the University of Birmingham and working with many experts and talents in this four years. Firstly, I would like to express my sincere gratitude to my supervisors, Prof. Owen Thomas and Dr. Erini Theodossiou. Without your excellent guidance and enormous patience, I would not have managed to complete this work. Prof. Thomas is a wonderful supervisor, his scientific guidance, strict standard on academic expression and technical contents shaped me from a normal student to a better researcher. I feel so lucky to have Dr. Theodossiou as my other supervisor. She has been extremely helpful for discussing all the details in my research project, conference posters and proofreading my PhD thesis.

I would like to express my acknowledgements to Prof. Franzreb and Dr. Bolle in the Karlsruher Institution of Technology for providing me ferrofluid. Also many thanks to the technical staffs in my university for their valuable assistance: Ms. Jennings and Ms. Mittchel for helping and advice me in lab; Ms. Morris for assistance with SEM and TEM; and Dr. Zakotnik for helping with VSM.

I would also like to thank all of the friends in the Biochemical Engineering Building: Tom as a genius in chemistry and Poppy as an excellent collaborator and advisor;

Isaac as a 'brother from different parents' sharing all my happiness and sadness; and students in group: Ping, Jiazhang, Haiyang, Reza, Kris and everybody else who has helped me during my PhD.

Importantly, I need to thank my parents, Yao Jiming and Wang Lanying, for their love, support and guidance since I was born; and all of the trust and encouragement during my PhD. Last but not least, I need thank my wife, Ni Rui, for standing by me and encouraging me whatever my research was up or down. With your love, the cold winter in UK feels as warm as the spring.

Table of contents

Thesis abstract.....	i
Acknowledgements.....	ii
Table of contents.....	iv
List of figures.....	x
List of tables.....	xv
1. Introduction.....	1
1.1 The application of magnetic separation.....	2
1.1.1 Basic theory of magnetic separation.....	2
1.1.2 Forms of magnetism.....	4
1.1.2.1 Ferromagnetism.....	4
1.1.2.2 Paramagnetism.....	6
1.1.2.3 Diamagnetism.....	7
1.1.2.4 Superparamagnetism.....	7
1.1.3 Historical development of magnetic separation.....	9
1.2 Design of magnetic supports for biotechnological application.....	16
1.2.1 Design strategy for the manufacture of magnetic adsorbents.....	16
1.2.1.1 Magnetic core material design.....	16
1.2.1.1.1 Selection of magnetic core material.....	16
1.2.1.1.2 Magnetic property of core material.....	17
1.2.1.1.3 Stabilization of magnetic core material.....	17
1.2.1.2 Magnetic support design.....	20
1.2.1.2.1 Fouling and cleaning.....	20
1.2.1.2.2 Particle size and surface area.....	21
1.2.1.2.3 Chemical and physical stability.....	22
1.2.1.2.4 Magnetic behavior and magnetic core content.....	22
1.2.2 Manufacture of magnetic adsorbents.....	23

1.2.2.1 Manufacture of core materials.....	23
1.2.2.2 Manufacture of magnetic supports.....	25
1.2.2.2.1 Coating techniques.....	26
1.2.2.2.2 Infiltration techniques.....	31
1.2.2.2.3 Encapsulation techniques.....	33
1.3 Liquid-liquid two phase polymerization types reactions.....	35
1.3.1 Emulsion formation and stabilization in liquid-liquid two phase system.....	35
1.3.2 Types of liquid-liquid two phase polymerization reactions.....	37
1.3.3 Inverse phase polymerization in liquid-liquid two phase system.....	39
1.4 Project overview.....	42
 2. Preparation of beaded poly(acrylamide-co-ethylenebis acrylamide) supports by an inverse liquid-liquid two phase polymerization method.....	 44
Abstract.....	44
2.1 Introduction.....	45
2.2 Materials.....	46
2.3 Description of equipment.....	47
2.4 Experimental methods.....	48
2.4.1 Selection of optimum initiator concentration.....	48
2.4.2 Selection of optimum dispersion to continuous phase ratio.....	49
2.4.3 Selection of optimum operation time.....	51
2.4.4 Selection of optimum agitation speed.....	51
2.5 Analytical techniques.....	52
2.5.1 Particle size distribution analysis using optical counting technique.....	52
2.5.2 Microstructure study with Cryo-SEM.....	52
2.6 Result and discussion.....	53
2.6.1 Selection and optimization of initiator.....	53
2.6.2 Selection of optimum dispersion to continuous phase ratio.....	54

2.6.3 Selection of optimum operation time.....	57
2.6.4 Selection of optimum agitation speed.....	60
2.7 Conclusion.....	62
 3. Preparation of beaded magnetic poly(acrylamide-co-ethylenebisacrylamide) composite supports by inverse liquid-liquid two phase polymerization methods.....	63
Abstract.....	63
3.1 Introduction.....	65
3.2 Materials.....	68
3.3 Experimental method.....	69
3.3.1 Synthesis of poly(methacrylic acid) coated ferrofluid.....	69
3.3.2 Preparation of beaded magnetic poly(acrylamide-co-ethylenebisacrylamide) composite supports.....	70
3.3.2.1 Preparation of magnetic poly(acrylamide-co-ethylenebisacrylamide) composite supports using an APS/TEMED initiator/ accelerator system, 'Arlacel® 83/ Isopar M' continuous phase and various types of magnetic elements.....	71
3.3.2.2 Preparation of magnetic poly(acrylamide-co-ethylenebisacrylamide) composite supports using a 1,1'-azobis(cyclohexanecarbonitrile) initiator system, 'Arlacel® 83/ cyclohexane' continuous phase and PMAA-coated ferrofluids.....	72
3.3.2.2.1 Preliminary protocol.....	72
3.3.2.2.2 Optimization experiments (support batches #4 – #12).....	74
3.3.3 Analytical techniques.....	75
3.3.3.1 Particle sizing techniques.....	75
3.3.3.1.1 Dynamic light scattering.....	75
3.3.3.1.2 Low angle light scattering.....	75
3.3.3.1.3 Optical counting.....	77
3.3.3.1.4 Calculation of Sauter mean diameters.....	78
3.3.3.2 Samples drying methods.....	79

3.3.3.2.1 Drying <i>in vacuo</i>	79
3.3.3.2.2 Critical point drying.....	79
3.3.3.3 Specific surface area measurement.....	80
3.3.3.4 X-ray diffraction.....	80
3.3.3.5 Thermogravimetric analysis.....	81
3.3.3.6 Vibrating Sample Magnetometry.....	81
3.3.3.7 Scanning Electron Microscopy.....	82
3.3.3.8 Transmission Electron Microscopy.....	82
3.3.3.9 Energy dispersive X-ray analysis.....	83
3.4 Result and discussion.....	83
3.4.1 Preparation of magnetic poly(acrylamide-co-ethylenebisacrylamide) supports using an APS/TEMED initiator/accelerator system, 'Arlacel® 83/ Isopar M' continuous phase and naked magnetite powder.....	84
3.4.2 Preparation of magnetic poly(acrylamide-co-ethylenebisacrylamide) supports using an APS/TEMED initiator/accelerator system, 'Arlacel® 83/ Isopar M' continuous phase and oleic acid and poly(acrylic acid) coated ferrofluids.....	88
3.4.3 Preparation and characterization of poly(methacrylic acid) coated ferrofluid.....	98
3.4.4 Preparation of magnetic poly(acrylamide-co-ethylenebisacrylamide) composite supports using PMAA-coated ferrofluids.....	104
3.4.4.1 Comparison of 'initiator + continuous phase' combinations: 'APS/TEMED + Arlacel® 83/ Isopar M' vs. 'ABCN + Arlacel® 83/ cyclohexane'.....	104
3.4.4.2 Influence of agitation speed during emulsification on the preparation of magnetic poly(acrylamide-co-ethylenebisacrylamide) supports using ABCN + Arlacel® 83/ cyclohexane + PMAA-coated ferrofluid.....	110
3.4.4.3 Influence of PMAA ferrofluid loading on the preparation of magnetic poly(acrylamide-co-ethylenebisacrylamide) supports using ABCN + Arlacel® 83/ cyclohexane + PMAA-coated ferrofluid.....	114

3.4.4.4 Influence of surfactant content (Arlacel® 83) on the preparation of magnetic poly(acrylamide-co-ethylenebisacrylamide) supports using ABCN + Arlacel® 83/ cyclohexane + PMAA-coated ferrofluid.....	121
3.5 Conclusions.....	125
4. 'One-pot' synthesis of beaded magnetic ion exchange adsorbents by inverse phase emulsion polymerization routes.....	128
Abstract.....	128
4.1 Introduction.....	129
4.2 Materials.....	133
4.3 Experimental methods.....	134
4.3.1 'One-pot' synthesis of magnetic anion exchange DEAE adsorbents.....	134
4.3.2 'One-pot' synthesis of magnetic cation exchange adsorbents.....	135
4.3.2.1 Synthesis of magnetic cation exchange adsorbents with PMAA coated ferrofluid.....	135
4.3.2.2 Synthesis of magnetic cation exchange adsorbents with TMAOH coated ferrofluid.....	136
4.3.3 Human serum albumin binding and elution study.....	136
4.3.4 Analytical techniques.....	138
4.3.4.1 Particle sizing techniques.....	138
4.3.4.1.1 Dynamic light scattering technique.....	138
4.3.4.1.2 Low angle light scattering technique.....	139
4.3.4.2 Specific surface area measurement.....	139
4.3.4.3 Vibrating Sample Magnetometry.....	139
4.3.4.4 Scanning Electron Microscopy.....	140
4.3.4.5 Transmission Electron Microscopy.....	140
4.3.4.6 Determination of ionic capacity of magnetic anion exchange adsorbents....	140
4.4 Results and discussion.....	142

4.4.1 'One-pot' synthesis of magnetic anion exchange DEAE adsorbents.....	142
4.4.1.1 Magnetic property.....	142
4.4.1.2 Particle size distribution and specific surface area.....	143
4.4.1.3 Particle morphology study.....	144
4.4.1.4 Ionic capacity of the magnetic anion exchange adsorbents.....	146
4.4.1.5 Human serum albumin protein binding and elution study.....	148
4.4.2 'One-pot' synthesis of magnetic cation exchange adsorbents.....	152
4.4.2.1 Synthesis of magnetic cation exchange adsorbents with PMAA coated ferrofluid.....	152
4.4.2.2 Synthesis of magnetic cation exchange adsorbents with TMAOH coated ferrofluid.....	154
4.4.2.2.1 Particle morphology.....	156
4.4.2.2.2 Magnetic property.....	157
4.4.2.2.3 Characterization of tetramethylammonium hydroxide (TMAOH) coated ferrofluid.....	158
4.5 Conclusions.....	160
5. Concluding remarks.....	163
6. Appendix.....	167
6.1 A pre-work toward surface molecularly imprinted adsorbents.....	167
6.1.1 Introduction.....	167
6.1.2 Materials.....	171
6.1.3 Experimental methods.....	171
6.1.3.1 Synthesis of N-(4-vinyl)-benzyl iminodiacetic acid (VBIDA)	171
6.1.3.2 Preparation of methacrylate-silica supports.....	172
6.1.3.3 Preparation of molecularly imprinted adsorbents.....	172
6.1.3.4 Batch protein binding and elution study.....	173

6.1.3.5 Analytical analysis.....	175
6.1.3.5.1 Molecule structure analysis of the synthesized VBIDA with NMR.....	175
6.1.3.5.2 Elemental analysis.....	175
6.1.3.5.3 UV spectrophotometry.....	175
6.1.4 Result and discussion.....	176
6.1.4.1 Synthesis of N-(4-vinyl)-benzyl iminodiacetic acid (VBIDA)	176
6.1.4.2 Elemental analysis.....	177
6.1.4.3 Protein batch binding.....	178
6.1.5 Conclusions.....	180
6.2 Chloride ions standard curve for calculation of ionic exchange capacity of magnetic anion exchanger.....	181
6.3 Protein Calibration curves for protein binding studies.....	182
7. Reference.....	184

List of figures

Figure 1.1 Schematic diagram of rotation and increasing size of domains in ferromagnetic material due to applied external magnetic field.....	5
Figure 1.2 Schematic diagram of the alignment of magnetic moments in a paramagnetic material.....	7
Figure 1.3 Schematic diagram of the magnetization of superparamagnetic nano scale particles.....	9
Figure 1.4 Schematic diagram of the steric repulsion between two surfactant coated magnetic particles.....	19
Figure 1.5 Schematic diagram of iron oxide oxidation pathway.....	25
Figure 1.6 Magnetic support designs afforded by coating, infiltration and encapsulation techniques.....	26

Figure 1.7 Schematic diagram of layer-by-layer adsorption technique to produce magnetic supports.....	27
Figure 1.8 Schematic diagram of a silanized iron oxide support.....	28
Figure 1.9 Schematic diagram of graft polymerization method producing nonporous magnetic supports.....	29
Figure 1.10 Classification of hydrophilic-lipophilic balance of surfactant.....	40
Figure 1.11 Schematic illustration of a typical inverse phase emulsion polymerization reaction.....	41
Figure 2.1 Image of the Silverson L5 M high shear laboratory mixer used in this work.....	47
Figure 2.2 Sketch of the equipment set-up used for the manufacturing of composite supports.....	48
Figure 2.3 Generation of free radicals from ammonium persulfate.....	54
Figure 2.4 Effect of dispersion to continuous phase ratio on particle size distribution.....	55
Figure 2.5 Illustration of the mixing mechanism behind the rotor-stator type high shear mixer.....	56
Figure 2.6 Effect of operation time on particle size and particle size distribution.....	58
Figure 2.7 Images of polymeric gels obtained at operation condition of 2000 rpm and 60 min.....	59
Figure 2.8 Cryo-SEM image of the gel produced following mixing at 2000 rpm for 60 minutes.....	59
Figure 2.9 Effect of agitation speed on particle size and particle size distribution.....	61
Figure 3.1 Light micrographs of magnetic poly(acrylamide-co-ethylenebisacrylamide) supports.....	85
Figure 3.2 Particle size distributions of magnetic poly(acrylamide-co-ethylenebis	

acrylamide) supports synthesized using naked Fe_3O_4 powder.....	86
Figure 3.3 Magnetic poly(acrylamide-co-ethylenebisacrylamide) supports synthesized using the oleic acid coated ferrofluid.....	89
Figure 3.4 VSM curve for magnetic poly(acrylamide-co-ethylenebisacrylamide) supports prepared using the poly(acrylic acid) coated ferrofluid.....	91
Figure 3.5 Scanning electron micrographs of magnetic poly(acrylamide-co-ethylenebisacrylamide) supports prepared using poly(acrylic acid) coated ferrofluid.....	93
Figure 3.6 Transmission electron micrographs ($40,000 \times$ magnification) of (A) magnetic poly(acrylamide-co-ethylenebisacrylamide) supports prepared using poly(acrylic acid) coated ferrofluid.....	94
Figure 3.7 Representative EDAX spectra and elemental compositions corresponding to defined regions within a magnetic poly(acrylamide-co-ethylenebisacrylamide) support prepared using a poly(acrylic acid) coated ferrofluid.....	95
Figure 3.8 TEM image of the poly(acrylic acid) coated ferrofluid employed in the manufacture of Batch 'C' magnetic poly(acrylamide-co-ethylenebisacrylamide) supports.....	97
Figure 3.9 XRD pattern of magnetic nano-sized crystals in the PMAA coated ferrofluid.....	99
Figure 3.10 Thermogravimetric weight loss curve for the PMAA coated ferrofluid prepared in this work.....	100
Figure 3.11 Hysteresis curve of poly(methacrylic acid) coated ferrofluid.....	102
Figure 3.12 DLS particle size distribution of the PMAA coated ferrofluid.....	103
Figure 3.13 TEM image of the PMAA coated ferrofluid prepared in this work.....	104
Figure 3.14 VSM curves for magnetic poly(acrylamide-co-ethylenebisacrylamide) supports prepared using PMAA coated ferrofluid.....	105
Figure 3.15 Transmission electron micrographs of cross-sections through magnetic supports in batch #1 and #2 prepared using PMAA coated ferrofluid.....	106

Figure 3.16 Representative EDAX spectra and corresponding elemental compositions of dark and pale areas within batch #1 and batch #2 magnetic poly(acrylamide-co-ethylenebisacrylamide) support particles prepared using PMAA coated ferrofluid.....	108
Figure 3.17 VSM curves for magnetic poly(acrylamide-co-ethylenebisacrylamide) supports prepared using ABCN + Arlacel® 83/ cyclohexane + PMAA-coated ferrofluid at various agitation speeds.....	111
Figure 3.18 SEM images of magnetic poly(acrylamide-co-ethylenebisacrylamide) supports prepared using ABCN + Arlacel® 83/ cyclohexane + PMAA-coated ferrofluid at various agitation speeds.....	113
Figure 3.19 Transmission electron micrographs of cross-sections through magnetic poly(acrylamide-co-ethylenebisacrylamide) supports prepared using ABCN + Arlacel® 83/ cyclohexane + PMAA-coated ferrofluid at various agitation speeds.....	114
Figure 3.20 VSM curves for magnetic poly(acrylamide-co-ethylenebisacrylamide) supports prepared using ABCN + Arlacel® 83/ cyclohexane + PMAA-coated ferrofluid at 5000 rpm and various combinations of ferrofluid and surfactant.....	116
Figure 3.21 SEM images of magnetic poly(acrylamide-co-ethylenebisacrylamide) support from batches #4, #7 and #9 prepared using a surfactant/ferrofluid ratio of 0.8 mg/mg.....	119
Figure 3.22 SEM images of magnetic poly(acrylamide-co-ethylenebisacrylamide) support from batches #5, #6 and #8 prepared using a surfactant/ferrofluid ratios of 0.40-0.60 mg/mg.....	120
Figure 3.23 TEM images of magnetic poly(acrylamide-co-ethylenebisacrylamide) support batches #4, #7 and #9 prepared using a surfactant/ferrofluid ratio of 0.8 mg/mg.....	121
Figure 3.24 VSM curves for magnetic poly(acrylamide-co-ethylenebisacrylamide) support batches #4, #7, #11 and #12.....	122
Figure 3.25 SEM images of magnetic poly(acrylamide-co-ethylenebisacrylamide)	

support batches #10, #4 and #11 prepared using PMAA coated ferrofluid loading of 500 mg and various Arlacel® 83 loadings.....	124
Figure 3.26 SEM images of magnetic poly(acrylamide-co-ethylenebisacrylamide) support batches #5, #7 and #12 prepared using PMAA coated ferrofluid loading of 1000 mg and various Arlacel® 83 loadings.....	125
Figure 4.1 Hysteresis curves of magnetic adsorbents.....	143
Figure 4.2 Electron micrographs of the magnetic particles following sputter coating of the samples with platinum.....	145
Figure 4.3 Cross section TEM images of the magnetic adsorbents.....	146
Figure 4.4 Schematic diagram of determination of anionic exchange capacity.....	147
Figure 4.5 Equilibrium binding isotherms for HSA to magnetic anion exchanger DEAE and unfunctionalized adsorbents.....	149
Figure 4.6 Comparison of human serum albumin elution data from magnetic anion exchange DEAE and unfunctionalized supports.....	151
Figure 4.7 Photographs of magnetic crystals excluded from monomer droplets during the preparation of magnetic cation exchange adsorbents.....	153
Figure 4.8 Magnetic collection of magnetic cation exchange adsorbents.....	156
Figure 4.9 SEM images of cation exchange adsorbents after sputter coating the samples with platinum.....	157
Figure 4.10 Hysteresis curves of cation exchange adsorbents.....	158
Figure 4.11 Image of observation of TMAOH coated ferrofluid.....	159
Figure 4.12 Hysteresis curve and image of TEM for TMAOH coated ferrofluid.....	160
Figure 6.1 Schematic illustration of molecular imprinting process.....	167
Figure 6.2 Schematic illustration of RNase A imprinting on silica surface derivatized with methacrylate groups.....	169
Figure 6.3 PDB Deepview surface images of myoglobin from equine heart and bovine	

pancreas α -chymotrypsinogen.....	160
Figure 6.4 400-MHZ NMR spectrum of N-(4-vinyl)-benzyl iminodiacetic acid.....	167
Figure 6.5 Protein binding isotherm on myoglobin imprinted adsorbents.....	178
Figure 6.6 Protein binding isotherm on α -Chymotrypsinogen A imprinted adsorbents....	
.....	179
Figure 6.7 Protein binding isotherm on non imprinted (NIPs) adsorbents.....	179
Figure 6.8 Standard curve used for calculation of chloride ions concentration after measurement of solution absorbance at 460 nm.....	181
Figure 6.9 Calibration curve used for calculation of human serum albumin (HSA) concentration after measurement of solution absorbance at 280 nm.....	182
Figure 6.10 Calibration curve used for calculation of myoglobin (Mb) concentration after measurement of solution absorbance at 525 nm.....	183
Figure 6.11 Calibration curve used for calculation of α -Chymotrypsinogen A (Chym) concentration after measurement of solution absorbance at 280 nm.....	183

List of tables

Table 1.1 Example of commercial magnetic adsorbent particles.....	13
Table 2.1 List of chemicals involved in this chapter.....	46
Table 2.2 Preparation of initiator system.....	49
Table 2.3 Preparation of liquid-liquid two phase systems in different dispersion phase to continuous phase ratio.....	50
Table 3.1 List of chemicals involved in this chapter.....	68
Table 3.2 Summary of conditions employed for the preparation of magnetic poly(acrylamide-co-ethylenebisacrylamide) composite supports using different magnetic elements.....	72
Table 3.3 Summary of conditions employed for the preparation of magnetic poly(acrylamide-co-ethylenebisacrylamide) composite supports using PMAA coated ferrofluid (batches #1-4).....	74
Table 3.4 Summary of second phase optimization experiments, corresponding	

particle batch numbers and compositions of the dispersion and continuous phases. The agitation speed during emulsification was 5000 rpm.....	75
Table 3.5 Summary of magnetic properties, refraction index and particle sizing data for Batch 'C' magnetic poly(acrylamide-co-ethylenebisacrylamide) supports synthesized using a poly(acrylic acid) coated ferrofluid.....	92
Table 3.6 Summary of magnetic properties, refraction index and particle sizing data for magnetic poly(acrylamide-co-ethylenebisacrylamide) supports synthesized using PMAA coated ferrofluid.....	106
Table 3.7 Summary of magnetic properties, refraction index, particle sizing and specific surface area data for magnetic poly(acrylamide-co-ethylenebisacrylamide) supports prepared using ABCN + Arlcel® 83/ cyclohexane + PMAA-coated ferrofluid at three different agitation rates.....	112
Table 3.8 Summary of magnetic properties, refraction index, particle sizing and specific surface area data for magnetic poly(acrylamide-co-ethylenebisacrylamide) supports prepared using ABCN + Arlcel® 83/ cyclohexane + PMAA-coated ferrofluid at 5000 rpm and various combinations of ferrofluid and surfactant.....	118
Table 3.9 Summary of magnetic properties, refraction index and particle sizing data for magnetic poly(acrylamide-co-ethylenebisacrylamide) supports batches prepared at 500 and 1000 mg loadings of PMAA coated ferrofluid and various Arlcel® 83 loadings.....	123
Table 4.1 Examples of ion exchange groups used in protein purification.....	131
Table 4.2 List of chemicals involved in this chapter.....	133
Table 4.3 Solvents used to wash the magnetic adsorbents prepared in section 4.2.2.4.2.....	136
Table 4.4 Results of particle size distribution and specific surface area for anion exchange and unfunctionalized magnetic adsorbents.....	144
Table 4.5 Ionic exchange capacities of the Streamline™ QXL; the magnetic anion exchanger DEAE and the unfunctionalized adsorbent.....	148

Table 4.6 Langmuir constants for the curves fitted in Figure 4.5.....	149
Table 6.1 List of chemicals involved in this chapter.....	171

1. Introduction

At the present rate of progress it is realistic to envisage commercial magnetic systems for bioseparation arising within the next 5-10 years. Bespoke bioprocess-scale magnetic separator systems have been successfully tested, and the first small pilot-scale high gradient magnetic fishing system has recently entered production. The biggest stumbling block however, remains the provision of process-scale quantities of 'suitable' magnetic adsorbents at low cost. Most commercially available magnetic supports are too expensive to suit for bioprocess use, and importantly the methods employed for their manufacture do not lend themselves to multi-kilogram scale production.

This project introduces a simple, fast and scalable 'one-pot' manufacturing route to cheap magnetic adsorbents for bioprocessing. The approach relies on incorporating coated ferrofluid into inverse emulsion polymerization reactions performed under high shear stress. The properties of finished supports are strongly influenced by changes in shear rate, type and amount of coated ferrofluid.

This project is supported by the European Commission Framework VI (NanoBioMag) and VII (MagPro²Life) Programmes.

1.1 The application of magnetic separation

1.1.1 Basic theory of magnetic separation (Gerber and Birss, 1983; Spaldin, 2003; Getzlaff, 2008)

Magnetic fields are generated when electric charges move. A magnetic field can be defined by either its cause (e.g. an electric current within a wire), or by its effect (e.g. the measured force acting on a small permanent magnet). The effect of a magnetic field is defined by the theoretical force acting on a 1 m length of wire, which is located within the field carrying a current of 1 Amp. The ratio between the force, F_m , the product of the current, I , and the wire length, L , is a measure of the field intensity and is called the magnetic flux density, B :

$$B = \frac{F_m}{I \cdot L} \quad (1.1)$$

The flux density is a vector pointing into the direction of the magnetic field and is measured in units of Tesla:

$$1 \frac{N}{A \cdot m} = 1 \frac{W \cdot s}{A \cdot m^2} = 1 \frac{V \cdot s}{m^2} = 1 \text{ Tesla}$$

If the wire has been coiled to form a cylindrical shape, the magnetic flux density inside of the coil can be expressed by the following correlation:

$$B = \mu_r \cdot \mu_0 \cdot I \cdot \frac{n}{L} \quad (1.2)$$

where n is the number of coils; L is the length of the coil; μ_r is the permeability (equals

1 in vacuum); μ_0 is the permeability of free space; and in SI unit, it has the value $4\pi \times 10^{-7} \text{ V s A}^{-1} \text{ m}^{-1}$. The magnetic field intensity, H , is independent of μ_r and μ_0 , and is thus defined as following equation:

$$H = I \cdot \frac{n}{L} \quad (1.3)$$

Combining equations 1.2 and 1.3, magnetic flux density and magnetic field intensity can be correlated as follows:

$$B = \mu_r \cdot \mu_0 \cdot H \quad (1.4)$$

The relationship between magnetic flux density B and magnetic field intensity H is a property of the magnetic material. At the outside of the magnetic material, B is a linear function of H , when in vacuum:

$$B = \mu_0 \cdot H \quad (1.5)$$

Inside the magnetic material, the relationship between magnetic flux density and magnetic field intensity is more complicated due to the magnetization, M , of the medium, and can be correlated according to the following equation:

$$B = \mu_0(H+M) \quad (1.6)$$

where M depends on how the dipole moments of the ions, atoms and molecules

interact with each other. The magnetization is thus defined as the total magnetic moment per volume unit.

$$M = m \cdot \frac{N}{V} \quad (1.7)$$

where, m is magnetic moment, a measure of the strength of a magnetic source; N is the number of magnetic moments in the magnetic material; and V is the volume of the material.

Magnetic separations are depended on the magnetic force (F_m), which is the result of the interaction between the magnetic core of the support and the external magnetic field and can be expressed as follows:

$$F_m = \frac{1}{2} \mu_0 \cdot V_s \cdot (\chi_s - \chi_f) \cdot \nabla \cdot H^2 \quad (1.8)$$

where, V_s is the support volume; χ_s and χ_f , are the magnetic susceptibilities (the extent of magnetization of a material to response the applied magnetic field) of the solid and the fluid respectively; $\nabla \cdot H^2$ is the magnetic gradient; and μ_0 is the permeability.

1.1.2 Forms of magnetism

1.1.2.1 Ferromagnetism

Ferromagnetic materials (e.g. nickel, iron, cobalt, magnetite and their alloys) consist

of microscopic domains, each magnetized in the same direction (Heebøll-Nielsen, 2002). Magnetic domain is a region in magnetic material with a uniform magnetisation; it was mentioned and theorized by French physicist Pierre-Ernest Weiss in 1906 (Cullity and Graham, 2009). Ferromagnetic materials require minimizing the energies effect on equilibrium of crystal lattices. As a result, a certain magnetic domain configuration occurs for the minimization of total energy (Cullity and Graham, 2009). If a ferromagnetic material has never been previously magnetized or has been thoroughly demagnetized, the magnetization vectors in different domains point randomly at different orientations, and the total magnetization averages to zero. When ferromagnetic material is placed into an external magnetic field, all of the domains rotate and the magnetic moments finally orient in the same parallel direction to maintain a lowered energy state (Getzlaff, 2008). The magnetic moments will remain in the parallel orientation, even when the external magnetic field has been removed (see Fig. 1.1), i.e. residual magnetization remains in the ferromagnetic material.

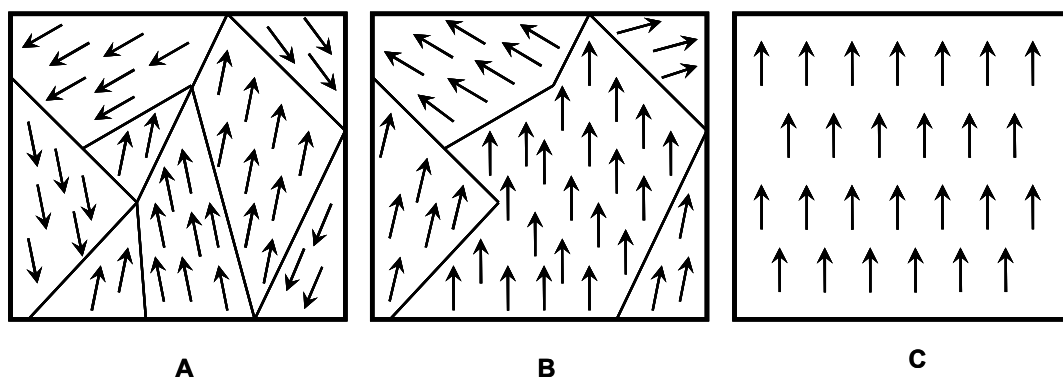


Figure 1.1 Schematic diagram of rotation and increasing size of domains in ferromagnetic material due to applied external magnetic field. (A: in the absence of external magnetic field; B: rotation and increased size of domains when an external

magnetic field is applied; C: all magnetic moments orient in the same parallel direction following magnetic saturation or even removal of the magnetic field).

Due to their residual magnetization, ferromagnetic materials tend to aggregate and form clumps. Even though they make excellent permanent magnet materials (Hatch and Stelter, 2001), when used in separations of biological products, permanent aggregation of product loaded adsorbents can severely compromise their efficiency during wash and product recovery steps (Hubbuck *et al.*, 2001), and are therefore unsuitable for the fabrication of magnetic adsorbents.

1.1.2.2 Paramagnetism

Paramagnetic materials (e.g. hematite) do not retain any magnetization in the absence of an external magnetic field. Their magnetic moments are only weakly coupled to each other, and so thermal energy causes the magnetic moments to orient randomly. When an external magnetic field is applied, the magnetic moments start to align, but only a small fraction will be oriented by the field (see Fig. 1.2). Paramagnetic materials respond linearly to the magnetic field (Dunlop *et al.*, 1984) and their response is proportional to the field strength. Following removal of the external magnetic field, all magnetic moments orient randomly again, and the support has no magnetic memory (Hatch and Stelter, 2001).

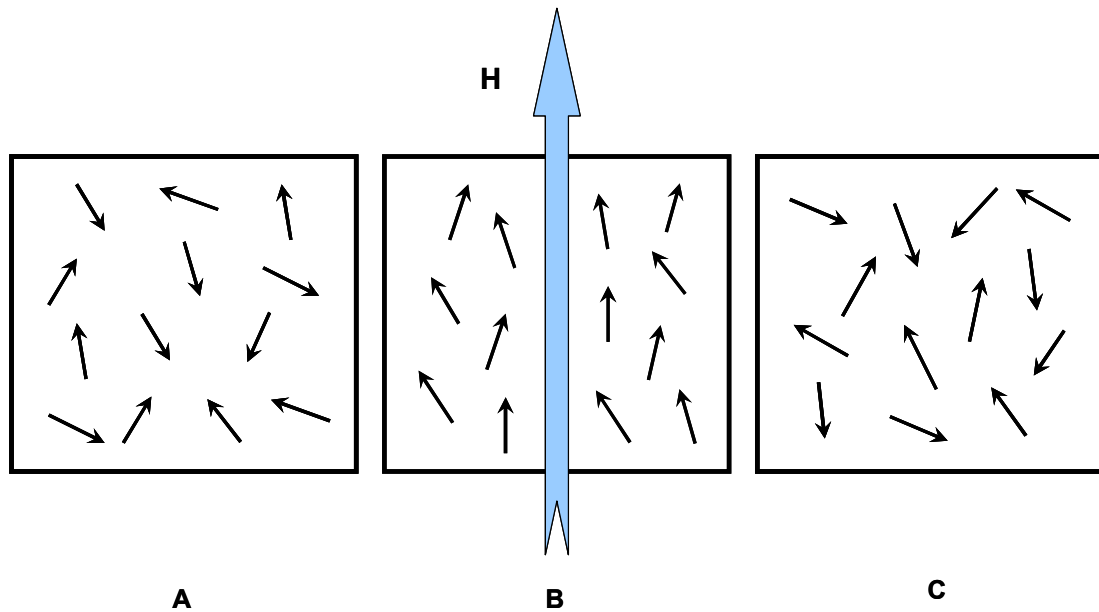


Figure 1.2 Schematic diagram of the alignment of magnetic moments in a paramagnetic material. (A: in the absence of external magnetic field; B: in the presence of an externally applied magnetic field; C: following removal of the external magnetic field).

1.1.2.3 Diamagnetism

Diamagnetism occurs in all kinds of material, but it is a very weak interaction and is often overshadowed by much stronger interactions such as ferromagnetism or paramagnetism. Diamagnetism can only be observed in some pure materials (e.g. bismuth, copper and diamond), which have not unpaired electrons. Diamagnetic materials can create a magnetic field in opposition to an externally applied magnetic field, thus causing a repulsive effect (Jiles, 1991).

1.1.2.4 Superparamagnetism

If a ferromagnetic material is smaller than approximately 30 nm in size and consists of

a single magnetic domain with one magnetic moment, it will exhibit superparamagnetism (Dave and Gao, 2009). In this kind of nano sized particles, magnetization can randomly flip direction by Brownian motion at room temperature. The mean time between two flips is called Néel relaxation time, τ , and is given by the following Néel-Arrhenius equation (Krishnan *et al.*, 2006):

$$\tau = \tau_0 \exp\left(\frac{K \cdot V}{k_B \cdot T}\right) \quad (1.9)$$

where, τ_0 is the measurement time; K is anisotropy constant of the bulk material, it has the value $1.1\text{-}1.3 \times 10^5 \text{ erg cm}^{-3}$ (Guardia *et al.*, 2006); V is the volume of the nano sized particle, k_B is the Boltzmann constant; and T is the temperature. In the absence of an external magnetic field, when the measurement time is much longer than the Néel relaxation time, the net magnetization of the nano sized particle therefore average to zero (Dave and Gao, 2009). However, when an external magnetic field is applied, the magnetic moments in these single domain particles align in the same direction as the magnetic field but this alignment will not remain after the removal of the magnetic field (See Fig. 1.3). Superparamagnetic adsorbents are very important during magnetic separations of biotechnological products because undesirable permanent particle agglomeration is avoided, and therefore desorption, cleaning and re-use of the adsorbents can be achieved.

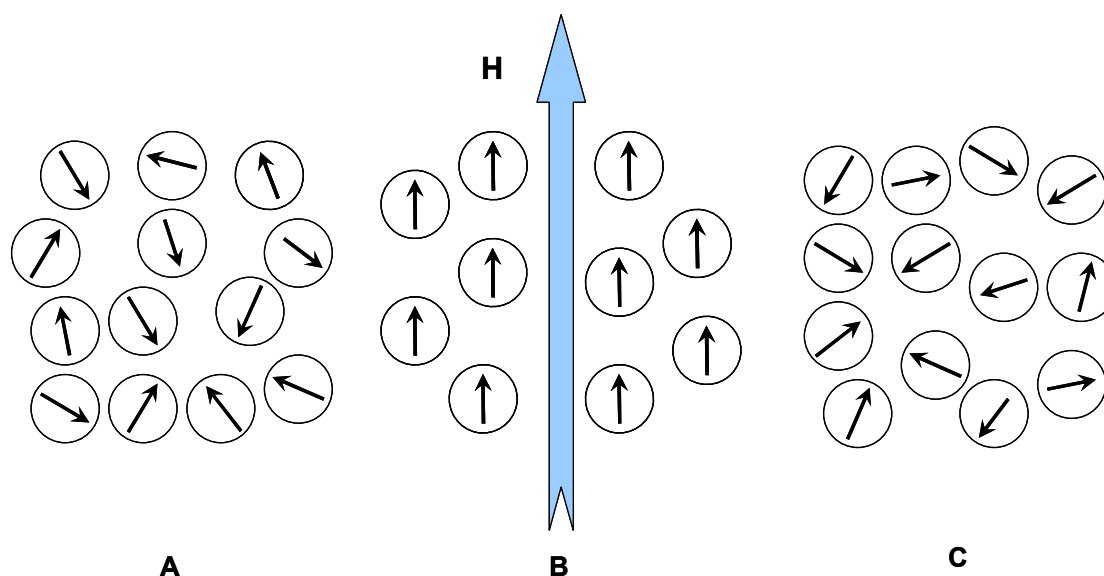


Figure 1.3 Schematic diagram of the magnetization of superparamagnetic nano scale particles. (A: in the absence of an external magnetic field; B: when an external magnetic field is applied; C: following removal of the external magnetic field).

1.1.3 Historical development of magnetic separations

People have been interested in magnetism for over 2,500 years. According to the Greek philosopher Aristotle, Thales of Miletus referred to the subject of magnetism around 550 BC (Fowler, 1997); in ancient China, Wang Xu quoted in 400 BC: "The lodestone makes iron come or it attracts it" (Fang, 1993); and during the first century BC, the magnetic spoon-like compass was used by seamen for direction (Kartsev, 1975).

Magnets were first used in separations in 1792 when William Fullarton filed a patent on the magnetic separation of iron minerals (Parker, 1977; Yavuz *et al.*, 2009). In the following one hundred years, a framework of the theory about electromagnetism was

established by a series of discoveries by Faraday, Maxwell, Gauss and Helmholtz. Once the mysterious magnetic force was discovered, it was quickly put to use in industry. In 1852, a New York company developed the first conveyor belt separator to select magnetite from apatite, and thereafter a variety of devices were introduced for the separation of magnetite and iron from minerals (Yavuz *et al.*, 2009).

During the 20th century, the applications of magnetic separations were not limited in the handling of large and strongly magnetic susceptible solids for the mineral industry, but were also applied in other large scale industry processes, such as clay, nuclear processing and waste water treatment. Urbain and Steman (1941) introduced a magnetoflocculation process to purify waste water by electrostatic adsorption. Flocculants and magnetite particles were added into waste water streams, where they formed a colloidal structure with organic impurities, which was allowed to settle under the influence of a magnetic field, thereby providing a rapid and economical process. In 1973, the first high gradient magnetic separation (HGMS) device was developed by Kolm in the search for the elusive Dirac monopole (a magnetic material with single magnetic pole) in ocean bottom sediments (Oberteuffer, 1973). These devices use filamentous ferromagnetic materials, such as stainless steel wool mesh, in the presence of a strong magnetic field. The irregular surface generates high magnetic gradients and thus strongly attracts magnetic susceptible materials (even weakly paramagnetic particles in a fast flow stream can be captured; Waston, 1975). HGMS

was quickly developed further and applied extensively in the mineral process industry (Oberteuffer, 1974; Sovaboda and Fujita, 2003).

Magnetic separations were first employed in biotechnology during the 1970s. Robinson and colleagues (1973) reported a successful preparation of immobilised enzymes (α -chymotrypsin and β -galactosidase) on magnetic iron oxide cellulose particles for an immobilised enzyme reactor. In this way, magnetic supports could directly capture the target product from the crude feedstock and then easily separated from various impurities by applying a magnetic field. Dunnill and Lilly (1974) developed magnetic bioaffinity adsorbents to purify β -galactosidase and L-asparaginase from *Escherichia coli* homogenates. Mosbach and Andersson (1977) magnetically recovered alcohol dehydrogenase from crude liver homogenates, whilst Halling and Dunnill (1979; 1980) used non-porous magnetic supports to recover lactase catalyst from whole milk and successfully immobilised α -chymotrypsin. The first commercially available magnetic supports, Enzacyl FEO-(M) and Magnogel, appeared at the later half of the 70s (Franzreb *et al.*, 2006). Shortly after, these early supports were replaced by more refined products, such as Biomag[®], Dynabeads[®] and Estapor[®] M (see Table 1.1). Today magnetic supports are derivatised with various ligands used in chromatography (e.g. ion exchange, affinity, hydrophobic *etc.*) and have found applications in vary areas including, amongst others, cell separation, immunoassays, and isolation of viruses and organelles (Franzreb *et al.*, 2006).

Magnetic separation processes consists of few steps: i) target molecule adsorption to superparamagnetic adsorbents; ii) rapid collection of the product loaded adsorbents in a strong magnetic field; iii) desorption and recovery of target molecule from the adsorbents (Heebøll-Nielson, 2002). It is therefore simple, fast, and scalable; and is a good alternative to expensive chromatography. Compared with traditional bioseparation methods, magnetic separation has many advantages, such as direct application in crude sample containing suspend solid material, fast collection with the aid of a magnetic field, easy cleaning and re-use, short operation time and consequently low capital and running costs (Safarik and Safarikova, 2004).

Table 1.1 Example of commercial magnetic adsorbent particles.

Manufacturer (Country)	Product	Description	Ref.
Ademtech SA (France)	Masterbeads Adembeads	<ul style="list-style-type: none"> Masterbeads are non porous monodispersed and superparamagnetic beads composed of magnetic core encapsulated by a highly cross-linked hydrophilic polymer shell. Sizes available: 0.5 μm in diameters; Specific surface area: $5\text{ m}^2\text{ g}^{-1}$; M_s: approx. 40 emu g^{-1}; Iron oxide content: approx. $\sim 70\%$. Adembeads are monodispersed and superparamagnetic beads composed of magnetic core encapsulated by a highly cross-linked hydrophilic polymer shell. Sizes available: 0.2 μm in diameters; M_s: approx. 40 emu g^{-1}; Specific surface area: $5\text{ m}^2\text{ g}^{-1}$; Iron oxide content: approx. $\sim 70\%$. 	A
Bangs Laboratories Inc. (USA)	ProMag TM COMPEL TM BioMag [®] , BioMag [®] Plus and BioMag [®] Maxi	<ul style="list-style-type: none"> Highly uniform polymer-based magnetite spheres. Size available: 1μm and 3μm in diameters. Highly uniform superparamagnetic microspheres ideal for applications that demand uniform particle response, such as miniaturized bioassays and separations. Sizes available: 3, 6 and 8 μm in diameters. High performance superparamagnetic microparticles used in the magnetic separation of biological and non-biological systems. Size available: 0.5-1.5 μm for BioMag[®] and BioMag[®] Plus; 3-12 μm for BioMag[®], BioMag[®] Plus; Iron oxide content $>90\%$ w/w. 	B
Chemagen Biopolymer Technologie AG (Germany)	M-PVA	<ul style="list-style-type: none"> Magnetite crystals encapsulated in cross-linked polyvinyl alcohol bead. Size available: 0.5-3 μm; Magnetite content: 50-60 %. 	C
Chemicell GmbH (Germany)	SiMAG beadMAG fluidMAG	<ul style="list-style-type: none"> Uniform superparamagnetic silica beads processes either highly porous or a non-porous silica surface. Sizes available: 0.5, 0.75 & 1μm; Surface area: $50\text{ m}^2\text{ g}^{-1}$. Superparamagnetic particles covered with a hydrophilic matrix of cross-linked starch. Sizes available: 1 μm in diameter. Magnetic iron oxides crystals covered with hydrophilic polymers. Size available: 0.05, 0.1 and 0.2 μm in diameters. 	D
Cortex Biochem (USA)	MagaPhase [®]	<ul style="list-style-type: none"> Pure magnetite encapsulated in polysaccharide or acrylic polymer beads. Size available: 1-10 μm, 1-60 μm & monosized 3.2 μm; Magnetite content: 33-60% w/w. 	E
Industrie Biologique Francaise (France)	Magnogel	<ul style="list-style-type: none"> Nonporous magnetic support prepared by copolymerization of acrylamide, melted agarose and iron oxide mixture. Size: 50-100 μm in diameter; iron oxide content: 7% w/w. 	F
Invitrogen AS (USA)	Dynabeads [®]	<ul style="list-style-type: none"> Non-porous uniform monodisperse superparamagnetic beads with size of 2.8 μm in diameters. 	G

Table 1.1 Example of commercial magnetic adsorbent particles (continued).

Manufacturer (Country)	Product	Description	Ref.
Merk Chimie SAS (Germany)	Estapor [®] M	<ul style="list-style-type: none"> Superparamagnetic crystals uniformly distributed in impervious polystyrene bead. Sizes available: 0.25-0.4 μm, 0.16-0.24 μm and 1.7-2.7 μm in diameters, Iron oxide content: 20-60% w/w. 	H
	Estapor [®] EM	<ul style="list-style-type: none"> Superparamagnetic core particle encapsulated in impervious polystyrene Available size: 0.8-1.8 μm, Iron oxide content: 36-50% w/w. 	
	Bio- Estapor [®]	<ul style="list-style-type: none"> Building upon Estapor[®] microsphere, Bio-Estapor[®] product line include streptavidin, anti-IgG, protein A & G coating microsphere. It will be launched soon. 	
Micromod Partikeltechnologie GmbH (Germany)	NanoMag [®]	<ul style="list-style-type: none"> Uniform chitosan, dextran or silica-fortified dextran iron oxide composite particles. Size available: 0.13-0.5 μm in diameters; $M_s > 75 \text{ emu g}^{-1}$. 	I
	PLA-Particles -M	<ul style="list-style-type: none"> Monodisperse supports prepared by encapsulation of magnetite within polylactic acid. Size available: 30, 100 and 250 μm in diameters. 	
	Sicastar [®] -M	<ul style="list-style-type: none"> Non-porous monodisperse supports coated with silica. Size available: 1.5 and 6 μm in diameters. 	
	Micromer [®] -M	<ul style="list-style-type: none"> Non-porous monodisperse supports prepared by encapsulation of magnetite within styrene-maleic acid copolymer matrix and subsequent coating with polysaccharide or silica. Size available: 2-12 μm in diameters. 	
Miltenyi Biotec (Germany)	MACS MicroBeads	<ul style="list-style-type: none"> Non-porous polysaccharide coated magnetic iron oxide crystals. Size available: approx. 50 nm in diameters. 	G
	MACSiBead [™] Particles	<ul style="list-style-type: none"> Non-porous monodisperse superparamagnetic particle covalently coupled to anti-biotin antibodies with size of 3.5 μm diameters. 	
Polysciences Inc. (UK)	BioMag [®] and BioMag [®] Plus ProMag [™]	<ul style="list-style-type: none"> Non-porous superparamagnetic silanized iron oxide. Size available: 0.5-1.5 μm diameters. Highly uniform polymer-based magnetite spheres. Size available: 1 μm and 3 μm in diameters. 	K
Promega GmbH (Germany)	MagneSil [™]	<ul style="list-style-type: none"> Magnetic core coated in porous silica shell. Size available: 2-14 μm diameters; Magnetic content : about 55% w/w. 	L
Roche Applied Science Inc. (Germany)	Magnetic Glass Particles (MGP)	<ul style="list-style-type: none"> Magnetic core particle encapsulated in nonporous glass shell. (No size information from manufacturer). 	M

Table 1.1 Example of commercial magnetic adsorbent particles (continued).

Manufacturer (Country)	Product	Description	Ref.
Thermo Fisher Scientific Inc. (USA)	Pierce® Glutathione Magnetic Beads Pierce® Streptavidin Magnetic Beads MagnaBind™ Magnetic Beads Sera-Mag™ magnetic Beads	<ul style="list-style-type: none"> ● Iron oxide particles with reduced glutathione attached to the surface and encapsulated in cross-linked agarose. Available size: 1-10 µm. ● Iron oxide particles covalently coated with a monolayer of recombinant streptavidin protein. Available size: 1 µm in diameter. ● Superparamagnetic silanized iron oxide particle. Size available: 1-4 µm in diameter; specific surface area: 100 m² g⁻¹. ● Non-porous magnetic beads with highly textured binding surface. Size Available: 0.7-3 µm in diameters. 	N
Sigma-Aldrich (USA)	Enzacryl FEO-(M) Anti-FLAG® M2 Magnetic Beads	<ul style="list-style-type: none"> ● Magnetite encapsulated in porous synthetic polymer matrix. Particle size: 40-70 µm in diameter. ● Magnetic affinity resin. (No size information from manufacturer). 	O
Spherotech Inc. (USA)	SPHERO™ Magnetic Particles	<ul style="list-style-type: none"> ● Non-porous magnetic monosphere coated a layer of polystyrene. Size available: 2, 3, 4 and 5 µm in diameters; Magnetite content: 15% w/w. 	P
Whatman (UK)	Magarose	<ul style="list-style-type: none"> ● Porous magnetic sphere by encapsulation of magnetite within cross-linked agarose. Available size: 20-160 µm in diameters. 	Q

Note:

A: <http://www.ademtech.com>

B: <http://www.bangslabs.com>

C: <http://www.chemagen.com>

D: <http://www.chemicell.com>

E: <http://www.cortex-biochem.com>

F: (Guesdon *et al.*, 1977)

G: <http://products.invitrogen.com>

H: <http://www.estapor.com>

I: <http://www.micromod.de>

G: <http://www.miltenyibiotec.com>

K: www.polysciences.com

L: <http://www.promega.com>

M: <http://www.roche-applied-science.com>

N: <http://www.piercenet.com> and <http://www.thermoscientific.com>

O: <http://www.sigmaaldrich.com>

P: <http://www.spherotech.com>

Q: (Levison *et al.*, 1998)

1.2 Design of magnetic supports for biotechnological applications

Since the middle 1970s, commercial functionalized magnetic adsorbents varying from nano sized particles (50-600 nm, mostly 50-200 nm), to macrosized ($>>10\mu\text{m}$) and microsized (0.6-10 μm , mostly 0.8-5 μm) particles have been widely used in biotechnological applications. These magnetic adsorbents share common properties, such as high magnetic susceptibility and can handle crude feedstocks. When combined with high gradient magnetic separation technology, they can be used in high gradient magnetic fishing (HGMF), a magnetic separation system developed at the Technical University of Denmark (Heebøll-Nielsen *et al.*, 2004). In the following sections, the design strategies and the various manufacturing methods employed in the production of magnetic adsorbents for biotechnological applications are presented.

1.2.1 Design strategy for the manufacture of magnetic adsorbents

1.2.1.1 Magnetic core material design

1.2.1.1.1 Selection of magnetic core material

There are many different substances that can be used as core materials and endow a support magnetic properties. These are iron, steel, nickel, magnesium alloy, chromium dioxide and ferrites. Ferrite is a chemical compound with structure $\text{MO}\cdot\text{Fe}_2\text{O}_3$, where M is typically Fe, Ni, Mn, MnZn or MgCu (McCurrie, 1994). Of these, the iron oxide (magnetite, Fe_3O_4), is the most common type of ferrite used as a core

material. It is a black ferromagnetic mineral with cubic inverse spinel structure, containing both Fe^{II} and Fe^{III} (Cornell and Schwertmann, 1996). Maghemite, $\gamma\text{-Fe}_2\text{O}_3$, is another type of ferrite with red-brown colour and isostructure with magnetite (Cornell and Schwertmann, 1996). Maghemite can be easily produced by oxidation of magnetite, and gives a relative reduction of magnetic moment. Thus, the actual component of the magnetic core in most supports contains both magnetite and maghemite. The magnetic core materials can be either a single magnetic core or many nano sized magnetic stabilized crystals (ferrofluid). The form of the core material has large impact on the appearance, performance and the application of the final magnetic support. Of particular importance is the crystal size and whether it is coated or not.

1.2.1.1.2 Magnetic properties of core materials

Superparamagnetic materials display an intermediate behaviour between paramagnetic and ferromagnetic materials. The nano sized magnetic crystals must have sizes smaller than 30 nm (Hatch and Stelter, 2001) to ensure that each individual nano sized crystal contains only one magnetic domain, and therefore exhibits superparamagnetic behaviour.

1.2.1.1.3 Stabilization of magnetic core material

In the absence of surface coating, the strong and long-range magnetostatic

interactions and van de Waals attraction that exist between neighbouring nano sized particle, form aggregates and result in increased final particle sizes. Once two large clusters approach each other, each of them come into the magnetic field of the other and get further magnetized (Tepper *et al.*, 2003). Therefore, the stability of the nano sized magnetic crystals is a very important issue, and in order to prevent their aggregation and subsequent sedimentation, the crystals are stabilized with a layer of surfactant or polymer to produce a steric repulsion (Odebach, 2002A).

The sedimentation of magnetic nano sized crystals is due to either gravitational attraction or magnetic interaction. If the size of the magnetic particles is small enough (e.g. 10 nm), the Brownian motion of the particles themselves can provide sufficient mixing by random moving, and they remain well dispersed. In other words, if the thermal energy of the particles is strong enough to move them freely, they do not sediment (Odenbach, 2002B). The maximum size of the self-dispersed magnetic particle is given by the following expression:

$$d < \left(\frac{6k_B T}{\mu_0 M_0 \pi H} \right)^{\frac{1}{3}} \quad (1.10)$$

where, d is the maximum diameter of the particle. k_B is Boltzmann's constant; T is the absolute temperature; H is the applied magnetic field strength; and M_0 is the magnetization of the material of particle.

Nevertheless, controlling the maximum size of the magnetic particles can only prevent them from sedimentation but will not stop their agglomeration. When the particle size becomes very small, van de Waals forces dominate the interaction between nano sized crystals, thus causing particle agglomeration and subsequently sedimentation. Therefore, particle contact must be avoided to ensure suspension stability. Rosensweig (1985) introduced a layer of a long chain surfactant on the surface of the crystals that produced steric repulsion and efficiently stabilized the magnetic suspension. If the surface distance of the crystals is larger than twice the thickness of the surfactant layer, there is no repulsion between the coated crystals, otherwise the surfactant density is reduced and orientation becomes disordered (see Fig. 1.4; Odebach, 2002B).

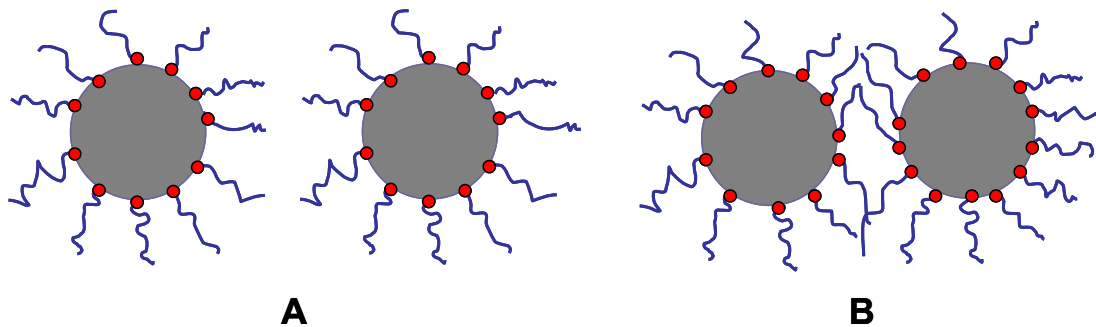


Figure 1.4 Schematic diagram of the steric repulsion between two surfactant coated magnetic particles (A: no repulsion between particles, as their surface distance is larger than twice the surfactant layer thickness. B: steric repulsion occurs, as long as the surface distance of two particles is smaller than twice the surfactant layer thickness).

1.2.1.2 Magnetic support design

Encasing magnetic nano sized crystals into organic polymers or inorganic materials to form magnetic susceptible supports protects the magnetic material from oxidizing and prevents core material leak (Ma *et al.*, 2007). This composite layer consequently promotes support dispersion and gives them chemical stability. Further features required for the creation of a successful magnetic support, include: ease of cleaning and reduced tendency to foul; uniform particle size distribution and high surface area; mechanical strength; and superparamagnetic behaviour. The degree to which each must be satisfied is related to the intended application and choice of the magnetic separation scheme.

1.2.1.2.1 Fouling and cleaning

Adsorption is the common way to separate the target product from a biological feedstock. However, some larger molecules and suspended solids can diffuse into the adsorbent, if an extensive porous framework exists inside of the adsorbent matrix. A study on porous expanded bed adsorption supports showed that only a part of the target product could be recovered from the support even after extensive washing, whilst the remaining molecules caused severe fouling of the expanded bed (Fernandez-Lahore *et al.*, 1999). In these cases, specific binding sites are blocked and the re-use of the adsorbent matrix is severely compromised (Dainiak *et al.*, 2002; Vilorio-Cols, 2004).

1.2.1.2.2 Particle size and surface area

Nonporous adsorbents have the advantage of less fouling and therefore can be cleaned easier than their porous counterparts. However, only their external surface is involved in the binding of the target product, and consequently nonporous adsorbents have a relatively smaller surface area available for binding than the porous adsorbents of the same size, which results in lower binding capacity. To achieve comparable binding surface area per unit weight (specific surface area) compared to porous adsorbents, non porous supports must be of small size. Watson (1973; 1975) used the following expression to describe the theoretical particle velocity, v_m , caused by the magnetic force in the direct vicinity of the wire:

$$v_m = \frac{2}{9} \cdot \frac{\chi \cdot M_s \cdot H_0 \cdot r_p^2}{a \cdot \eta} \quad (1.11)$$

where χ is the susceptibility of the adsorbent; M_s is the saturation magnetization (the highest state which magnetization can reach); H_0 is the applied field; η is the viscosity of the fluid; a is the wire radius; and, r_p is the radius of adsorbent. As the particle radius is a function of the particle velocity, very small adsorbents have low collection velocity and consequently poor magnetic separation efficiency. Therefore, the proper balance between surface area and adsorbent size must be considered in adsorbent design. Ideally, a magnetic adsorbent should be no smaller than 0.5 μm and have a specific surface area of 20-100 $\text{m}^2 \text{g}^{-1}$ (Franzreb *et al.*, 2006).

1.2.1.2.3 Chemical and physical stability

Magnetic adsorbents must be stable and able to tolerate the harsh chemicals employed in support cleaning and regeneration. The surface coating material must be chemically inert, hydrophilic and easy to derivatize to high ligand density, preferably using standard, inexpensive chemistries adopted in the manufacture of approved biochromatography and membrane materials. Furthermore, good physical stability is highly desirable as the vigorous agitation in the stirred tank reactor involved in the HGMF recycle loop, can cause mechanical attrition of the magnetic adsorbents and reduce their lifespan. In order to achieve both chemical and physical stability, many commercial magnetic supports contain polystyrene, polyvinyl alcohol, cellulose, silica and glass (Safarik and Safarikova, 2004). Some polysaccharide gels (e.g. alginate, agarose and chitosan) that form a porous matrix layer and are sensitive to mechanical damage should be avoided in the design of magnetic adsorbents.

1.2.1.2.4 Magnetic behaviour and magnetic core content

Magnetic aggregation is employed in mineral industry to enhance the recovery of ferromagnetic minerals (Svoboda, 1987). However, permanent magnetic support aggregation is very undesirable and must be avoided in bioseparations. Once significant adsorbent aggregation occurs and the particle size increases, the specific surface area will be reduced dramatically. Additionally, agglomerated adsorbents have

dead spaces that promote fouling. The most efficient way to prevent permanent aggregation is to use a superparamagnetic core material which enables fast collection under an applied field, and ease of resuspension after the field is removed (Safarik and Safarikova, 2004).

To ensure rapid collection, the product loaded adsorbents must exhibit high magnetic susceptibility. To achieve high saturation magnetization, sufficient amount of magnetic material must be encased into the adsorbents. However, due to the high density of the magnetic components (e.g. magnetite has a density of 5.2 g cm^{-3}), magnetic adsorbents require vigorous agitation to overcome gravitational settling. To avoid subsequent mechanical attrition of the adsorbents and high energy consumption, the percentage of the magnetic core content of the adsorbent is critical. The ideal superparamagnetic adsorbents should be roughly $0.5\text{-}1 \text{ }\mu\text{m}$ in size, possess a magnetic core content of $\geq 50\%$ ($M_s > 35 \text{ emu g}^{-1}$; $\rho = 3\text{-}4 \text{ g cm}^{-3}$), settle very slowly at zero field, and be rapidly separated at moderate magnetic fields (Brown, 2008).

1.2.2 Manufacture of magnetic adsorbents

1.2.2.1 Manufacture of core materials

Magnetite is usually the more desirable core material compared to maghemite because of its ferromagnetic behaviour in bulk, and higher saturation magnetization and magnetic susceptibility (Wohlfarth, 1980). Generally, magnetite nano sized

crystals can be produced by adding alkali into a mixture of ferrous and ferric salt solutions (Khalafalla and Reimers, 1980). The magnetite crystals start growing and complete precipitation at pH 9-14 (Odenbach, 2002A). The reaction formula can be written as follows (Cornell and Schwertmann, 1996):



The above reaction must be carried out in an oxygen free environment, otherwise, Fe^{2+} and Fe^{3+} are deprotonated to $\text{Fe}(\text{OH})_y^{2-y}$ and $\text{Fe}(\text{OH})_x^{3-x}$, after a series of reactions finally transformed to hematite ($\alpha\text{-Fe}_2\text{O}_3$), which can severely change the chemical and physical properties of the core material (see Fig. 1.5). In order to prevent magnetic core material from undesirable oxidation, the reaction system is usually purged with nitrogen before and during the reaction. In addition, coating with a layer of organic material during precipitation can very efficiently prevent oxidation and consequent agglomeration of the magnetic crystals during long term storage (Gupta and Gupta, 2005).

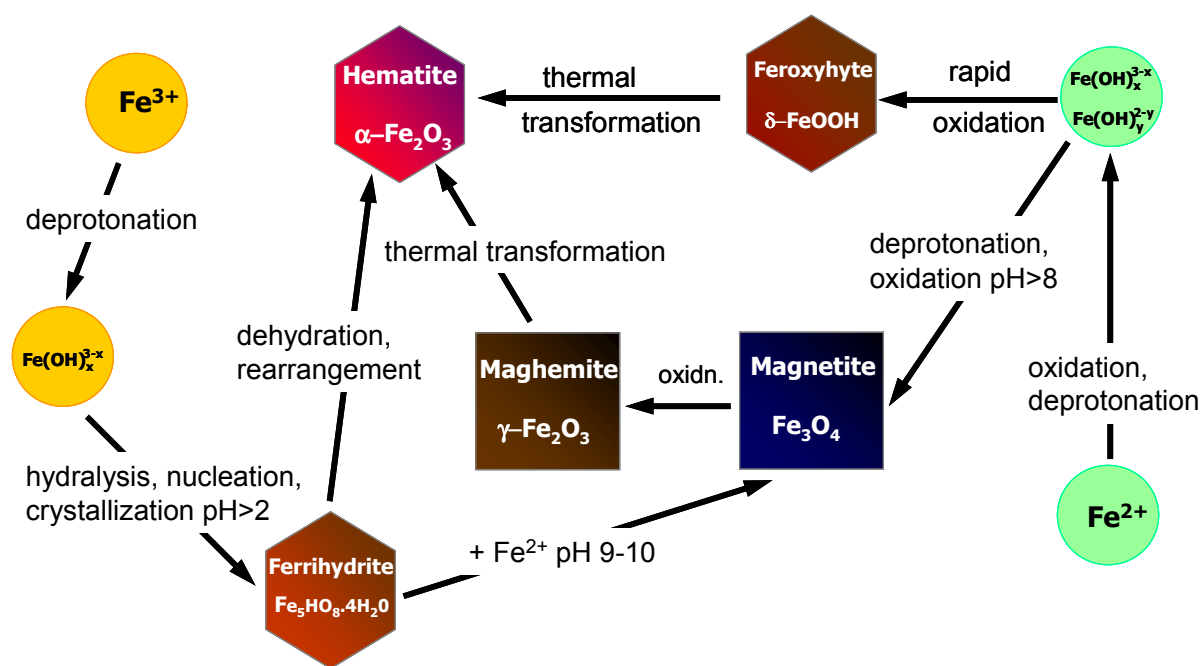


Figure 1.5 Schematic diagram of iron oxide oxidation pathway (Courtesy of O.R.T. Thomas, University of Birmingham, UK).

1.2.2.2 Manufacture of magnetic supports

Magnetic supports can be created by incorporation of the magnetic core material into a layer of organic polymer or polymeric matrix, thereby making them suitable for bioprocessing, as well as preventing iron leaching and protecting the magnetic core from oxidization. To achieve this various methods have been developed (see Fig 1.6), namely (i) coating, (ii) infiltration, (iii) encapsulation and a combination of (i) and (ii) or (i) and (iii).

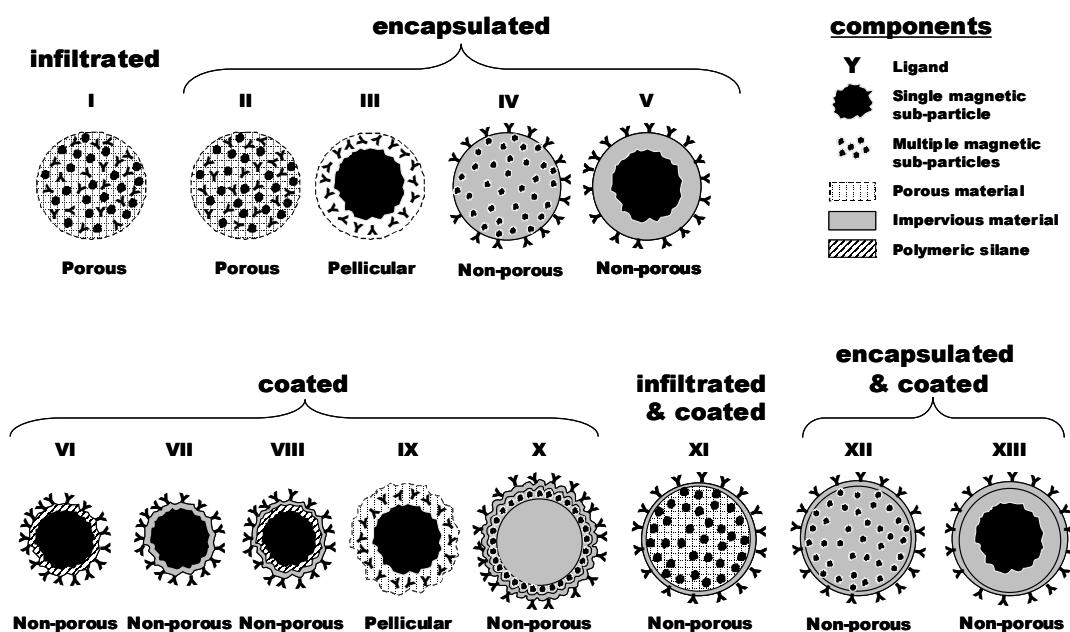


Figure 1.6 Magnetic support designs afforded by coating, infiltration and encapsulation techniques. For simplicity, only the primary location of ligands is depicted. (Courtesy of O.R.T.Thomas, University of Birmingham, UK).

1.2.2.2.1 Coating techniques

Magnetic core materials can be coated in a variety of ways to allow for ligand attachment and stabilization of a given support structure. Four different approaches are introduced in here, namely layer-by-layer adsorption, silanization, graft polymerization and co-precipitation.

Cheaper water soluble polyamines, such as polyethyleneimine or polyvinyl amine can be electrostatically adsorbed onto the charged surface of the magnetic nano sized crystals (design VII, Fig. 1.6). A more elaborate example using layer by layer adsorption technique making magnetic supports has been described as electrostatic

encrusting porous silica onto magnetic crystals to form a pellicular coating (design IX, Fig. 1.6). Goetz and colleagues (1991) firstly introduced this technique as colloidal silica and an oppositely charged polymer were electrostatically deposited onto the magnetic core material stepwise (10-50 times). Following deposition of the desirable layers, the supports were subject to two controlled heating steps, to burn out the polymer and then sintered the silica coating (Goetz *et al*, 1991). This approach is shown in Fig. 1.7. Lately, this technique has been developed to produce superparamagnetic monodispersed magnetic spheres (Caruso *et al.*, 1999) and controllable sized monodispersed magnetic silica (Zhu *et al.*, 2003).

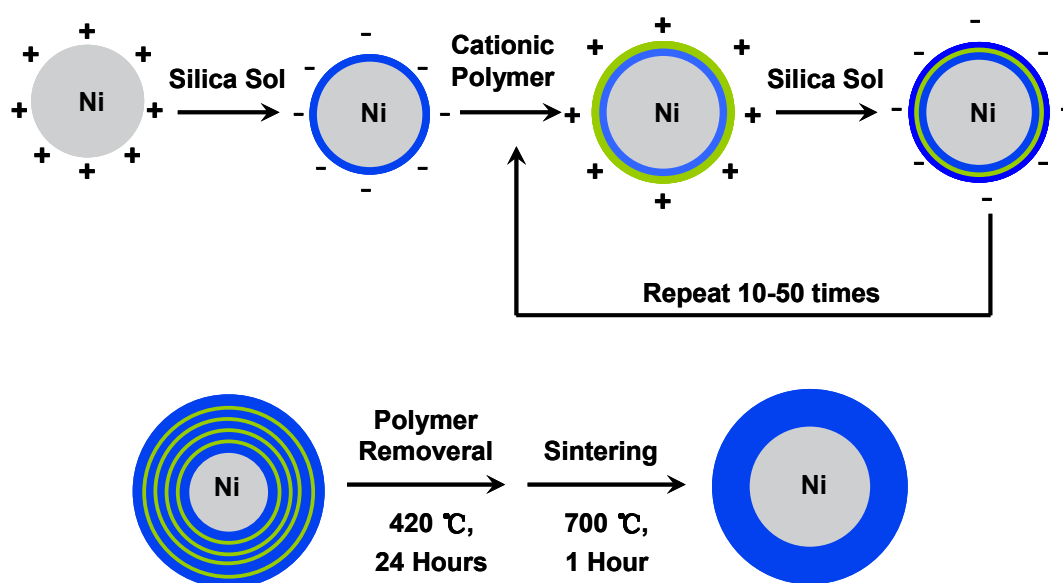
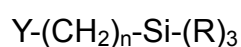


Figure 1.7 Schematic diagram of layer-by-layer adsorption technique to produce magnetic supports. Positively charged nickel core is represented in grey, silica sol is represented in blue and polyelectrolyte is shown in green (Reproduced from Goetz *et al.*, 1991).

Silane coupling agents are frequently employed to introduce reactive organic functionalities onto magnetic nano sized particles by silanization. Silane coupling agents are organosilicone compounds having two functional groups; one of the two functional groups reacts with organic materials and the other reacts with inorganic materials, such as glass, silica and metal oxide (TCI America, 2010). Their general structure is as follows:



where Y is the organic functional moiety (e.g. vinyl, epoxy and amino group); R is the inorganic functional moiety (e.g. chlorine, alkoxy, and acetoxy group). Iron oxide nano sized crystals can be covalently silanized with various silane coupling agents and subsequently form hydrophilic amine group or hydrophobic allyl group shell (see Fig. 1.8; Durdureanu-Angheluta, 2008).

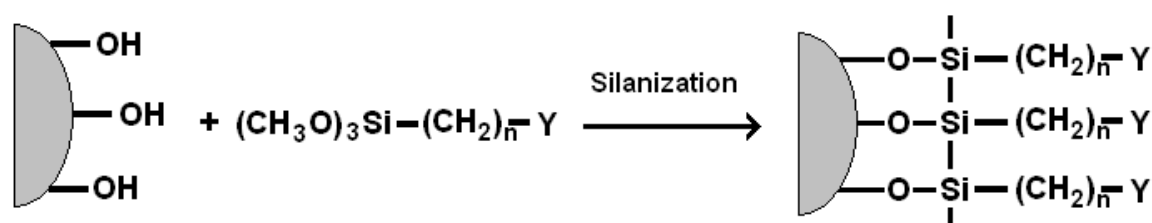


Figure 1.8 Schematic diagram of a silanized iron oxide support. The iron oxide core is represented in gray; -Y could be vinyl, epoxy and amino group.

This approach provides an ideal anchorage for future covalent grafting of specific ligands. Perhaps the best-known commercial available magnetic support of this type

(design VI, Fig. 1.6) is the micron sized, silane-coated BioMag[®] particle (Polysciences, Inc., Warrington, UK), which possesses a highly-textured exterior, imparting a specific surface area of more than 100 m² g⁻¹.

As it has been explained in section 1.2.1.2.1, porous magnetic adsorbents are susceptible to fouling, difficult to sanitize once fouled and mass transfer limited by diffusion. Thus, nonporous magnetic adsorbents with superparamagnetic property are highly suitable to handle large volumes of dirty crude feedstocks. Halling and Dunnill (1979) introduced an elegant and inexpensive, two step approach to the manufacturing of stable coated nonporous magnetic supports, namely graft polymerization method (see Fig. 1.9).

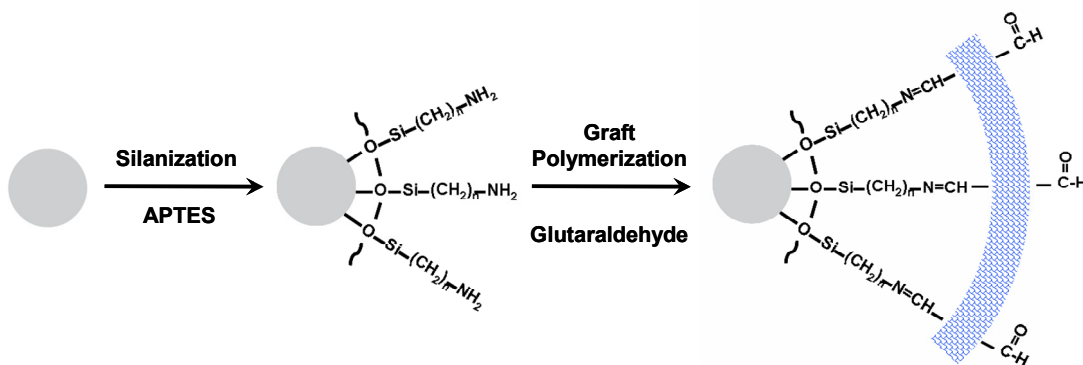


Figure 1.9 Schematic diagram of graft polymerization method producing nonporous magnetic supports. Iron oxide core is represented in grey and polyglutaraldehyde layer is in light blue.

This approach was subsequently developed further by O'Brien *et al.* (1996),

Zulqarnain (1999), and has been routinely employed during HGMF studies (Hubbuck *et al.*, 2001; Hubbuck and Thomas, 2002; Heebøll-Nielsen *et al.*, 2004). Iron oxide nano sized crystals are firstly silanized with silane coupling agent, such as: 3-aminopropyltriethoxysilane (APTES) to create amine terminated surface. Then these amine terminated magnetic particles surface are coated with an ultra thin layer of polyglutaraldehyde to form nonporous submicron particles which can be easily derivatised with various functional ligands (Heebøll-Nielsen *et al.*, 2004). When used in large scale preparations of magnetic adsorbents, this technique produced high binding capacity adsorbents ($> 200 \text{ mg g}^{-1}$) successfully employed in HGMF separations (design VIII, Fig. 1.6; Heebøll-Nielsen, 2002). Polymer graft coating techniques can also be applied to the surfaces of encapsulated nonporous magnetic adsorbents (designs IV & V, Fig. 1.6), resulting in materials with the appearance of types XII and XIII (See Fig. 1.6).

Conventionally, magnetic nano sized crystals (magnetite and/or maghemite) can be synthesized via co-precipitation of ferrous and ferric salt solutions by addition of an alkaline solution. The final size, shape and component of the magnetic nano sized crystal depend on the initial molar ratio of ferrous and ferric ion from 1:1.5 to 1:2 and the type of alkali used (e.g. KOH, NaOH and NH_4OH) (Odenbach, 2002A). An increasingly popular and cheap route for preparing coated, magnetic nano sized crystals is simply to introduce an appropriate polymer (e.g. polyethylene glycol,

polylactic acid, chitosan and dextran) into the iron salt solution prior to the alkaline addition (design VII, Fig. 1.6). The adsorbed coat material surrounding the single crystals is often stabilized by a chemical cross linking treatment. In addition, various surfactants, such as fatty acids (Wooding *et al.*, 1991; Shen *et al.*, 1998), citric acid (Raacuci *et al.*, 2006) or tetramethylammonium hydroxide (Berger *et al.*, 1999) can also be introduced into the iron salt solution prior to alkaline addition to form a stabilized colloidal suspension of nano sized magnetic crystals (ferrofluid).

1.2.2.2.2 Infiltration techniques

Preparation of single crystal magnetic adsorbents has been explored extensively by many researchers; it involves several steps, is time consuming, and the final adsorbents are small in size which limits their separation efficiency when employed in high gradient magnetic fishing (Heebøll-Nielsen, 2002). Despite that, they are highly suitable for laboratory scale separations and biomedicine applications (Heebøll-Nielsen, 2002). An alternative route to the creation of multi-crystals magnetic supports is via infiltration (design I, Fig. 1.6).

Initially, a ferrofluid with an average particle size of 10 nm was recycled through a bed of affinity chromatography Sepharose matrix and the resulted magnetic nano sized particles were entrapped and consequently introduced magnetic properties into these chromatography adsorbents (Mosbach and Anderson, 1977). Later, Hirschbein and

Whitesides (1982) produced magnetic supports by simply mixing synthetic agarose with magnetite, followed by washing and removal by filtration of any excess magnetite present.

A novel route, called 'activated swelling process', involving multiple steps is used to manufacture the well known commercial magnetic supports, Dynobead[®], invented by Ugelstad *et al.* (1983). The starting material is prepared by normal emulsion polymerization and uses a water soluble initiator. The resulted latex particles are highly porous, monodispersed, spherical and smooth surfaced. Oxidative amino groups (e.g. -NO₂, -ONO or -ONO₂) are then introduced into the pores and the particles are suspended in an aqueous ferrous salt solution. When the pH of the solution is raised and an iron oxyhydroxide intermediate Fe(OH)₂ is formed, oxidation takes place inside of pores by means of the amine group which continuously oxidizes Fe(OH)₂ to Fe(OH)₃. Therefore, Fe(OH)₂ is constantly transported from the outer solution inside the pores, and upon subsequent heating, it forms into small magnetite (or maghemite) crystals, which are uniformly dispersed throughout these latex particles. To protect the ferrite crystals from corrosion and prevent leakage of soluble ferric ions, these ferrite-containing particles are finally treated with epoxy compounds or synthetic polymers, which fill up most of the pores, coat the exterior surface and yield a nonporous surface (design XI, Fig. 1.6). This coating step also introduces anchor points for the attachment of appropriate ligands to the external surface.

1.2.2.2.3 Encapsulation techniques

Instead of infiltration, encapsulation is another alternative route to improve the dispersion characteristics, chemical stability and functionality of the magnetic particles. Early on, magnetic powders were introduced into a monomer suspension and subsequently gelled into a block. The polymer block was then ground down and sieved, and often yields crude materials with irregular shape, large size and wide size distribution (Safarik and Safarikova, 1993). In later studies, large, beaded adsorbents, featuring entrapped magnetic sub-particles were prepared by: (i) simple, metal ion-induced gelation of solutions of algal polymers (e.g. κ -carrageenan, alginate) containing magnetic sub-particles (Moffat *et al.*, 1994); (ii) polymerization of acrylamide in the presence of agarose and magnetite (Pollak *et al.*, 1980); and (iii) cross-linking of bovine serum albumin with glutaraldehyde in the presence of suspended Fe_3O_4 in an emulsion suspension system (Halling and Dunnill, 1980).

Inorganic support matrices offer certain advantages over the use of polymers, including high mechanical strength, thermal stability and resistance to solvent and microbial attack. Magnetic nano sized particles can also be encapsulated within glass, glass ceramics and other inorganic materials, but the methods are quite different to those employed with organic materials. For example, the Magnetic Glass Particle (MGP) adsorbent is prepared by a sol-gel processing route (Roche Diagnostics

GmbH, 2000), which involves mixing a sol consisting of alkoxides of network-forming components (e.g. SiO_2 , B_2O_3 , Al_2O_3 , TiO_2 , ZrO_2 , GeO_2) and oxides and salts of other components in an alcohol solution with magnetic nano sized particles, and then spray-drying the mixture to gel the sol layers encasing the magnetic cores. Subsequent, high temperature heating in a nitrogen-purged atmosphere yields magnetic cores encased in a substantially pore-free glass (design V, Fig. 1.6).

Since the late 1970s, liquid-liquid two phase polymerization techniques have been used to fabricate a great many micron and sub-micron sized magnetic supports encased in various synthetic, natural and hybrid matrices (e.g. Denkbass *et al.*, 2002; Ramirez and Landfester, 2003; Saravanan, *et al.*, 2004; Xu *et al.*, 2004; Pich *et al.*, 2005; Muller-Schulte and Schmitz-Rode, 2006). Relying on these techniques, magnetic particles encapsulated in synthetic polymers can be produced by rapidly mixing a solution of magnetic iron oxides, monomers and co-monomers in a hydrophobic phase, such as isoparaffinic oil. Agitation disperses the solution, forming beaded droplets, whose size is determined by the agitation conditions. Solidified adsorbents are subsequently formed by polymerization; the porosity of the resulting supports is influenced by the choice of monomer, co-monomer and polymerization conditions; magnetic property is influenced by encapsulation of various magnetic materials. Therefore, the physical and chemical properties of the resulting particles are more controllable.

Unlike the coating and infiltration techniques, liquid-liquid two phase methods involve a one-pot synthesis of the magnetic supports using one off free radical reaction; in this way they avoid complicated multi-step preparations, are low-cost and permit the rapid production of primary support particles. In addition, they are easy to scale up as a large number of agitation equipment are commercially available in various types and work capacities; these liquid-liquid two phase reactions are presented in more detail in the following sections.

1.3 Liquid-liquid two phase polymerization type reactions

1.3.1 Emulsion formation and stabilization in liquid-liquid two phase system

A liquid-liquid two phase system is formed through the process of emulsification, during which, immiscible droplets are dispersed through a continuous phase. This can be achieved with the aid of various emulsification equipments, such as sonifiers, homogenizers and high shear mixers. Sonifiers produce ultrasound waves during continuous compression and depression cycles, and these wave shocks result in the breakup of the emulsion droplets (Bondy and Sollner, 1935). Homogenizers are designed to force emulsion droplets pass through a narrow gap at high velocity, thereby subjecting them to high share stress and causing their collapse and breakage into smaller size particles (Anton *et al.*, 2008). In high shear mixers big emulsion droplets are broken by the collision with turbulence flow eddies and the minimum size

of the emulsion droplet that can be achieved will depend on the smallest size of the turbulence eddies (Asus, 2002). High shear mixers have many advantages over sonifiers and homogenizers because they are inexpensive, simple to operate and are commercially available in various types and working capacity, which makes their scale up quite easy and straightforward.

In liquid-liquid two phase systems, the breakup of dispersion phase droplets creates large surface area. This process raises the interfacial energy, resulting in positive Gibbs free energy of the emulsion formation and introducing thermodynamic instability to the system (Anton *et al.*, 2008). If the liquid-liquid two phase system can be considered as an isolated system, it has following equilibrium correlation:

$$\Delta G_f = \gamma \Delta A - T \Delta S_f \quad (1.13)$$

where, ΔG_f , is the Gibbs free energy of the emulsion formation; $\gamma \Delta A$, is the interfacial energy, in which γ and ΔA respectively represent the surface tension and the surface area gained from breakup; and, $T \Delta S_f$, is the entropy of droplet formation. If: $\Delta G_f > 0$, the system is thermodynamically unstable; $\Delta G_f = 0$, the system is in equilibrium. Therefore, to maintain system equilibrium the individual droplets spontaneously merge to minimize their interfacial area, which can lead to emulsification failure, which is very undesirable during liquid-liquid two phase polymerization. Thus, the system stabilization can only rely on lower surface tension.

Surfactant is an organic amphiphilic compound which consists of a hydrophilic head and a hydrophobic tail (Rosen, 1989). In liquid-liquid two phase systems, the hydrophilic head gets into contact with the polar phase, while the hydrophobic tail extends into the non-polar phase. The surfactant layer which is formed at the interfacial area reduces the surface tension of the emulsion droplet, decreases the free interfacial energy and maintains the equilibrium of the system (see Eq. 1.13). It therefore prevents the coalescence of the emulsion droplets and stabilizes the system.

1.3.2 Types of liquid-liquid two phase polymerization reactions

The history of liquid-liquid two phase polymerization dates back to the early 20th century, and was first employed within the field of synthetic rubber manufacture (Whitby and Katz, 1933). Kurt Gottlob (1915) invented a natural macromolecule (e.g. starch and albumin) stabilized aqueous monomer emulsion to produce synthetic rubber to meet the increasing needs of natural rubber was expanded during the First World War. In the following 100 years, liquid-liquid two phase polymerization was extensively investigated, and three major types of reactions have been developed; namely: dispersion/precipitation polymerization; emulsion polymerization; and, suspension polymerization. Though the definitions of these polymerization reactions have not been codified by the International Union of Pure and Applied Chemistry, they

appear in the wide literature and thereby are commonly accepted by general agreement (Elbert, 2011).

Dispersion polymerization is a type of liquid-liquid two phase reaction, which exploits the difference in solubility between the monomer and the final polymer (Elbert, 2011). Initially, the monomer, the surfactant and the initiator are dissolved in a homogeneous single phase, in which the final polymer is insoluble; shortly after the initiation of the polymerization reaction, polymer chains start to grow, new particles occur by nucleation and because the longer polymer chains have lower solubility compared to the shorter ones (Flory, 1942), phase separation happens when the polymer weight reaches a specific value. Later on, the formed particles continue to grow by capturing the low concentration of polymer chains before nucleation of new particles happens (LaMer and Dinegar, 1950), and since nucleation takes place in a very short period, this type of polymerization usually results in monodisperse particles. Precipitation polymerization is very similar to dispersion polymerization, with the only difference being that no surfactant is used; coalescence thus occurs between the new particles resulting in irregular shaped preparations with broad particle size distributions (Barrett, 1975).

Unlike dispersion polymerization, the monomer and initiator of direct emulsion polymerization are soluble in the monomer droplets and the continuous phase

respectively, and initiation occurs in the micelles which are located outside of the monomer droplets (Schildknecht, 1956). Excess surfactant creates an increased number of micelles in the continuous phase, from which polymer chains grow rapidly by radical reaction and polymeric particles are created (Oadian, 1970).

During suspension polymerization, the monomer and initiator are both soluble in the dispersion phase of the liquid-liquid two phase system and polymerization occurs in each individual monomer droplet (Schildknecht, 1956). The resulting particle size is thereby determined by the rate at which the monomer droplets break and reform (Elbert, 2011).

1.3.3 Inverse phase polymerization in liquid-liquid two phase system

The liquid-liquid two phase polymerization technique can be employed in both water-in-oil (W/O) emulsion and oil-in-water (O/W) emulsion. If the emulsion is formulated as oil immiscible droplets dispersed through water (O/W), it is often classified as 'direct' whereas, the system of water-in-oil emulsion is classified as 'inverse' (Pross *et al.*, 1998).

Inverse phase emulsion can be created by employing a W/O type surfactant during emulsification. The most suitable surfactant can be chosen using the concept of the hydrophilic-lipophilic balance (HLB). The HLB was first defined as a function of the

weight percentage of the hydrophilic portion of the surfactant molecules (Griffin, 1949; Al-Sabagh, 2002). Later, the HLB was employed (as a scale from 0 to 20) to describe the hydrophilicity and hydrophilicity of a molecule based on its chemical formula (Davies, 1957).

$$\text{HLB} = \Sigma (\text{hydrophilic group numbers}) - n (\text{group number per } \text{CH}_2 \text{ group}) + 7 \quad (1.14)$$

where n is the number of the CH_2 groups of the surfactant molecule (relative values of group numbers can be found in the literature; Davies, 1957). As shown in Fig. 1.10, in order to select a surfactant for inverse phase (W/O) polymerization, its HLB should be in the range of 3.5 to 6.

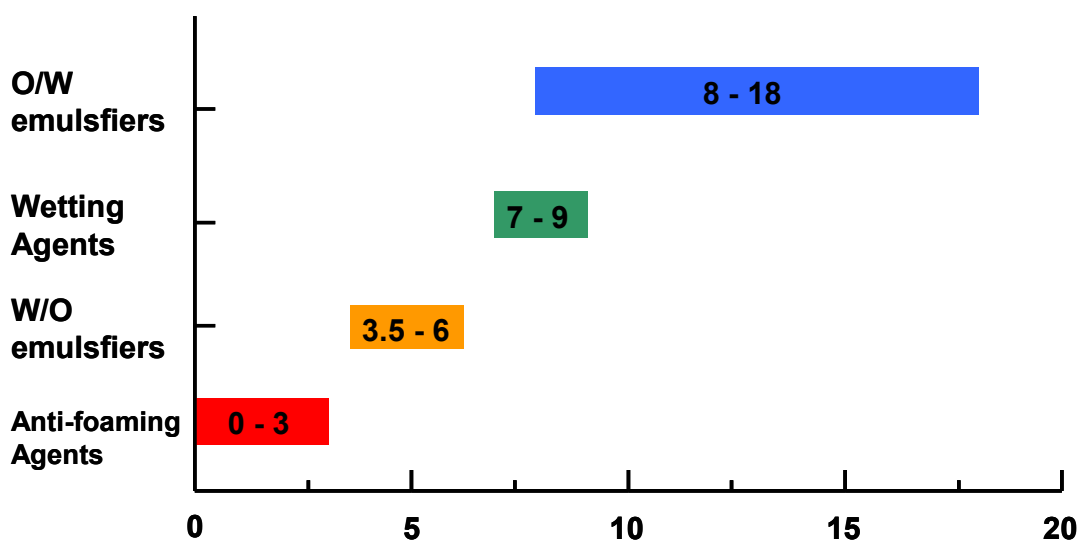


Figure 1.10 Classification of hydrophilic-lipophilic balance of surfactant (Reproduced from Davies, 1957).

The reaction mechanism of the inverse phase emulsion polymerization is different to

that of the direct phase emulsion polymerization, in which the radical reaction occurs in the monomer droplets instead of the micelles (Elbert, 2011). Especially, when a large external energy is employing in inverse system, the emulsion droplets are resulted in submicron domain with narrow particle size distribution and large surface area. Due to the large total surface area, capture of free radicals by the monomer droplets is efficient and initiation thus occurs in aqueous monomer droplets, even if initiator is in the continuous phase (see Fig 1.11; Elbert, 2011). In this case, inverse phase emulsion polymerization resembles an inverse suspension polymerization, and its resulted particle size will be influenced with input of mechanical energy. In addition, some monomer droplets do not capture radicals, but contribute to growing particles; therefore, the resulted polymeric particle size is bigger than the size of droplet (Lovell and El-Aasser, 1997).

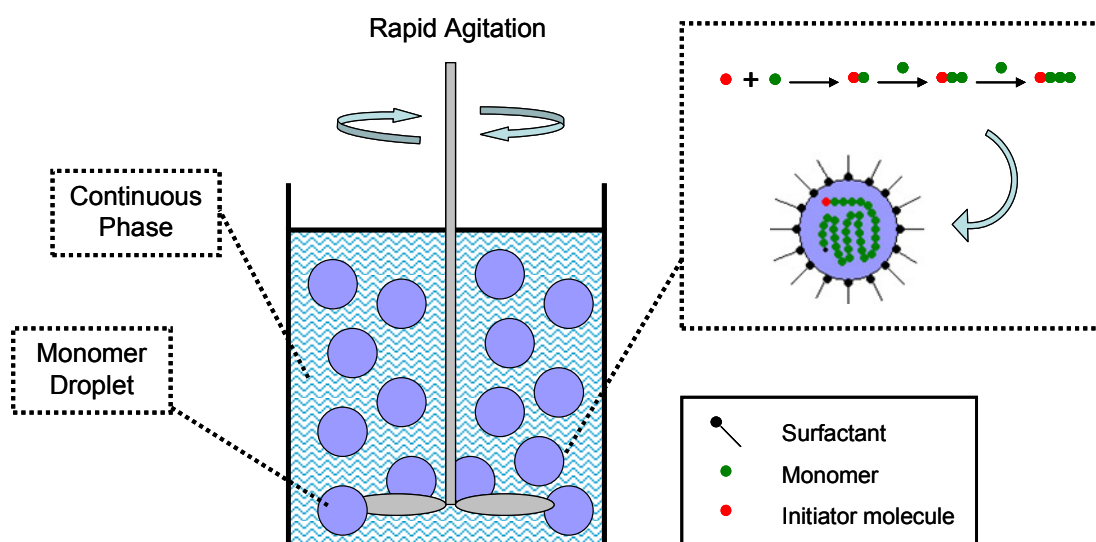


Figure 1.11 Illustration of a typical inverse phase emulsion polymerization reaction.

1.4 Project overview

This project focuses on an 'one-pot' manufacturing route to produce magnetic adsorbents for the large scale purification of biological molecules.

The first chapter introduces the background knowledge of this thesis, where the basic theory of magnetic separation, forms of magnetism, the historical development of magnetic separations, and the principles of magnetic support design and manufacturing approaches suitable for biotechnological applications are introduced. The latter part of the chapter contains a short overview of the various types of liquid-liquid two phase polymerization reactions use in the manufacture of composite particles.

Chapter two presents some 'ground' work on the use of inverse liquid-liquid two phase polymerization and a high shear mixing device to produce suitable polymer particles without any magnetic core material. Various operating conditions, such as concentration of initiator, dispersed to continuous phase ratio, time of operation and agitation speed were systematically investigated to identify the optimum manufacturing conditions for the production of polymer beads.

In chapter three, various magnetic core materials such as uncoated magnetite powder

and different ferrofluids were incorporated into the polymer [poly(acrylamide-co-ethylenebisacrylamide)] support matrix, and the efficiency of encapsulation was studied with regards to particle size distribution, particle morphology, and magnetic properties. Furthermore, the agitation speed of the high shear mixer as well as the magnetite and surfactant loadings were further investigated to produce magnetic/polymer composites of desirable size distribution.

In the next chapter (chapter four), functional monomers were added to the polar phase, and magnetic anion and cation exchange adsorbents were synthesized following the 'one-pot' inverse phase emulsion polymerization route. The above adsorbents were subsequently tested under binding and elution conditions using model proteins.

The final chapter (chapter five) in this thesis contains the main conclusions drawn from the work carried out so far and also point out to future directions and further applications of the 'one-pot' manufacturing process in the area of bioprocessing.

In the appendix, a preliminary work toward surface molecularly imprinted adsorbents was carried out as a side work by using sequence-recognition surface metal coordination imprinting approach to familiar surface protein imprinting techniques for future manufacturing magnetic molecularly imprinted adsorbents.

2. Preparation of beaded poly(acrylamide-co-ethylenebisacrylamide) supports by an inverse liquid-liquid two phase polymerization method

Abstract

In this chapter, inverse liquid-liquid two phase polymerization method is employed to produce beaded materials in absence of magnetic core materials. Through systematic variation of initiator concentration, dispersion to continuous phase ratio, operation time and agitation speed, the influence on the varying of particle size and particle size distribution were investigated and the optimum operation conditions of manufacturing non-magnetic beaded materials via liquid-liquid two phase polymerization have been confirmed. Optical counting technique was used in particle size distribution analysis. Cryo Scanning Electron Microscopy technique was dedicated to the microstructure study of the particle preparation following 48 minutes and 60 minutes mixing.

2.1 Introduction

Various liquid-liquid two phase polymerization methods have been used in the past to produce magnetic polymeric particles with optimal physical properties, such as shape, size and magnetic content (Ma *et al.*, 2007; Philippova *et al.*, 2011). Of these, suspension polymerization is an easy to perform process, during which the polymerization occurs in each individual monomer droplet. Magnetic particles produced this way have usually ten to hundred micrometers in size and broad particle size distribution (Cocker *et al.*, 1997; Lee *et al.*, 2003; Liu *et al.*, 2010); therefore their sizes are too big to provide enough surface area for efficient bioseparation. Dispersion polymerization is another simple and efficient method, which can produce micron size and monodispersed magnetic particles (Ma *et al.*, 2005). However, dispersion polymerization initially begins as a solution polymerization in a single phase (Elbert, 2011); this nature limits its application in producing magnetic surface molecularly imprinted adsorbents. Emulsion polymerization is the most extensively studied method for making magnetic composite particles, which measure between ten to several hundred nanometers in size and have a relative high saturation magnetization (in some cases, the saturation magnetization can be as high as 47 emu g^{-1} ; Wormuth, 2001; Xu, *et al.*, 2004; Mori and Kawaguchi, 2007; Zhang *et al.*, 2007). Even though emulsion polymerization has already been successfully adapted to produce magnetic polymeric particles, there is still room for improvement regarding the use of different monomers, initiators, phase solvents, operating conditions and type of equipment

which will ultimately affect the final physical particle properties (for example, shape and size).

In this work, a series of non-magnetic polymeric particle preparations were made using inverse liquid-liquid two phase polymerization. Various parameters such as: initiator concentration; dispersion to continuous phase ratio; operation time; and, agitation speed were systematically investigated, in order to produce suitable particles of uniform size distribution and optimum size, upon which the future production of magnetic polymeric particles will be based.

2.2 Materials

Table 2.1 List of chemicals involved in this chapter

Chemical	Abbr.	Supplier	Description
Acrylamide	AM	Sigma-Aldrich	Neutral monomer
N,N'-ethylenebisacrylamide	EBA	Sigma-Aldrich	Cross linker
Ammonium persulfate	APS	Sigma-Aldrich	Initiator
N,N,N',N'-tetramethylethylenediamine	TEMED	Sigma-Aldrich	Accelerator
Isopar M	N.A.	Multisol	Continuous phase solvent
sorbitan sesquioleate (Arlacel [®] 83)	N.A.	Sigma-Aldrich	Surfactant; HLB: 3.7
Ethanol	N.A.	Fisher Scientific	Wash resulting particles

The double distilled water used in this work was generated from a Hamilton water boiler (Hamilton Laboratory glass Ltd., Margate, UK). Nitrogen was supplied by the BOC Group (Dudley, UK). Resulting polymeric particle suspensions were contained in 50 mL or 15 mL centrifuge tubes (Sarstedt UK Ltd., Leicester, UK).

2.3 Description of equipment

In this work, the emulsification of the monomer solution was carried out in a Silverson L5 M rotor-stator type high shear mixer (shown in Figure 2.1; Silverson Machines Ltd., Chesham, UK), equipped with a single phase motor (250 W, 50/ 60 Hz), that can reach a maximum agitation speed of 6000 rpm under full load (Silverson Machines Ltd., 2010).



Figure 2.1 Image of the Silverson L5 M high shear laboratory mixer used in this work, showing: (A) mixer; (B) workhead; (C) rotor; (D) stator; (E) bottom view of the rotor; (F) bottom view of the work head. The workhead consists of a 4 bladed impeller (D: 31 mm, H: 12.5 mm) and an emulsor screen (D: 33 mm (ext.), H: 17 mm). A 0.175 mm gap is left between the edges of the rotor blades and internal wall of the stator (Silverson Machines Ltd., 2010).

Mixing was carried out in a glass jacketed vessel (D: 70 mm (ext.), D: 55 mm (int.), H: 90 mm), made by the Department of Chemistry Workshop (University of Birmingham, UK). A Grant W6 water-bath with pump (Grant instrument Ltd., Cambridge, UK) was connected to the heating jacket of the glass reactor to maintain the desired temperature during polymerization (Fig. 2.2).

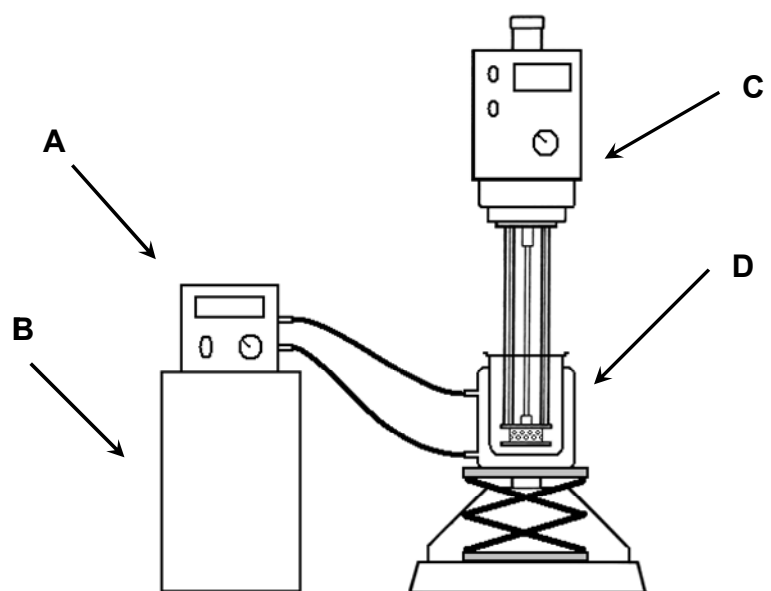


Figure 2.2 Sketch of the equipment set-up used for the manufacturing of composite supports showing: (A) pump; (B) water bath; (C) Silverson L5 M high shear laboratory mixer; (D) glass jacketed vessel.

2.4 Experimental methods

2.4.1 Selection of optimum initiator concentration

White and Thomas (1990) indicated what a final concentration of 0.19% (w/v) is the

lowest amount of initiator required to provide a optimum polymerization rate and a uniform and sturdy gel properties when ammonium persulfate and N,N,N',N'-tetramethylethylenediamine (TEMED) were respectively used as initiator and accelerator in one initiator system. According to White's result, the optimum initiator concentration was studied as following: 8 g of acrylamide and 1.36 g of N,N'-ethylenebisacrylamide were dissolved into double distilled water to create 36 mL of monomer solution, which was then purged with nitrogen for 30 minutes and split into four equal fractions. One milliliter of various concentrations of ammonium persulfate and their corresponding volume of accelerator (see Table 2.2) were then added into the above solutions and following brief mixing with a VM20 vortex mixer at maximum speed setting for 10 s. The mixtures were left to stand overnight to achieve complete polymerization.

Table 2.2 Preparation of initiator system

Final initiator ratio (w/v)	Ammonium persulfate (mg mL ⁻¹)	TEMED (μ L)
0.05%	5	6.5
0.1%	10	13
0.2%	20	26
0.4%	40	52

2.4.2 Selection of optimum dispersion to continuous phase ratio

Acrylamide (6 g) and 1.02 g of N,N'-ethylenebisacrylamide were dissolved into double distilled water to create 27 mL of dispersion phase, which was purged with nitrogen for 30 minutes and then split into three equal fractions. Arlacel[®] 83 (400 mg) was

added into each of three different volumes of Isopar M (20 mL, 40 mL and 80 mL) to create the continuous phase, which were purged with nitrogen for 30 minutes. A combination includes 26 μL of TEMED and 1 mL of ammonium persulfate solution (20 mg mL^{-1}) were added in and mixed with each dispersion phase. These dispersion phases were respectively added into the three different volumes of continuous phases and resulted on final dispersion phase to continuous phase ratios as 1:2, 1:4 and 1:8 (see Table 2.3).

Table 2.3 Preparation of liquid-liquid two phase systems in different dispersion phase to continuous phase ratio

Exp. No.	Monomer solution (mL)	Initiator solution (mL; 20 mg mL^{-1})	TEMED (μL)	Continuous Phase (mL)	Final dispersion phase to continuous phase ratio
1	9	1	26	20	1:2
2	9	1	26	40	1:4
3	9	1	26	80	1:8

Vigorous agitation was introduced with a Silverson high shear mixer at 2000 rpm for 12 minutes. The final emulsion was left to stand overnight and then the particles were washed once with ethanol and three times with double distilled water. Between each wash step, the particles were collected using a Jouan C422 centrifuge (DJB Lab care Ltd., Newport Pagnell, UK) operated at 4000 rpm for 5 minutes. The particle size distribution was determined using optical counting as described in section 2.2.4.1.

2.4.3 Selection of optimum mixing time

Acrylamide and N,N'-ethylenebisacrylamide (2 g and 0.34 g respectively) were dissolved into double distilled water to create 9 mL of dispersion phase, which was purged with nitrogen for 30 minutes. Four hundred milligrams of Arlacel[®] 83 were mixed with 40 mL of Isopar M to create the continuous phase, which was then purged with nitrogen for 30 minutes. A combination includes 26 μL of TEMED and 1 mL of ammonium persulfate solution (20 mg mL^{-1}) were added in and mixed with the dispersion phase. The dispersion phase was immediately added into the continuous phase and emulsified using the Silverson L5 M mixer operated at 2000 rpm for: 3, 6, 12, 24, 30, 48 and 60 minutes. The final emulsion was left to stand overnight and then the particles were washed once with ethanol and three times with double distilled water. Between each wash step, the particles were collected using a Jouan C422 centrifuge operated at 4000 rpm for 5 minutes. The particle size distribution was determined using optical counting as described in section 2.2.4.1. The particle preparation following 60 minutes of mixing was analysed by Cryo Scanning Electron Microscopy (see section 2.2.4.2), while the particle preparation following 48 minutes of mixing was analysed in the same manner as control.

2.4.4 Selection of optimum agitation speed

Dispersion and continuous phases were created and mixed as described above

(section 2.2.3.3) and then emulsified using the Silverson L5 M mixer for 48 minutes at the following agitation speeds: 1800, 2000, 2200, 2400, 2600, 2800, 3000, 3200 and 3400 rpm. The final emulsion was left to stand overnight and then the particles were washed once with ethanol and three times with double distilled water. Between each wash step, the particles were collected using a Jouan C422 centrifuge operated at 4000 rpm for 5 minutes. The particle size distribution was determined using optical counting as described in section 2.2.4.1.

2.5 Analytical techniques

2.5.1 Particle size distribution analysis using optical counting

The particle size distribution of the various preparations was determined using an Olympus BX50 light microscope (Olympus UK Ltd., Essex, UK), which was connected to a COHU high performance CCD camera (COHU's OEM Products Group, San Diego, USA). The images were taken at 1000 times magnification. A graticule slide with 1 mm grid was imaged in the same manner, and the particle size was calculated using the Droplet Detection System V1.5 (Compucon S.A, Thessaloniki, Greece).

2.5.2 Microstructure study using Cryo Scanning Electron Microscopy (Cryo SEM)

A thin piece of sample was sliced from the particle preparation after 60 minutes mixing, fixed onto the sample holder, and frozen at -198 °C in nitrogen slush under vacuum. Fracturing of the sample was conducted at -180 °C within the preparation chamber to

obtain a fresh surface, before it was sputtered under the platinum cathode for 60 seconds to increase conductivity and finally transferred into the sample chamber to be imaged with a Philips XL-30 Environmental Scanning Electron Microscope (FEI Co., Hillsboro, USA) at 5.0 kV and -130 °C. A drop of sample from particle preparation after 48 minutes mixing was directly loaded into sample holder, then prepared and imaged with the Philips XL-30 Environmental Scanning Electron Microscope in the same manner.

2.6 Results and discussion

2.6.1 Selection and optimisation of initiator

Azo compounds, such as azobisisobutyronitrile (AIBN), are the most commonly used initiators for emulsion polymerization. However, as they are highly flammable, toxic, irritating and can cause serious eye damage, AIBN is either not supplied in the UK (Oladosu, 2007), or incurs high delivery charges (O'Connor, 2008), which defeats the object of employing a cheap 'one-pot' manufacturing method.

In contrast, ammonium persulfate is an inexpensive strong oxidizing agent, which is usually applied together with the accelerator N,N,N',N'-tetramethylethylenediamine (TEMED), to generate free radicals for polymerization (see Fig. 2.3). Ammonium persulfate therefore was chosen as the most suitable substitute to AIBN in this work.

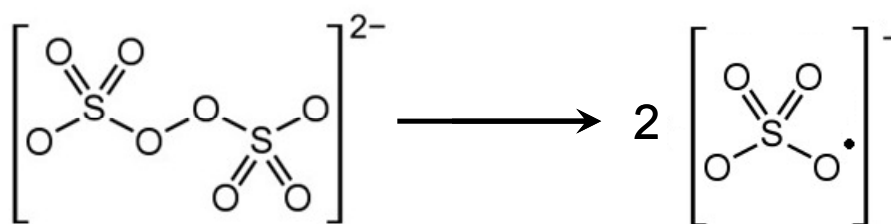


Figure 2.3 Generation of free radicals from ammonium persulfate.

Of the four concentrations of initiator tested (Table 2.1), both the 0.2% and 0.4% (w/v) gave quite uniform and sturdy gel structures. In contrast, using 0.1% (w/v) of initiator produced wobbly and weak gels. At a concentration of 0.05% (w/v) the mixture was still in liquid state even after it was left to stand overnight, indicating that there was not enough ammonium persulfate present to initiate the polymerization reaction. Therefore 0.2% (w/v) initiator concentration was chosen as the optimum to conduct further experiments.

2.6.2 Selection of optimum dispersion to continuous phase ratio

Based on the results of Desnoyer and co-workers (2003), which reported that phase ratios of 2:3 and above could result in phase inversion, the following three different dispersion to continuous phase ratios were investigated: 1:8; 1:4; and 1:2, whilst the mixing speed and time were kept constant at 2000 rpm and 12 minutes respectively. In addition, the task of this section is to find out optimal phases ratio only regarding to making the small particle size and narrow size distribution particles as starting point to further magnetic supports manufacture; these dynamic studies (e.g. energy input per

kilogram) will not be included because of the limited time. As illustrated in Fig. 2.4, the particle size decreases with the increasing fraction of the dispersion phase volume in the system, which is contrary to those has been reported in the literature using a normal high shear mixer (Kraume *et al.*, 2004; Razzaghi and Shahraki, 2010).

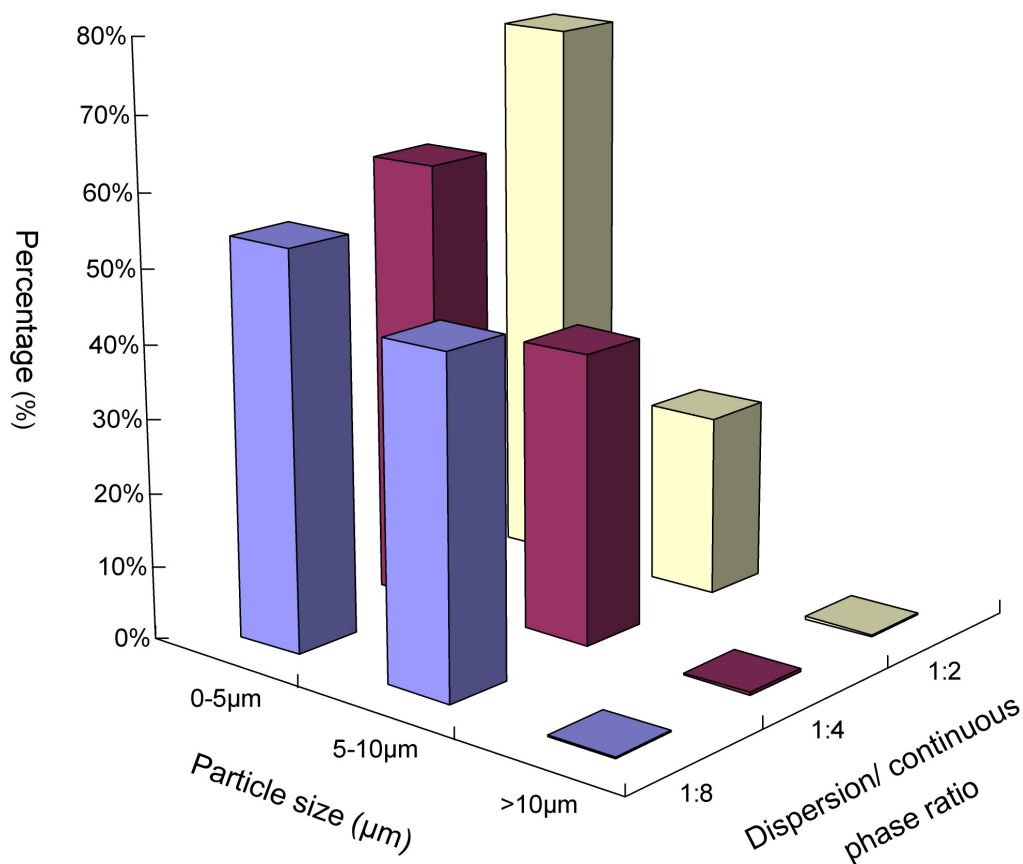


Figure 2.4 Effect of dispersion to continuous phase ratio on particle size distribution.

This contradictory result can be attributed mainly to the type of mixer used in this work. The mixing profile of a rotor-stator type high shear mixer is different to that of the traditional high shear mixers used for the breakup of emulsion droplets. According to

literature provided by Silverson Machines Ltd. (2011), in the case of the rotor-stator type high shear mixer, the breakup of droplets mainly takes place inside the workhead, since the high speed rotation of rotor blades exert a powerful suction to draw emulsion droplets into its centre (see Fig. 2.5 A). The emulsion droplets are then centrifugally driven to the periphery of the workhead, where they encounter a milling force between rotor and emulsor screen (stator), and followed by intense hydrodynamic shear when they are forced through the narrow pores of the emulsor screen at high speed (see Fig 2.5 B & C). Finally, the emulsion droplets are discharged from the workhead, and fresh emulsion droplets are drawn into it (see Fig 2.5 D).

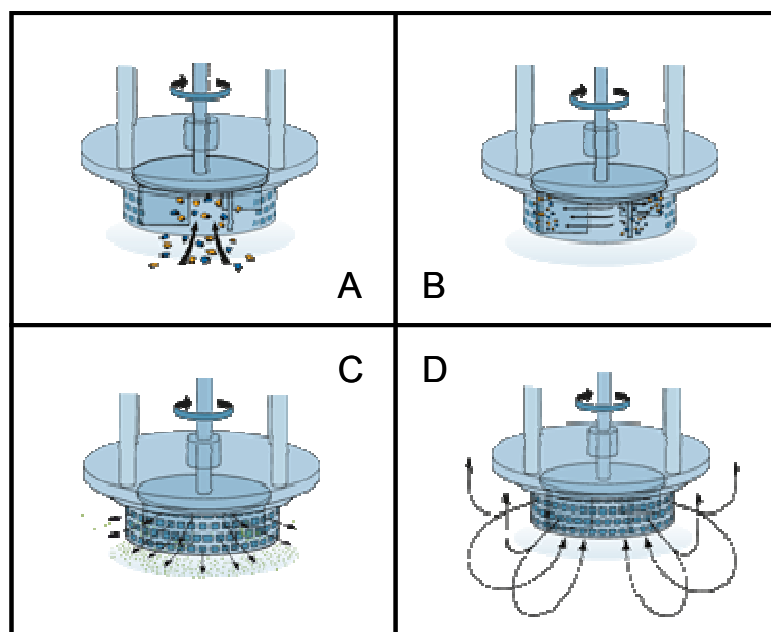


Figure 2.5 Illustration of the mixing mechanism behind the rotor-stator type high shear mixer (taken from Silverson Machines Ltd., UK).

Based on the above, the formation of the emulsion droplets presented in this work is the result of milling force and hydrodynamic shear, rather than the collision with turbulence eddies occurring in traditional high shear mixers. The higher dispersion to continuous phase ratio produces higher droplet concentration and thereby increased chances of droplets to go through the workhead and be subjected to milling force and hydrodynamic shear. Therefore, at constant mixing speed and operation time, the larger dispersion to continuous phase ratio will produce the smaller emulsion droplets and consequently the smaller size particles. However, the total volume of the liquid-liquid two phase system decreases with the increasing of the dispersion to continuous phase ratio when keeping a constant dispersion phase volume. Therefore, the workhead was unable to be completely immersed into the liquid-liquid two phase system when 1:2 of dispersion to continuous phase ratio was employed. Consequently, the air in the top space was introduced into the system as a third phase and resulted in emulsion system change. Thus, 1:4 of dispersion phase to continuous phase ratio has been selected as the optimum ratio.

2.6.3 Selection of optimum operation time

The effect of the operation time on the final particle size distribution was investigated at the dispersion to continuous phase ratio of 1:4 and 2000 rpm mixing speed, and the results are illustrated in Fig. 2.6. It is clear that with increasing mixing time from 3 to 48 minutes, the particle size distribution becomes narrower, and the total particle size is

reduced markedly, which is a direct consequence of prolonged exposure to shear forces.

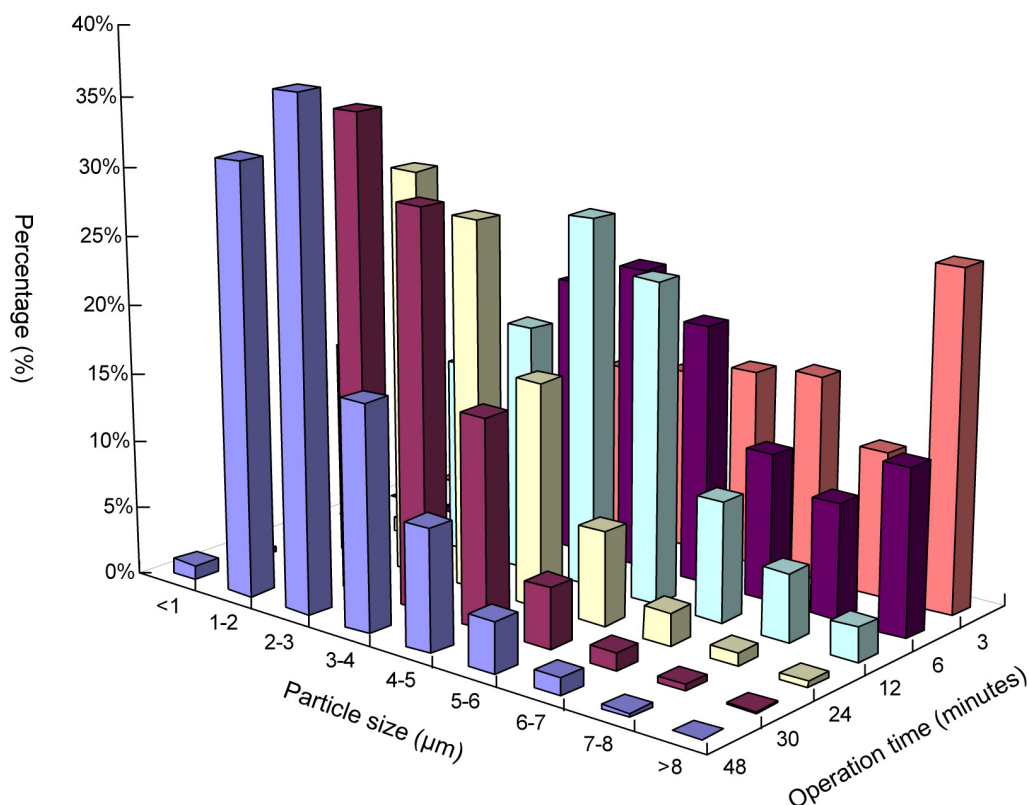


Figure 2.6 Effect of operation time on particle size and particle size distribution.

However, after 60 minutes of mixing, a continuous lump of smooth and uniform polymeric gel was formed, instead of distinct polymeric particles. When the process was repeated once again, it produced the same result, as depicted in Figure 2.7. The above gels were further analysed with Cryo-SEM (Figure 2.8), which revealed the presence of many ellipsoid particles with sizes below 15 microns dispersed throughout the continuous gel structure. In contrast, the Cryo SEM image of the

sample from the particle preparation following 48 minutes of mixing exhibits individual and distinct polymeric spherical particles.

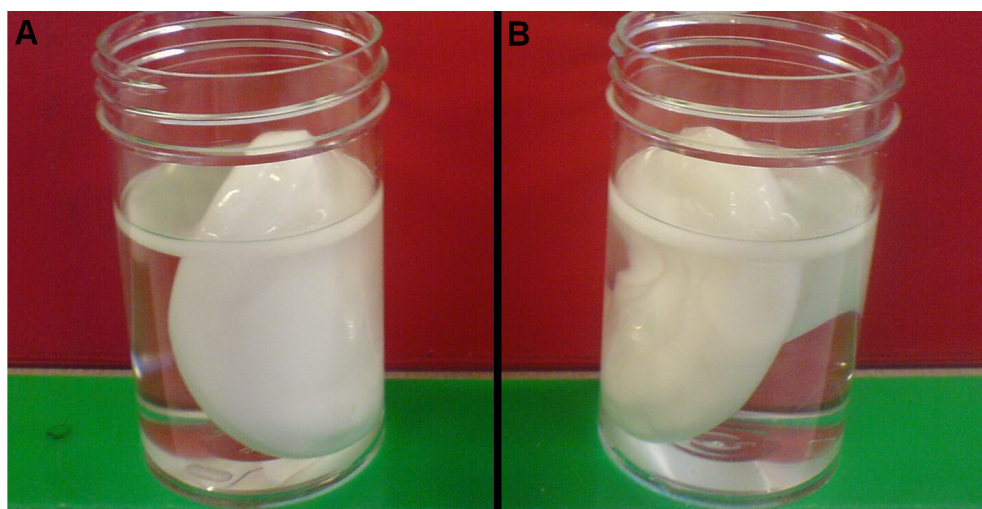


Figure 2.7 Images of polymeric gels obtained at operation condition of 2000 rpm and 60 minutes (A: first attempt; B second attempt).

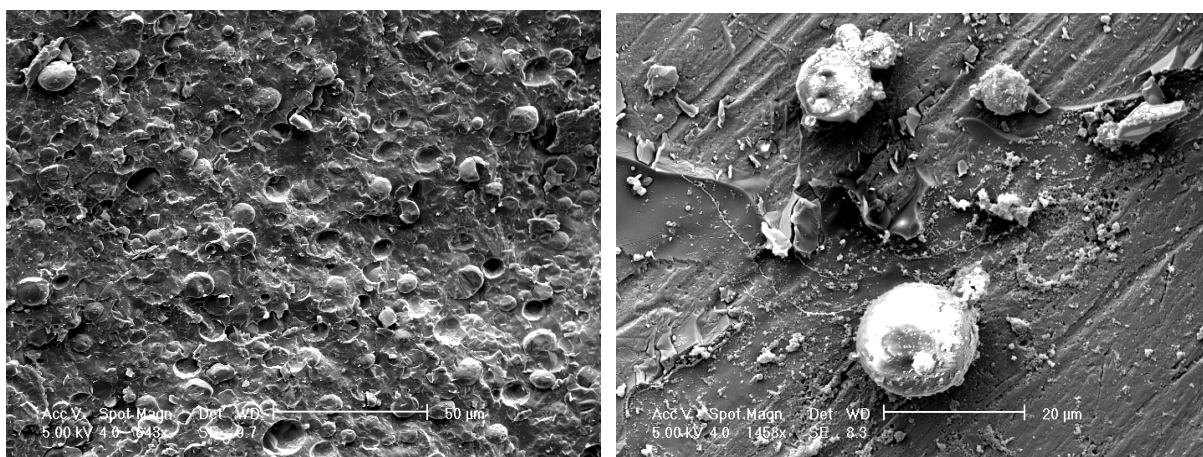


Figure 2.8 Cryo-SEM image of the gel produced following mixing at 2000 rpm for 60 minutes (the ellipsoid particles are believed to be frozen Isopar M droplets; left) and particles produced following mixing at 2000 rpm for 48 minutes mixing (right).

Long term agitation causes accumulation of heat energy in the liquid-liquid two phase system and consequently temperature increase. Shinoda and co-workers (1968, 1969) introduced the concept of Phase Inversion Temperature (PIT) and indicated that temperature changes can modify the affinities of the surfactant to the water and oil phases and therefore alter the relative values of the hydrophilic and hydrophobic group numbers. As can be seen from equation 1.14 and Fig. 1.11 (Section 1.3.3), when the hydrophilic-lipophilic balance (HLB) of a surfactant becomes higher than 8, the surfactant becomes an O/W rather than a W/O type. Subsequently, the liquid-liquid two phase system undergoes a transitional emulsion phase inversion as the relative affinity of the surfactant for both dispersive/ continuous phases is changed with a gradual modification of the temperature (Anton *et al.*, 2008). Prolonged mixing (1 hour) resulted in this phase inversion and Isopar M formed emulsion droplets which were dispersed within the continuous aqueous phase formed by the monomer, cross-linker and the initiator solution. In order to avoid phase inversion and at the same time achieve small particles of narrow size distribution, the optimum mixing time was set at 48 minutes.

2.6.4 Selection of optimum agitation speed

The effect of the agitation speed on the final particle size distribution was investigated and the results are presented in Fig. 2.9. As expected, increased mixing speed had a positive effect on both the particle size and size distribution and at 3000 rpm 70.4% of

particles were in the range of 0.5-2 μm . However, further increases in agitation speed (*i.e.* 3200 and 3400 rpm) appeared to produce bigger particles (respectively, 67% and 61.5% of particles were in the range of 0.5-2 μm).

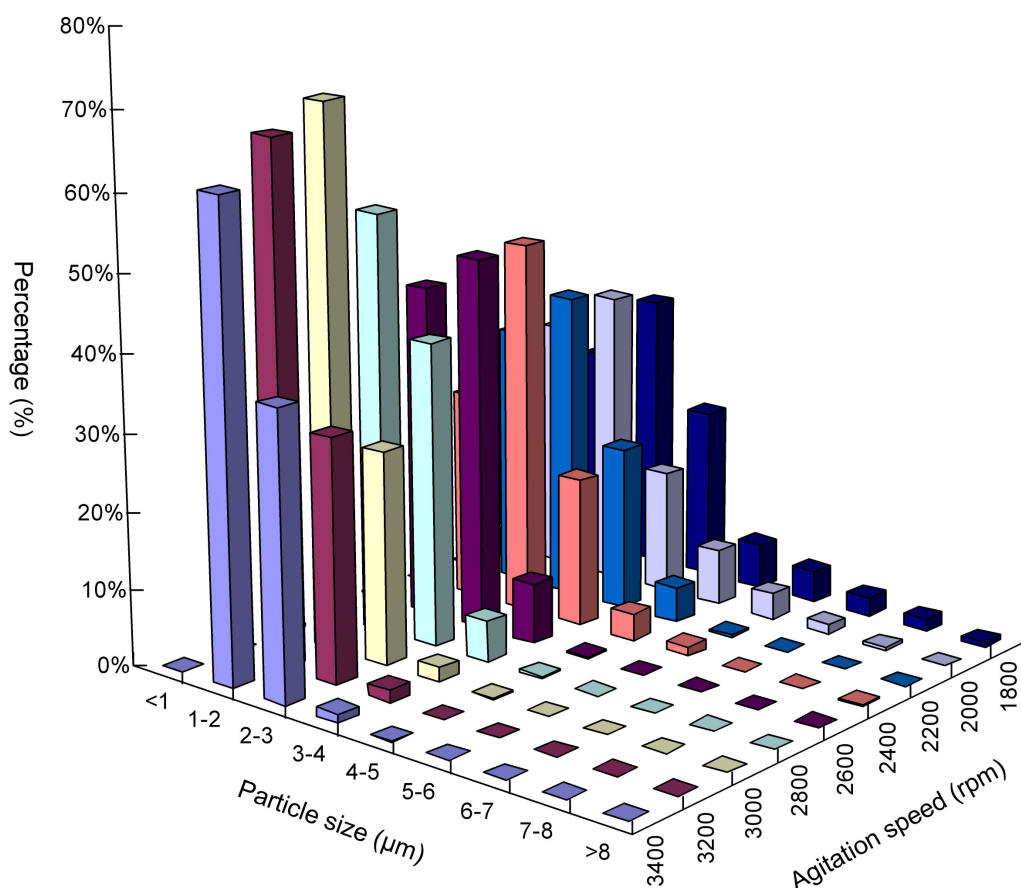


Figure 2.9 Effect of agitation speed on particle size and particle size distribution.

As discussed previously (Section 2.3.2) the droplets break up as a result of the milling force and the hydrodynamic shear exerted by the workhead of the Silverson high shear mixer. At the same time, the random collisions between the emulsion droplets on the outside of the workhead cause them to break up and coalesce. If there is

sufficient surfactant present in the liquid-liquid two phase system, it will be absorbed fast onto the newly created interfacial area of the broken emulsion droplets thereby stabilizing them and preventing their potential coalescence. However, once all the surfactant has been used, further breakage of emulsion droplets will create surfactant free surface areas that tend to agglomerate in order to reduce their interfacial energy and remain stable. At this point, equilibrium has been reached between droplet breakup and coalescence. Further rise in agitation speed and excess energy input will promote droplet aggregation rather than breakup, and the final particle size will increase. In view of the above results, 3000 rpm was selected as the optimum agitation speed for further studies.

2.7 Conclusion

The influence of several parameters, namely initiator concentration, ratio between the dispersion and continuous phases, and mixing time and speed, on the inverse liquid-liquid two phase polymerization for the production of beaded poly(acrylamide-co-ethylenebisacrylamide) supports has been investigated. The initiator concentration of 0.2% w/v was the lowest value to provide a good rate of polymerization and satisfactory polymer properties, and 1:4 and 48 minutes were respectively confirmed as optimum dispersion to continuous ratio and operation time. Finally, 70.4% of total polymeric particles' size distribution in a range of 0.5-2 μm (98% of particle size less than 3 μm) has been obtained under 3000 rpm of agitation speed.

3. Preparation of beaded magnetic poly(acrylamide-co-ethylenebisacrylamide) composite supports by inverse liquid-liquid two phase polymerization methods

Abstract

The 'one-pot' manufacture of beaded magnetic poly(acrylamide-co-ethylenebisacrylamide) supports via inverse liquid-liquid two phase emulsion polymerization performed under high shear stress is described. Naked fine particle magnetite powder, and two types of coated ferrofluid were initially screened for their ability to render poly(acrylamide-co-ethylenebisacrylamide) support beads magnetically susceptible. The efficiency of encapsulation of naked magnetite during emulsion polymerization was very poor (<10%), resulting in two distinct bead populations within the same preparation, i.e. large numbers of small (most between 0 and 10 μm) 'unoccupied' polymer beads and small numbers of much larger magnetic ones (most in the 10-30 μm range) with varying magnetic core contents. One of the coated ferrofluids (oleic acid coated) had lost its magnetic properties, most probably during storage via oxidation, and the resulting magnetic polymer composite supports could not be separated in a magnetic rack, while the other (poly(acrylic acid) coated) produced magnetic supports with non-uniformly distributed magnetic elements, i.e. preferentially concentrated at the support bead's perimeter. A new stably coated ferrofluid was subsequently prepared by co-precipitation of magnetite crystals in the

presence of poly(methacrylic acid), and following rigorous characterization it was employed as the magnetizable element in all subsequent preparations of magnetic polymer supports. Concerted attempts to simultaneously reduce the size of magnetic poly(acrylamide-co-ethylenebisacrylamide) supports, achieve more uniformly distributed entrapment of magnetic materials within them, and increase their loading with magnetic material, were undertaken. In a head-to-head comparison of two different initiator + continuous phase combinations, '1,1'-azobis(cyclohexanecarbonitrile + Arlcel[®] 83/cyclohexane' was found to be superior to the 'Ammonium persulphate/N,N,N',N'-tetramethylethylenediamine + Arlcel[®] 83/Isopar M' combination employed in Chapter 2, given that the only former ensured uniform distribution of poly(methacrylic acid) coated crystals throughout beaded poly(acrylamide-co-ethylenebisacrylamide) supports. The effects of varying agitation speed, ferrofluid and surfactant (Arlcel[®] 83) loadings during support preparation on the resulting properties were subsequently investigated, and optimal conditions for the 'one-pot' manufacture of small (Sauter mean diameter = 1.9 μm ; submicron under SEM) non-porous highly magnetic ($M_s = 42.2 \text{ Am}^2 \text{ kg}^{-1}$ equivalent to 55.1% w/w magnetite) beaded poly(acrylamide-co-ethylenebisacrylamide) supports, were established.

3.1 Introduction

During the last 10 years, the synthesis of magnetically responsive composite supports has become a rapidly expanding field of research. The most common design blueprint (see Chapter 1, Fig 1.6) of magnetically responsive support comprises tiny magnetically susceptible elements dispersed in a beaded polymeric matrix. The latter is often endowed with specific functional groups (or ligands), which may be introduced post-production (e.g. by conventional staged activation and coupling routes and/or via graft polymerization) or alternatively feature within the matrix starting material from the outset (Philippova *et al.*, 2011). By making an adsorbent material responsive to magnetic forces, it becomes possible to directly recover the material loaded up with adsorbed target species out of complex biological feedstocks such as whole blood, milk, fermentation broths and cell homogenates, simply by using an appropriate magnet. The efficiency of magnetic bio-separation processes relies on two factors: (i) efficient adsorption of the target species; and (ii) rapid separation of product-loaded adsorbents from the crude feedstock (Hubbuch *et al.*, 2001; Hubbuch and Thomas, 2002)). For the purposes of product recovery from complex biological feedstocks containing suspended solids and fouling materials the use of non-porous magnetic adsorbents offers numerous advantages over porous varieties. Of special importance is that the latter are acutely sensitive to fouling and are much more difficult to clean once fouled (pore plugging is especially problematic). Non-porous materials are by contrast far less prone to fouling and are much more effectively cleaned (Munro *et al.*,

1977; O'Brien *et al.*, 1996, 1997). However, in order to achieve comparable surface areas for target binding to porous adsorbents, a non-porous support must lie in the micron to sub-micron size range (O'Brien *et al.*, 1996). Since the late 1970's, encapsulation have been used to fabricate a great number of micron and sub-micron sized magnetic supports encased in various synthetic, natural and hybrid matrices. Emulsion based techniques permit the rapid production of primary support particles, and many appear amenable to low-cost, large-scale manufacturing (e.g. Chemagen's M-PVA). For example, magnetic particles encapsulated in synthetic polymers can be produced by rapidly mixing a solution of magnetic iron oxides, monomers and co-monomers (the 'dispersed phase' cocktail) in a 'continuous' hydrophobic phase. Agitation disperses the solution, forming beaded droplets, whose size is determined by the agitation conditions. Solidified adsorbents are subsequently formed by polymerization; the porosity of the resulting supports is influenced by the choice of monomer, co-monomer and polymerization conditions. Most commercial magnetic materials made in this way behave as non-porous supports.

For successful production of 'consistent' magnetic support preparations by encapsulation routes uniform distribution of the magnetic elements throughout each monomer droplet and finished magnetic bead, is desirable. Depending on the hydrophilicity/hydrophobicity of the monomer species, encapsulation can be conducted via W/O or O/W emulsion based procedures. While it has been possible to

introduce magnetic susceptibility into a polymeric support particle using naked magnetite particles or powders (for example see Ansell and Mosbach, 1988) increasingly it appears that ensuring high levels of incorporation of magnetic particle elements in the dispersed phase and within the finished magnetic support particle requires the use of coated ferrofluids. Entrapment of finely divided hydrophilic magnetite within hydrophobic polymer beads can be achieved as long as an appropriate stabilizing surfactant is employed to simultaneously (i) coat the iron oxide crystals, (ii) prevent their agglomeration and (iii) encourage dispersion of the magnetic elements within the non-polar dispersed phase droplets. Examples of surfactants that have been employed for stabilizing magnetite crystals, and which result in good dispersion within monomer droplets include, but are not limited to, the following:

- oleic acid – Csetneki *et al.* (2004) employed an oleic acid stabilized ferrofluid for making magnetic polystyrene particles;
- polyethylene glycol – Hu and coworkers (2009) introduced magnetic crystals into molecularly imprinted beads by means of a polyethylene glycol stabilized ferrofluid; and
- acrylic acid – Lin *et al.* (2005) prepared magnetic poly(NIPAAm-co-MAA) beads using a poly(acrylic acid) stabilized ferrofluid.

In this work, attempts to adapt the inverse emulsion procedures described in Chapter 2 to the 'one-pot' manufacture of viable magnetic supports were undertaken. Naked

magnetite powder and various coated ferrofluids were added into inverse emulsion polymerization reactions performed under high shear stress. The resulting supports were subjected to a series of physicochemical characterisation tests (particle sizing, light microscopy, image analysis, BET analysis, SEM, TEM, EDAX, thermogravimetry, XRD, VSM). The effects of a large number of operating parameters, i.e. type of initiator system and continuous phase solvent, agitation speed (shear stress) during emulsification, type and quantity of magnetic element in the dispersion phase, and concentration of surfactant in the continuous phase, were systematically investigated, and the conditions for consistent manufacture of effective support materials were optimized.

3.2 Materials

Table 3.1 List of chemicals involved in this chapter

Chemical Name	Abbr.	Supplier	Description
Acrylamide	AM	Sigma-Aldrich	Neutral monomer
N,N'-ethylenebisacrylamide	EBA	Sigma-Aldrich	Cross linker
Ammonium persulfate	APS	Sigma-Aldrich	Initiator
N,N,N',N'-tetramethylethylenediamine	TEMED	Sigma-Aldrich	Accelerator
1,1'-azobis(cyclohexanecarbonitrile)	ABCN	Sigma-Aldrich	Initiator
Cyclohexane	N.A.	Fisher Scientific	Continuous phase solvent
Isopar M	N.A.	Multisol	Continuous phase solvent
sorbitan sesquioleate (Arlacel® 83)	N.A.	Sigma-Aldrich	Surfactant
poly(methacrylic acid, sodium salt) solution	PMAA	Sigma-Aldrich	Ferrofluid stabilizer; Mw: 4000-6000, 40 wt. % in H ₂ O
Iron ^{II} chloride tetrahydrate	N.A.	Sigma-Aldrich	Production of magnetite
Iron ^{III} chloride hexahydrate	N.A.	Sigma-Aldrich	Production of magnetite
Ammonium hydroxide	N.A.	Sigma-Aldrich	Production of magnetite
Hydrochloric acid	N.A.	Sigma-Aldrich	pH adjuster
Iron ^{II} chloride tetrahydrate	N.A.	Sigma-Aldrich	Production of magnetite
Uncoated magnetite powder	N.A.	Sigma-Aldrich	Magnetic core material; size < 5 µm

Poly(acrylic acid) coated ferrofluid (magnetite: 70 mg mL⁻¹) and oleic acid coated ferrofluid (magnetite: 167 mg mL⁻¹) were received as gifts from Dr. Jens Bolle and Prof. Matthias Franzreb (KIT, Karlsruhe, Germany). The double distilled water used in this work was generated by a Hamilton water boiler (Hamilton Laboratory glass Ltd., Margate, UK) and nitrogen was supplied by the BOC Group (Dudley, UK).

3.3 Experimental Methods

3.3.1 Synthesis of poly(methacrylic acid) coated ferrofluid

FeCl₂·4H₂O (2.15 g) and 3.525 g of FeCl₃ (molar ratio: Fe³⁺:Fe²⁺ = 2:1) were dissolved into 40 mL of double distilled water. The aqueous iron chloride (II, III) solution was then incubated in a 60 °C water-bath for 30 minutes whilst continually purging with nitrogen. Subsequently 12.5 mL of 28% (w/v) solution of NH₄OH held at 60°C was pumped into the iron (II, III) chloride solution at a rate of 0.32 mL s⁻¹, and the two solutions were vigorously blended together with 4 bladed impeller rotating at 1500 rpm. After addition of NH₄OH, the black solution was kept in 60°C water-bath and stirred at 1500 rpm for an additional 30 minutes under a stream of bubbling nitrogen. The magnetite crystal suspension was subsequently transferred into four clean 50 mL Screw-capped Falcon tubes and cooled to room temperature. The stabilization of magnetite crystals was carried out according to the procedure described by Mendenhall *et al.* (1996). Briefly, this involved the following steps. Three millilitre

aliquots of poly(methacrylic acid) (hereafter abbreviated to PMAA) were added to the magnetite crystal suspension in each Falcon tube. The contents of each tube were then treated with a Philip Harris Scientific Status US70 Sonication Probe (Philip Harris Scientific, Bath, UK) operated at 85% of the maximum output for 4 minutes. After cooling to room temperature, the pH of each 'magnetite/PMAA' suspension was adjusted to 4 using 37% (w/v) hydrochloric acid, and the resulting PMAA coated ferrofluid was collected by magnetic separation on a Chemagic Stand 50k permanent magnetic rack (Chemagen AG, Baesweiler, Germany). The ferrofluid was then washed 5 times with double distilled water to remove Cl^- and excess PMAA; in between each wash the coated magnetic materials were recovered magnetically and mixing during washing was carried out with a VM20 vortex mixer (Chiltern Scientific Instruments, Wendover, UK). Finally, the pH of the PMAA coated ferrofluid was adjusted to 9.8 using 28% (w/v) NH_4OH before storing at 4°C prior to use. The appearance, size distribution and magnetic properties of the PMAA coated ferrofluid preparation so produced was analysed as described under 3.3.3 'Analytical techniques'.

3.3.2 Preparation of beaded magnetic poly(acrylamide-co-ethylenebisacrylamide) composite supports

In all 15 different types of magnetic poly(acrylamide-co-ethylenebisacrylamide) composite supports were prepared and characterized. All magnetic

poly(acrylamide-co-ethylenebisacrylamide) composite supports prepared using a poly(methacrylic acid) coated ferrofluid are identified by a specific batch number, i.e. batches #1 - #12. The remaining three support batches are identified by letters (i.e. A, B & C).

3.3.2.1 Preparation of magnetic poly(acrylamide-co-ethylenebisacrylamide) composite supports using an APS/TEMED initiator/ accelerator system, 'Arlacel® 83/ Isopar M' continuous phase and various types of magnetic elements

The optimal protocol for the preparation of beaded non-magnetic poly(acrylamide-co-ethylenebisacrylamide) supports (see Chapter 2) was employed as the starting point for manufacture of magnetic versions (see Table 3.2). Dispersion phases containing acrylamide (2 g), 0.34 g of N,N'-ethylenebisacrylamide and either 117 mg of magnetite powder or 500 mg quantities of oleic acid, poly(acrylic acid) or poly(methacrylic acid) coated ferrofluids were adjusted to final volumes of 9 mL with double distilled water and then purged with nitrogen for 30 minutes. Arlacel® 83 (400 mg) was mixed with 40 mL of Isopar M to create the 'continuous phase', which was also purged with nitrogen for 30 minutes. Next, 26 µL of TEMED was pipetted into 1 mL of a 20 mg mL⁻¹ ammonium persulfate solution before immediately mixing the combined accelerator and initiator cocktail into the dispersion phase and then immediately adding to the continuous phase and emulsifying together using a Silverson L5 M high shear mixer operated at 3000 rpm for 48 minutes. The final

emulsion was left to stand overnight at room temperature, before washing the finished magnetic composite supports once with ethanol and three times with double distilled water, before storing at 4°C until required.

Table 3.2 Summary of conditions employed for the preparation of magnetic poly(acrylamide-co-ethylenebisacrylamide) composite supports using different magnetic elements.

Batch ID		A	B	C	#1
Dispersion phase	AM (g)	2	2	2	2
	EBA (g)	0.34	0.34	0.34	0.34
	Magnetic element	Fe ₃ O ₄ powder (117 mg)	OA- ferrofluid (500 mg)	PAA -ferrofluid (500 mg)	PMAA-ferrofluid (500 mg)
	Final volume (mL)	10	10	10	10
Continuous phase	Arlacel [®] 83 (mg)	400	400	400	400
	Isopar M (mL)	40	40	40	40
Arlacel [®] 83 : magnetic material ratio (mg/mg)		3.42	0.80	0.80	0.80

Key: AM, Acrylamide; EBA, N,N'-ethylenebisacrylamide; OA-, oleic acid coated; PAA, poly(acrylic acid) coated; PMAA, poly(methacrylic acid) coated.

3.3.2.2 Preparation of magnetic poly(acrylamide-co-ethylenebisacrylamide) composite supports using a 1,1'-azobis(cyclohexanecarbonitrile) initiator system, 'Arlacel[®] 83/ cyclohexane' continuous phase and PMAA-coated ferrofluids

3.3.2.2.1 Preliminary protocol

The basic starting protocol described below employs the azo initiator compound, 1,1'-azobis(cyclohexanecarbonitrile) (hereafter abbreviated to ABCN), in place of the APS/TEMED system presented earlier (3.2.2.1). An additional change was made to

the solvent employed in the continuous phase, replacing Isopar M with one more compatible with the ABCN initiator, i.e. cyclohexane (Table 3.3). Ten millilitres of a nitrogen purged aqueous dispersion phase containing 2 g of acrylamide, 0.34 g of N,N'-ethylenebisacrylamide and 500 mg of PMAA coated ferrofluid was emulsified with the nitrogen purged continuous phase (400 mg of Arlacel[®] 83 in 40 mL of cyclohexane) as described previously (i.e. using a Silverson L5 M high shear mixer operated at 3000 rpm for 12 minutes). Subsequently, 150 mg of ABCN was added into the mixture, and the reaction was left to proceed at 67°C with a water bath under the continuous mixing at same speed for a further 36 minutes all the while purging continuously with nitrogen. The resulting magnetic supports were then collected on a magnetic rack as described previously, washed once with ethanol, followed by three times with double distilled water, and then stored at 4°C until required.

Table 3.3 Summary of conditions employed for the preparation of magnetic poly(acrylamide-co-ethylenebisacrylamide) composite supports using PMAA coated ferrofluid (batches #1 – 4).

Batch ID		#1	#2	#3	#4
Dispersion phase	AM (g)	2	2	2	2
	EBA (g)	0.34	0.34	0.34	0.34
	PMAA - ferrofluid (mg)	500	500	500	500
	Final volume (mL)	10	10	10	10
Continuous phase	Arlacel 83 (mg)	400	400	400	400
	Solvent	Isopar M	Cyclohexane	Cyclohexane	Cyclohexane
	Final volume (mL)	40	40	40	40
Arlacel 83:PMAA ferrofluid ratio (mg/mg)		0.80	0.80	0.80	0.80
Agitation speed (rpm)		3000	3000	4000	5000
Initiator system		APS/TEMED	ABCN	ABCN	ABCN
Phase initiator dissolved in:		Dispersion	Continuous	Continuous	Continuous

Key: AM, Acrylamide; EBA, N,N'-ethylenebisacrylamide; PMAA-, poly(methacrylic acid) coated.

3.3.2.2.2 Optimization experiments (support batches #4 – #12)

Starting from preparative conditions selected immediately above (3.2.2.3.1) a series of parameter variations were conducted. Briefly, the effects of agitation speed during emulsification (3000 – 5000 rpm) on particle properties were first investigated, whilst maintaining all other parameters fixed (see Table 3.2), and following this, combined variation of the dispersion phase PMAA coated ferrofluid loading (500 – 1500 mg) and continuous phase Arlacel 83 surfactant content (400 – 1200 mg) was evaluated at an agitation speed during emulsification of 5000 rpm (the paired combinations are summarized in Table 3.4).

Table 3.4 Summary of second phase optimization experiments, corresponding particle batch numbers and compositions of the dispersion and continuous phases. The agitation speed during emulsification was 5000 rpm.

Batch ID		#10	#4	#11	#5	#6	#7	#12	#8	#9
Dispersion phase	AM (g)	2	2	2	2	2	2	2	2	2
	EBA (g)	0.34	0.34	0.34	0.34	0.34	0.34	0.34	0.34	0.34
	PMAA - ferrofluid (mg)	500	500	500	1000	1000	1000	1000	1500	1500
	Final volume (mL)	10	10	10	10	10	10	10	10	10
Continuous phase	Arlacel 83 (mg)	200	400	800	400	600	800	1200	800	1200
	Cyclohexane (mL)	40	40	40	40	40	40	40	40	40
Arlacel 83:PMAA ferrofluid ratio (mg/mg)		0.40	0.80	1.6	0.40	0.60	0.80	1.20	0.53	0.80

Key: AM, Acrylamide; EBA, N,N'-ethylenebisacrylamide; PMAA-, poly(methacrylic acid) coated.

3.3.3 Analytical techniques

3.3.3.1 Particle sizing techniques

3.3.3.1.1 Dynamic light scattering (DLS)

The particle size of magnetic iron oxide crystals in ferrofluids was analyzed with a High Performance Particle Sizer MS2000 (Malvern Instruments Ltd., Malvern, UK). Samples were diluted 100 fold with double distilled water and 0.2 mL aliquots of these were transferred into disposable cuvettes (Fisher Scientific Ltd., Loughborough, UK) and placed in the sample chamber. Each sample was analysed three times and the average value was calculated.

3.3.3.1.2 Low angle light scattering

The particle size distributions of magnetic composite supports were measured with a

Mastersizer 2000 (Malvern Instruments Ltd, Malvern, UK) using low angle light scattering technique. The refractive indexes of water, poly(acrylamide-co-ethylenebisacrylamide) and magnetite used in computation of particle sizes of magnetic poly(acrylamide-co-ethylenebisacrylamide composite supports were set at 1.33, 1.49 (Polyanskiy, 2011) and 2.42 (Steitz *et al.*, 2007) respectively. A mixing speed of 2000 rpm was applied in the measuring cell loop to ensure complete dispersion of particles. The magnetic support suspensions were pipetted dropwise into the dispersion unit until the laser obscuration reached 11 % of its total value. Each sample was measured three times and an average value was calculated.

The low angle scattering technique is based on the phenomenon that when a laser beam passing through a particle suspension it will scatter light at an angle that is directly related to the particle size. The scattering angle increases logarithmically with decreasing particle size, thus larger particles result in narrow scattering angles with high intensity. The calculation of particle size distributions from light scattering data can be provided from Mie Theory (Kippax, 2005). For small particles, Mie Theory reduces to the Rayleigh Approximation as follows:

$$I = I_0 \left(\frac{1 + \cos^2 \theta}{2R^2} \right) \left(\frac{2\pi}{\lambda} \right)^4 \left(\frac{n^2 - 1}{n^2 + 2} \right)^2 \left(\frac{d}{2} \right)^6 \quad (3.1)$$

where, I is the intensity of the light scattered, I_0 is the original light intensity, θ is the

scattering angle, R is the distance from the particle, λ is the wavelength of the light, n is the refractive index of the particle, and d is the diameter of the particle. From the above equation, it is clear that refractive index gradients can logarithmically influence the particle size determined, and thus using an appropriate (i.e. correct) RI for the material being sized is essential. The RI of water (1.33) is employed in the calculation of particle size to determine background due to the suspending solvent. As water within the particle is the same as suspending solvent it does not result in scattering, thus the refractive index of different magnetic poly(acrylamide-co-ethylenebisacrylamide) supports is determined by the ratio of magnetite to poly(acrylamide-co-ethylenebisacrylamide). In other words, the RI to employ for a given magnetic poly(acrylamide-co-ethylenebisacrylamide) sample is given by:

$$RI_{\text{support}} = (RI_{\text{polymer}} \times \text{fractional polymer content}) + (RI_{\text{magnetite}} \times \text{fractional magnetite content}) \quad (3.2)$$

The magnetite content of PMAA coated ferrofluid and different magnetic poly(acrylamide-co-ethylenebisacrylamide) supports was determined by VSM (see 3.3.3.6).

3.3.3.1.3 Optical counting

The particle size distribution of the magnetic composite supports produced with naked

uncoated Fe₃O₄ powder was determined using an Olympus BX50 light microscope (Olympus UK Ltd., Essex, UK), which was connected to a COHU high performance CCD camera (COHU's OEM Products Group, San Diego, USA). The images were taken at 1000 times magnification. A graticule slide with 1 mm grid was imaged in the same manner, and the particle size was calculated using the Droplet Detector 1.5 software (Compucon S.A, Thessaloniki, Greece).

3.3.3.1.4 Calculation of Sauter mean diameters

In applications where active surface area is especially important such as catalysis, combustion and adsorption, mean particle sizes are commonly expressed as the Sauter mean diameter (SMD, $D[3,2]$ or d_{32}), which is defined as the mean diameter of a sphere that has the same volume/ surface area ratio as the particle of interest (Sauter, 1926,1928; Rawle, 2011). Accordingly, particle sizing data obtained above (3.3.3.1.2) were used to calculate Sauter Mean Diameters for the various magnetic poly(acrylamide-co-ethylenebisacrylamide) supports preparations produced in this work. Typically SMD is defined in terms of surface and volume diameters, d_s (eq 3.3) and d_v (eq 3.4) where A_p and V_p are respectively the surface area and volume of the particle.

$$d_s = \left(\frac{A_p}{\pi} \right)^{\frac{1}{2}} \quad (3.3)$$

$$d_v = \left(\frac{6V_p}{\pi} \right)^{\frac{1}{3}} \quad (3.4)$$

Usually d_s and d_v are measured directly without knowledge of A_p or V_p and the Sauter Diameter for a given particle preparation is given by equation 3.5:

$$SD = D[3,2] = d_{32} = \frac{d_v^3}{d_s^2} \quad (3.5)$$

3.3.3.2 Samples drying methods

3.3.3.2.1 Drying *in vacuo*

Samples of ferrofluid or magnetic poly(acrylamide-co-ethylenebisacrylamide) composite supports, contained in a porcelain crucibles, were placed into sample chamber of an Edwards vacuum dryer EF03 (Edwards Vacuum Ltd., West Sussex, UK). Samples were dried under 4.5 bar of pressure for 48 h.

3.3.3.2.2 Critical point drying

Magnetic poly(acrylamide-co-ethylenebisacrylamide) composite supports were critical point dried according to the technical brief supplied by Quorum Technologies Ltd. (2009). Briefly, supports were dehydrated by sequential resuspension and mixing (for 10 minutes each time) in an increasing ethanol concentrations (i.e. 50% v/v → 70% v/v → 80% v/v → 95% v/v) followed by 2 sequential washes with pure ethanol. Dehydrated samples were subsequently loaded into a porous specimen pot and then

placed into the pressure chamber. Pure ethanol was used as an intermediate fluid, and critical point drying was performed in a CO₂ critical point system (33°C; 110 bar) using a Critical Point Dryer E3000 (Quorum Technologies Ltd., Kent, UK).

3.3.3.3 Specific surface area measurement

Magnetic composite supports were critical point dried (see 3.3.3.2.2) prior to being analyzed for their specific surface area. Octane was used as surface adsorbing probe. The surface areas of the various magnetic composite supports were then measured by the Brunauer–Emmet–Teller (BET) method with Advantage 1 Dynamic Vapor Sorption Analyzer (Surface Measurement System Ltd., Alperton, UK).

3.3.3.4 X-ray diffraction (XRD)

The crystalline structure of nano-sized magnetite crystals in ferrofluids was analyzed with an X-ray Powder Diffractometer D5000 (Siemens-Nixdorf, Munich, Germany) employing monochromatic Cu-K α radiation ($\lambda = 1.54 \text{ \AA}$). Small amounts of ferrofluid sample previously dried *in vacuo* (see 3.3.3.2.1) were uniformly dusted on one half of a piece of Sellotape[®], and then folded once in the middle to seal the sample.¹ The Sellotape[®] was stuck onto the sample holder, which was then fixed in the XRD. The XRD profile of sample was recorded in the angular range between 10° and 70° with a step size of 0.02° and a step time of 153 s. Finally, the crystalline structure was

¹ To maximize the accuracy of the peak location, the layer of sample dust should be as thin as possible (Mahadevan *et al.*, 2007).

analyzed by comparing the XRD patterns obtained with the model patterns from the Joint Committee on Powder Diffraction Standard database.

3.3.3.5 Thermogravimetric analysis (TGA)

Thermogravimetric analysis was carried out with a Thermogravimetric Analyzer TG209F1 system (NETZSCH-Gerätebau GmbH, Wolverhampton, UK). PMAA ferrofluid dried *in vacuo* (see 3.3.3.2.1) was placed in a porcelain crucible and then placed into sample chamber. A stream of air was applied as the carrier gas at a flow rate of 50 mL per minute. The sample was heated from 25°C to 600°C at a heating rate of 10°C per minute, and the changes in mass of the sample recorded throughout the heating profile were analyzed from thermogravimetric curves.

3.3.3.6 Vibrating Sample Magnetometry (VSM)

The magnetic properties of PMAA coated ferrofluid and the magnetic poly(acrylamide-co-ethylenebisacrylamide) composite supports were measured with a Vibrating Sample Magnetometer 7300 (Lakeshore Ltd., Harpenden, UK). Samples dried *in vacuo* (3.3.3.2.1) were placed in a Perspex sample holder, which was attached to the end of a rod and aligned in the magnetic field along the x, y and z axis to ensure that the sample is insensitive to small rotations about the axes (Foner, 1956). A complete hysteresis loop was recorded at room temperature by sweeping the external magnetic field between ± 2.0 Tesla unless stated otherwise. In addition to

measuring the bulk magnetic properties M_s values determined by VSM were employed to calculate their individual magnetite contents, assuming an M_s of 76.6 $\text{Am}^2 \text{kg}^{-1}$ for pure magnetite in the ferrofluid (see later, 3.4.3). This permitted calculation of refractive index values necessary for accurate determination of particle size by low angle light scattering (3.3.3.1.2).

3.3.3.7 Scanning Electron Microscopy (SEM)

Samples were critical point dried (see 3.3.3.2.2) and then sputter coated under a platinum cathode for 60 s to increase conductivity. The sample was transferred into the sample chamber of a Philips XL-30 Environmental Scanning Electron Microscope (FEI Co., Hillsboro, OR, USA) and imaged at 5.0 kV (unless otherwise stated).

3.3.3.8 Transmission Electron Microscopy (TEM)

Sample cross-sections were prepared according to the procedure described by Thomas *et al.* (1988). Briefly, samples were dehydrated by sequential resuspension and mixing (for 10 minutes each time) in an increasing series of ethanol concentrations (i.e. 50% v/v \rightarrow 70% v/v \rightarrow 80% v/v \rightarrow 95% v/v) followed by 4 sequential washes with pure ethanol, before embedding in a 50% (v/v) LR White Hard Grade acrylic resin (Agar Scientific Ltd., Essex, UK) in ethanol for 12 h, and curing in 100% (v/v) LR White Hard Grade acrylic resin at 60°C for 48 h. Thin sections (150 nm) were then cut from the resin blocks using a Reichert-Jung Ultramicrotome knife

(Reichert Microscope Services, New York, USA), and then placed on a copper grid and fixed on the top of the sample holder. Finally, the sample was transferred into the sample chamber of a Jeol 1200 Transmission Electron Microscope (Jeol Ltd., Herts, UK) and imaged at 80 kV. Samples of poly(acrylic acid) and PMAA coated ferrofluid were also analysed by TEM in the Jeol 1200 TEM at 80 kV after drying at room temperature for 30 minutes.

3.3.3.9 Energy dispersive X-ray analysis

The elemental composition of selected areas on the thin sample cross-sections (see 3.3.3.8) were analyzed using an energy dispersive analysis of X-ray (EDAX) microanalysis system comprising an Oxford Inca X-sight Energy Dispersive Spectroscopy (Oxford Instruments, Abingdon, UK) linked to a Jeol JSM-7000F Field Emission Scanning Electron Microscope (Jeol Ltd., Herts, UK).

3.4 Results and discussion

This chapter details the preparation and detailed characterization of a stable poly(methacrylic acid) coated ferrofluid, and efforts to use this and other magnetic materials (naked magnetite powder, oleic acid and poly(acrylic acid) coated ferrofluids) to introduce magnetic susceptibility on beaded poly(acrylamide-co-ethylenebisacrylamide) supports in a 'one-pot' manufacturing process employing inverse liquid-liquid two phase polymerization methodology. In all

15 separate batches (13 different types) of magnetic poly(acrylamide-co-ethylenebisacrylamide) composite supports were prepared each differing in:

- precise method of manufacture (initiator system, continuous phase solvent, agitation rate during emulsification);
- type and amount of magnetic material used to magnetize the polymer support particles (naked magnetite and various coated ferrofluid); and
- surfactant concentration in the continuous phase.

Both the PMAA-coated ferrofluid and magnetite impregnated poly(acrylamide-co-ethylenebisacrylamide) supports were comprehensively characterized for particle size, morphology under light microscopy, scanning and transmission electron microscopy, EDAX, specific surface area and magnetic properties. The PMAA-coated ferrofluid was additionally subjected to thermogravimetric analysis and X-ray diffraction.

3.4.1 Preparation of magnetic poly(acrylamide-co-ethylenebisacrylamide) supports using an APS/TEMED initiator/accelerator system, 'Arlacel® 83/ Isopar M' continuous phase and naked magnetite powder

The first attempt to introduce magnetic susceptibility on beaded poly(acrylamide-co-ethylenebisacrylamide) supports via entrapment during inverse suspension polymerization employed a naked fine particle magnetite powder. Figure

3.1 shows light micrographs of the resulting supports taken before (Fig. 3.1A) and after (Fig. 3.1B) magnetic enrichment on a magnetic rack.

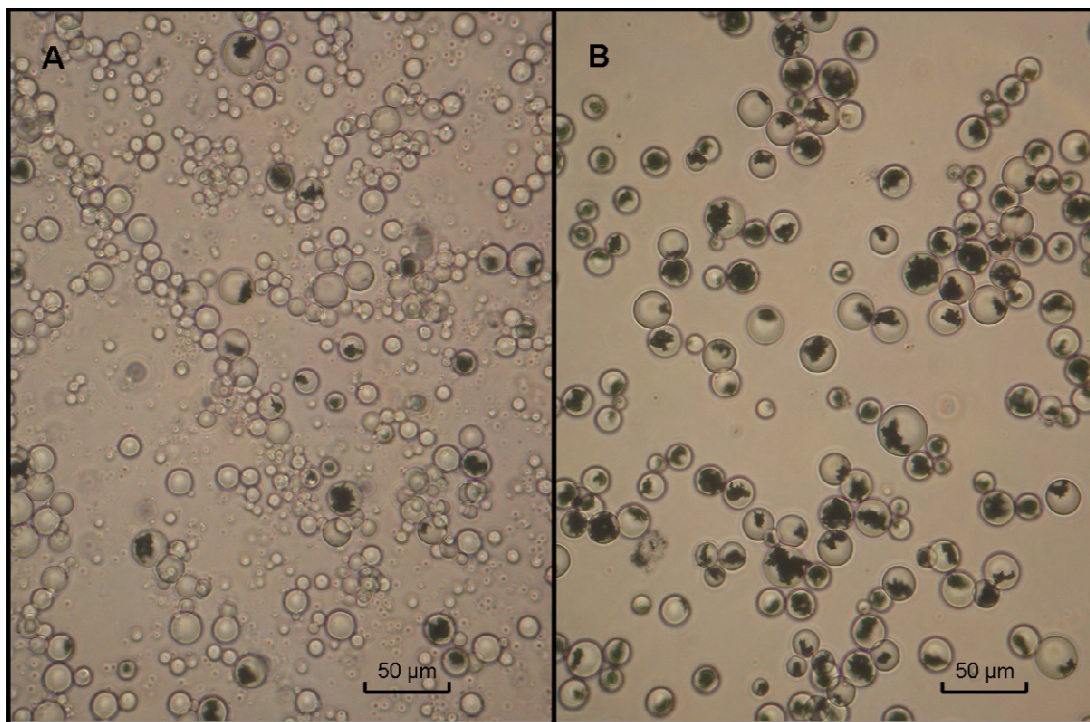


Figure 3.1 Light micrographs of magnetic poly(acrylamide-co-ethylenebisacrylamide) supports (Batch A, Table 3.1) synthesized using naked Fe_3O_4 powder. Before (A) and after (B) magnetic enrichment.

A number of striking features are evident. First, it is clear that only a small percentage of the particles visible in Fig. 3.1A actually contain magnetic particles, and these tend to be of significantly larger size compared to the transparent non-magnetic particles. Indeed, scrutiny of Fig. 3.2 shows that following magnetic enrichment the numbers of particles smaller than $10\text{ }\mu\text{m}$ dropped dramatically from $>63\%$ to only 9.3% , whereas the numbers of particles in the ' $10\text{-}20\text{ }\mu\text{m}$ ', ' $20\text{-}30\text{ }\mu\text{m}$ ' and ' $>30\text{ }\mu\text{m}$ ' ranges increased significantly, i.e. from ' $36\text{ to }80\%$ ', ' $0.5\text{ to }10.3\%$ ', and ' $0\text{ to }0.4\%$ ' respectively.

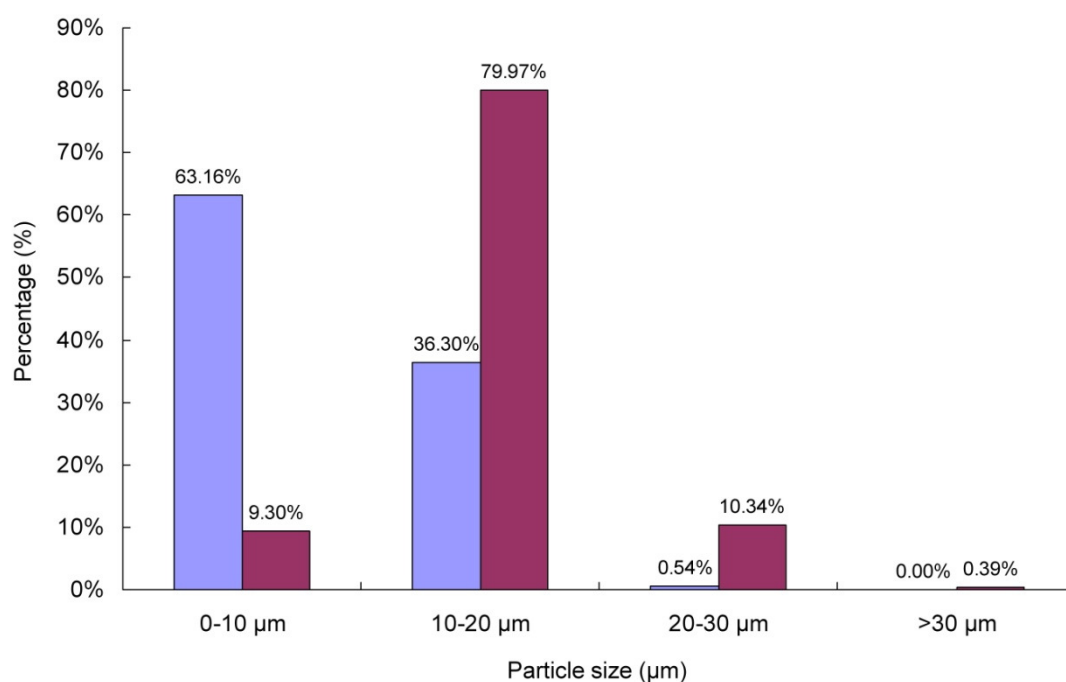


Figure 3.2 Particle size distributions of magnetic poly(acrylamide-co-ethylenebisacrylamide) supports (Batch A, Table 3.1) synthesized using naked Fe_3O_4 powder. Before (blue bars) and after (purple bars) magnetic enrichment.

It should be noted that under the same manufacturing conditions (see Section 2.4), but in the absence of added magnetic particles, very much smaller poly(acrylamide-co-ethylenebisacrylamide) bead sizes were produced, i.e. 98% were less than 3 μm . Satisfactory explanations for the gross difference in particle size of the magnetic and non-magnetic poly(acrylamide-co-ethylenebisacrylamide) particles are difficult to offer at the present time; clearly this requires further experimentation. This said, one possibility is offered below. While Fe^{2+} promotes polymerization Fe^{3+} inhibits it by terminating the polymer molecules. It is highly likely that traces of Fe^{2+} and Fe^{3+} ions leach away from the highly energetic surface of the naked magnetite powder.

Should leachable Fe^{2+} dominate over Fe^{3+} , then the polymerization rate in the vicinity of magnetite, i.e. within magnetite encapsulated monomer droplets should be higher than that in unoccupied monomer droplets, and consequently the latter should be more liquid/molten and more susceptible to further breakage during agitation. Second, an obvious point to highlight is that the distribution of magnetic elements clearly isn't uniform. Particles that do contain magnetic material possess single aggregates or clusters of fine particles of various size within their interiors (especially evident following magnetic enrichment, see Fig. 3.1B). The important consequences of this non-uniform distribution and loading of particles with magnetic material is that the individual particles in a given preparation possess very different magnetic susceptibilities which translate to marked differences in separation velocity towards a magnetic collector; larger particles with higher loading will be separated rapidly, whilst smaller more lightly loaded ones will require an extended separation time. Finally, serious disadvantages are that the manufacturing process produces large magnetic poly(acrylamide-co-ethylenebisacrylamide) supports, and is low yielding with <10% (v/v) of the particles produced being magnetically susceptible; thus post production an additional magnetic enrichment step is mandatory.

In subsequent experiments, concerted attempts to simultaneously: (i) improve the efficiency of entrapment; (ii) reduce particle size; and (iii) achieve more uniformly distributed entrapment of magnetic materials within

poly(acrylamide-co-ethylenebisacrylamide) supports, were undertaken. This involved replacing uncoated magnetite powder with various coated superparamagnetic ferrofluids, making changes to initiator and continuous phase solvent, and studying the effects of agitation rate during emulsification, ferrofluid and surfactant loadings.

3.4.2 Preparation of magnetic poly(acrylamide-co-ethylenebisacrylamide) supports using an APS/TEMED initiator/accelerator system, 'Arlacel® 83/ Isopar M' continuous phase and oleic acid and poly(acrylic acid) coated ferrofluids

Two ferrofluids received as gifts from Dr Jens Bolle (KIT, Karlsruhe) were screened for their ability to confer magnetic susceptibility on poly(acrylamide-co-ethylenebisacrylamide) supports. The first ferrofluid tested was coated with oleic acid. Oleic acid is an amphiphilic fatty acid, comprising a hydrophilic carboxyl head group and a hydrophobic C18 alkyl chain. The carboxylic head groups of oleic acid coordinate exposed hydroxyl groups on the surface of the magnetite; and the hydrocarbon C18 chains lend a hydrophobic sheath to the individual crystals of the ferrofluid (Khalafalla, 1980), conferring hydrophobicity on the magnetic material.

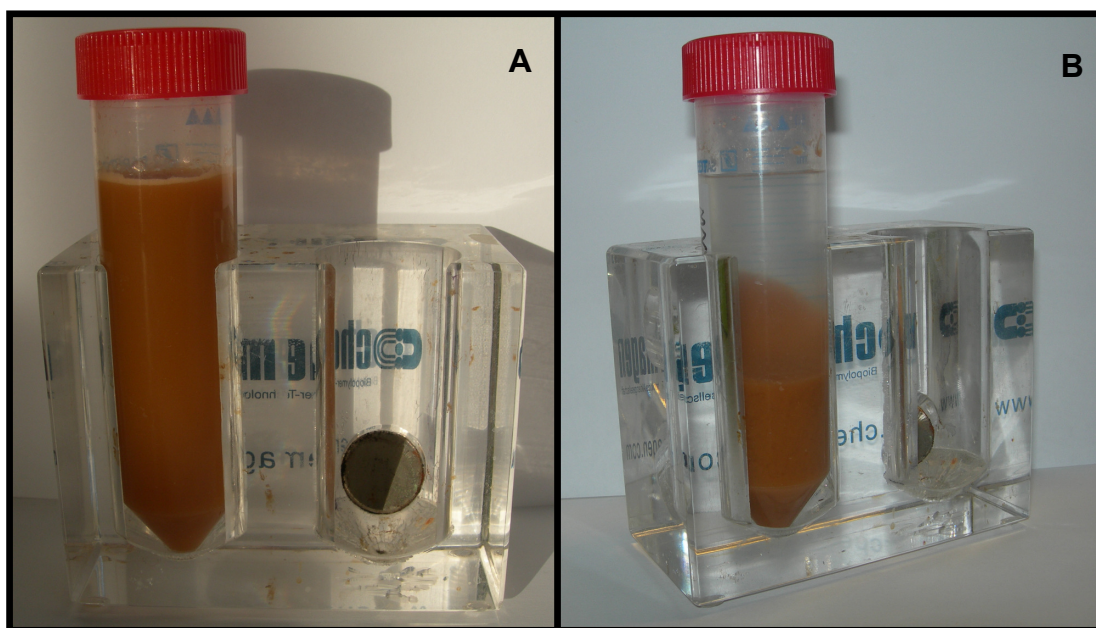


Figure 3.3 Magnetic poly(acrylamide-co-ethylenebisacrylamide) supports synthesized using the oleic acid coated ferrofluid (Batch B, Table 3.1). Photographs taken immediately before (A) and after (B) 5 h of exposure to a 0.15 Tesla magnetic field.

Magnetic poly(acrylamide-co-ethylenebisacrylamide) supports prepared using this oleic acid coated ferrofluid exhibited very low magnetic susceptibility and could not be separated efficiently using a 0.15 Tesla strength magnetic rack even after 5 h of exposure (Fig. 3.3). The most probable explanation is that the magnetic iron oxide crystals of the ferrofluid received had been transformed via oxidation to paramagnetic iron oxides (see Fig. 1.5). Strong evidence for this is that oleic acid coated ferrofluid encapsulated poly(acrylamide-co-ethylenebisacrylamide) supports appeared reddish-brown (Fig. 3.3), rather than the expected brownish-black. Given the nitrogen-rich environment during emulsion polymerization it is unlikely that oxidation of the magnetic iron oxides had occurred during support manufacture. The oleic acid

coated ferrofluid was also red-brown, implying that oxidation had occurred either during manufacture of the ferrofluid itself and/or during storage. However, owing to limited amounts of this ferrofluid it was not possible to confirm this by XRD and VSM.

The next coated ferrofluid evaluated was one synthesized by co-precipitation in the presence of poly(acrylic acid) (Bolle, 2009). Poly(acrylic acid) promotes the nucleation and inhibits the growth of the magnetic iron oxide, so that the average diameter of each individual magnetite crystal is 10 nm or less. Additionally, poly(acrylic acid) chains provide both electrostatic and steric repulsion against particle aggregation (Lin *et al.*, 2005).²

²Some of the hydroxyl groups of the poly(acrylic acid) coordinate with the magnetite surface, while others interact with water rendering the stabilized magnetite crystals hydrophilic, and the carboxyl groups prevent close approach of the coated crystals to one another.

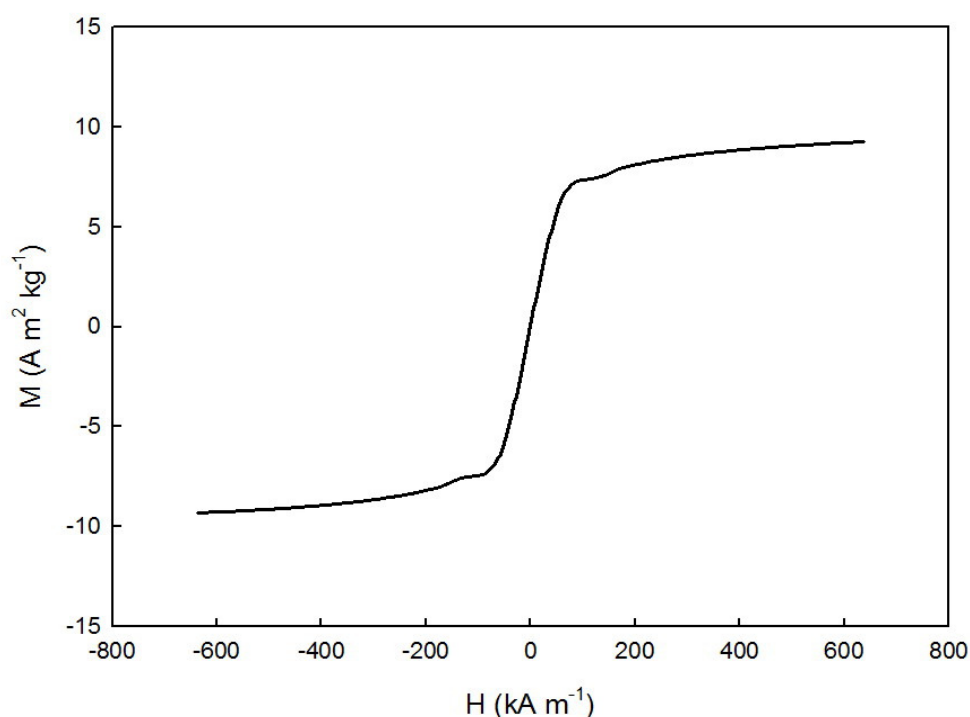


Figure 3.4 VSM curve for magnetic poly(acrylamide-co-ethylenebisacrylamide) supports prepared using the poly(acrylic acid) coated ferrofluid (Batch C, Table 3.1). The full magnetic hysteresis loop was recorded at room temperature, sweeping the external field between ± 0.8 Tesla.

Figure 3.4 shows a room temperature magnetic hysteresis loop for the magnetic poly(acrylamide-co-ethylenebisacrylamide) support preparation synthesized using the poly(acrylic acid) coated ferrofluid. Although the completely closed VSM loop is characteristic of an ideal superparamagnetic material (i.e. no remanence, no magnetic coercivity), the recorded saturation magnetization (M_s) of $9.3 \text{ Am}^2 \text{ kg}^{-1}$ was low. By assuming that the magnetic material in the ferrofluid is pure magnetite with an M_s of $76.6 \text{ Am}^2 \text{ kg}^{-1}$ (see later, 3.4.3) it is possible to calculate both the average magnetite content and corresponding refractive index values as 12.1% (w/w) and 1.603. The

latter is necessary to compute the particle size distribution of the various magnetic poly(acrylamide-co-ethylenebisacrylamide) support preparations (see 3.3.3.1.2).

Table 3.5 Summary of magnetic properties, refraction index and particle sizing data for Batch ‘C’ magnetic poly(acrylamide-co-ethylenebisacrylamide) supports synthesized using a poly(acrylic acid) coated ferrofluid.

Batch ID	M_s (Am ² kg ⁻¹)	Fe ₃ O ₄ content (% w/w)	RI	Particle size distribution (μm)			Sauter Diameter (μm)
				D(10)	D(50)	D(90)	
C (Table 3.1)	9.3	12.1	1.603	5.1	7.5	9.9	7.0

Batch ‘C’ magnetic poly(acrylamide-co-ethylenebisacrylamide) supports were examined under SEM at 12,500 × (Fig. 3.5A) and >100,000 × (Fig. 3.5B) magnifications. Most individual beaded support particles were considerably smaller than the Sauter mean diameter of 7 μm (Table 3.5) determined by low angle light scattering, lying between 1 and 3 μm. This size discrepancy likely originates from some particle shrinkage during the sample preparation for SEM (notably during the drying process), coupled with the fact that the majority of individual particles in solution likely form small clusters³ which are detected by the Mastersizer. The morphological appearance of support particles under SEM is distinctive, i.e. smooth spherical beads studded in a non-uniform fashion with much smaller spherical particles roughly 50 nm across (Fig. 3.5B).

³Indeed, small particle clusters in the Sauter diameter range are evident under SEM, although this clustering could be introduced during sample preparation.

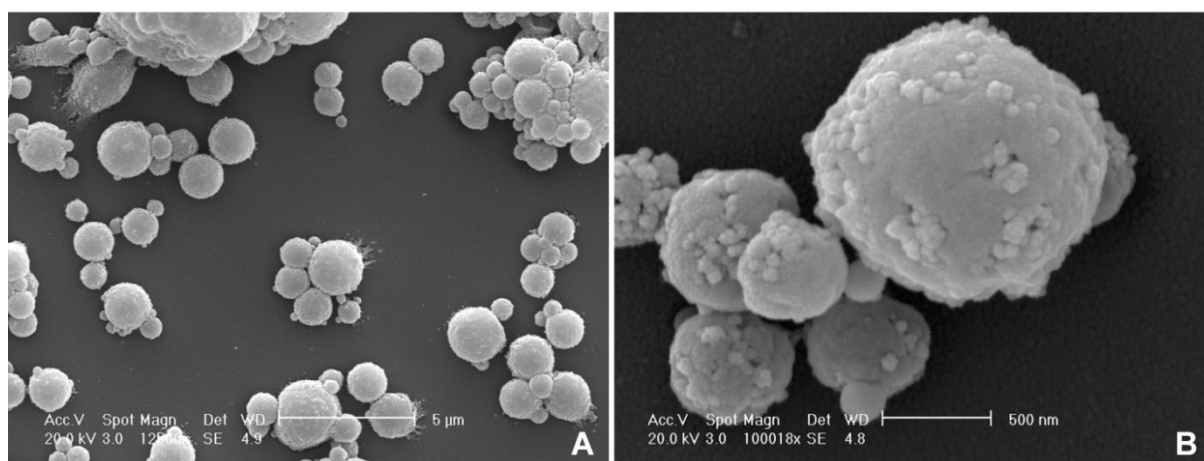


Figure 3.5 Scanning electron micrographs of magnetic poly(acrylamide-*co*-ethylenebisacrylamide) supports prepared using poly(acrylic acid) coated ferrofluid (Batch C, Table 3.1) at (A) 12,500 \times and (B) 100,018 \times magnification.

To confirm the identity of these smaller particles and also ascertain whether they were distributed within the interior of the beads or solely confined to the exterior surfaces, samples of batch C supports and controls⁴ were desiccated, embedded in LR white resin, sectioned with an ultramicrotome knife and examined by TEM (3.3.3.8) coupled with EDAX (3.3.3.9).

⁴i.e. poly(acrylamide-*co*-ethylenebisacrylamide) supports prepared under identical conditions in the absence of magnetic material.

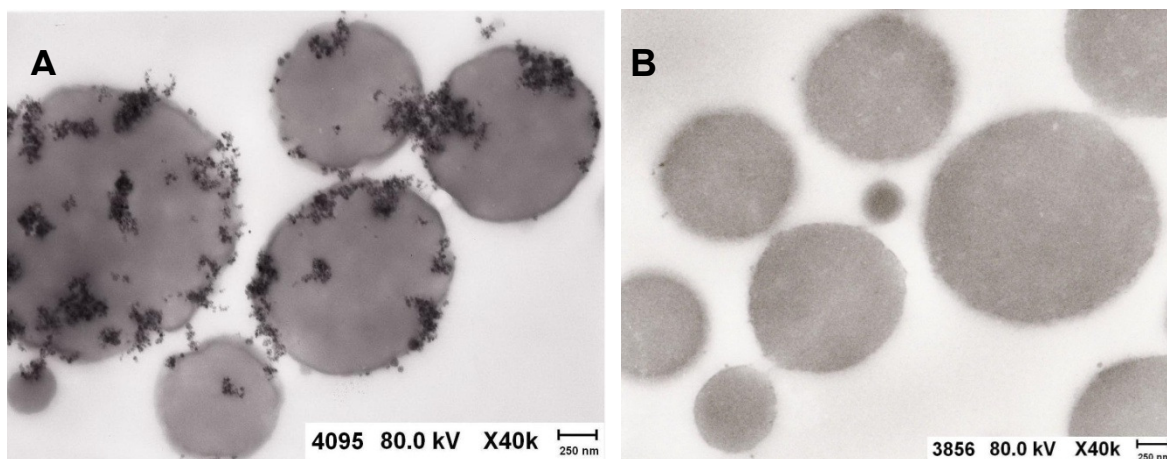


Figure 3.6 Transmission electron micrographs ($40,000\times$ magnification) of (A) magnetic poly(acrylamide-co-ethylenebisacrylamide) supports prepared using poly(acrylic acid) coated ferrofluid (Batch C, Table 3.1) and (B) non-magnetic poly(acrylamide-co-ethylenebisacrylamide) control beads (from particle preparation: 1:4 of dispersion to continuous phase ration, following 3000 rpm and 48 min mixing in Chapter 2)

Figure 3.6 shows the transmission electron micrographs obtained. Large numbers of electron dense grains are clearly visible in the magnetic batch C sample (Fig. 3.6A) and are entirely absent from the non-magnetic control poly(acrylamide-co-ethylenebisacrylamide) beads (Fig. 3.6B). The dark grains are not homogeneously distributed, appear as clusters rather than as single grains, and furthermore, greater numbers are located at or near the beads' perimeters. EDAX confirmed that the identity of electron dense solids as iron oxide (i.e. the ferrofluid) and the lighter areas as the polymer matrix. Figure 3.7A shows a spectrum corresponding to the electron dense grains. In addition to $K\alpha$ principal line peaks for carbon (0.3 keV) and oxygen (0.5 keV), peaks occurring at the $L\alpha$ (0.7 keV), $K\alpha$ (6.4

keV) and K β (7.1 keV) principal lines, corresponding to different oxidation states of iron, are clearly visible. The carbon and partial oxygen peaks most likely represent the poly(acrylamide-co-ethylenebisacrylamide) matrix, and the iron and other partial oxygen peaks correspond to magnetite, FeO•Fe₂O₃.

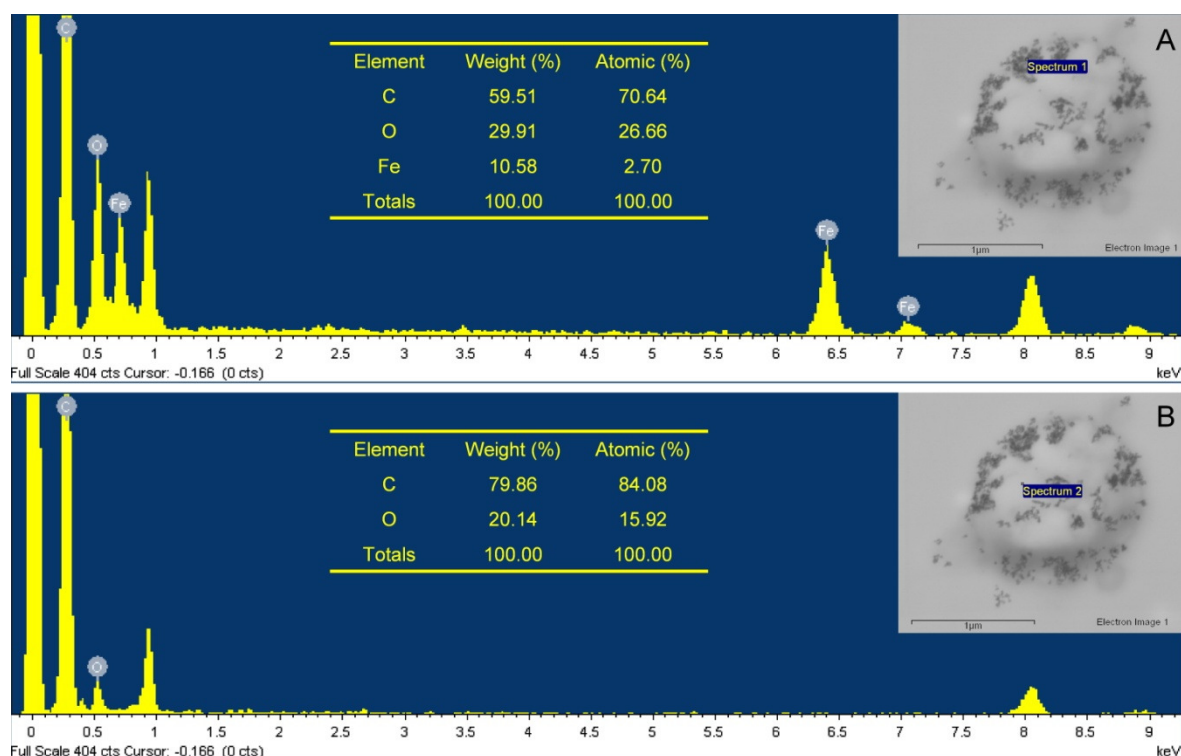


Figure 3.7 Representative EDAX spectra and elemental compositions corresponding to defined regions (A: dark electron dense; B: pale regions devoid of electron dense material) within a magnetic poly(acrylamide-co-ethylenebisacrylamide) support particle prepared using a poly(acrylic acid) coated ferrofluid (Batch C, Table 3.1).

In stark contrast, the spectrum of light areas devoid of electron dense material (Fig. 3.7B), only exhibits peaks corresponding to carbon (0.3 keV) and oxygen (0.5 keV). It should also be noted that the weight and atomic percentage values for oxygen are

substantially lower for the light *cf.* the dark electron dense regions (i.e. 20.14% and 15.92% *cf.* 29.91% and 26.66%). This is not surprising as in contrast to the oxygen peak in Fig. 3.7A, that in Fig. 3.7B is solely due the poly(acrylamide-co-ethylenebisacrylamide) matrix. Given the polar and negatively charged poly(acrylic acid) coating stabilizing the individual magnetic grains of the ferrofluid suspension, the non-uniform distribution of magnetite throughout the beaded poly(acrylamide-co-ethylenebisacrylamide supports is puzzling. The poly(acrylic acid) layer surrounding the magnetite crystals should encourage mutual compatibility with the dispersion phase (i.e. hydrophilic polymer droplets), and also prevent their aggregation with one another. The aggregation of magnetite noted in Fig 3.6A is also clear in transmission electron micrograph images of the poly(acrylic acid) coated ferrofluid (Fig. 3.8), may indicate that the poly(acrylic acid) coating of the ferrofluid isn't stably applied.

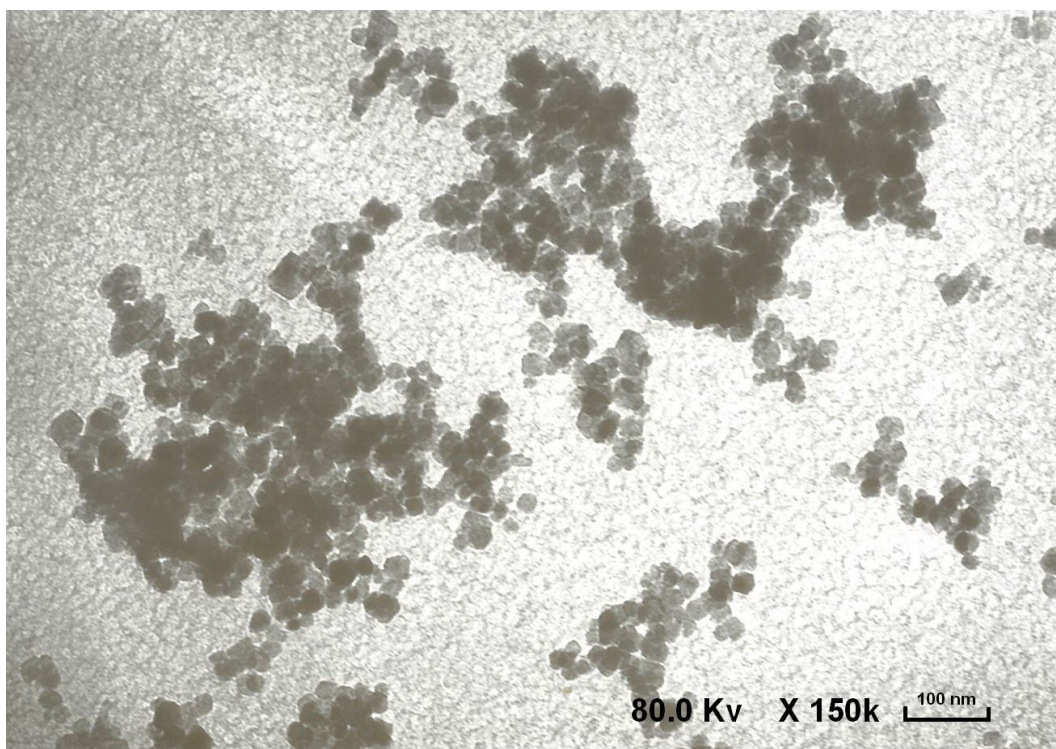


Figure 3.8 TEM image of the poly(acrylic acid) coated ferrofluid employed in the manufacture of Batch 'C' magnetic poly(acrylamide-co-ethylenebisacrylamide) supports (Table 3.2). The size of individual coated crystals within the ferrofluid is 10-20 nm.

It is possible, for example, that during long term storage of the ferrofluid at least some of the stabilizing poly(acrylic acid) had peeled away from the surface of magnetite crystals leaving them free to aggregate with one another, thereby compromising their affinity to enter the polymer droplets as homogeneously dispersed bodies. Support for this hypothesis comes from Wooding *et al.* (1992), who pointed out that the repeating unit of poly(acrylic acid) of only 2 carbons, may not be sufficient to provide satisfactory protection against penetration of water to the polymer/magnetite interface.

3.4.3 Preparation and characterization of poly(methacrylic acid) coated ferrofluid

Owing to instability/aggregation issues experienced with the oleic acid and poly(acrylic acid) coated ferrofluids initially employed to render poly(acrylamide-co-ethylenebisacrylamide) magnetic, efforts to produce a more stably coated ferrofluid were undertaken. Poly(methacrylic acid) coated ferrofluid was produced within a method involving co-precipitation, ultrasonication and stabilization at pH 9.8 prior to be thoroughly characterized by X-ray diffraction, thermogravimetric analysis, VSM, particle sizing and transmission electron microscopy. The XRD pattern observed in Fig. 3.9 shows X-ray intensity peaks at 2-theta angles of 30.081, 35.431, 43.06, 56.945 and 62.531. This series of peaks is characteristic of the cubic inverse spinel structure of magnetite.

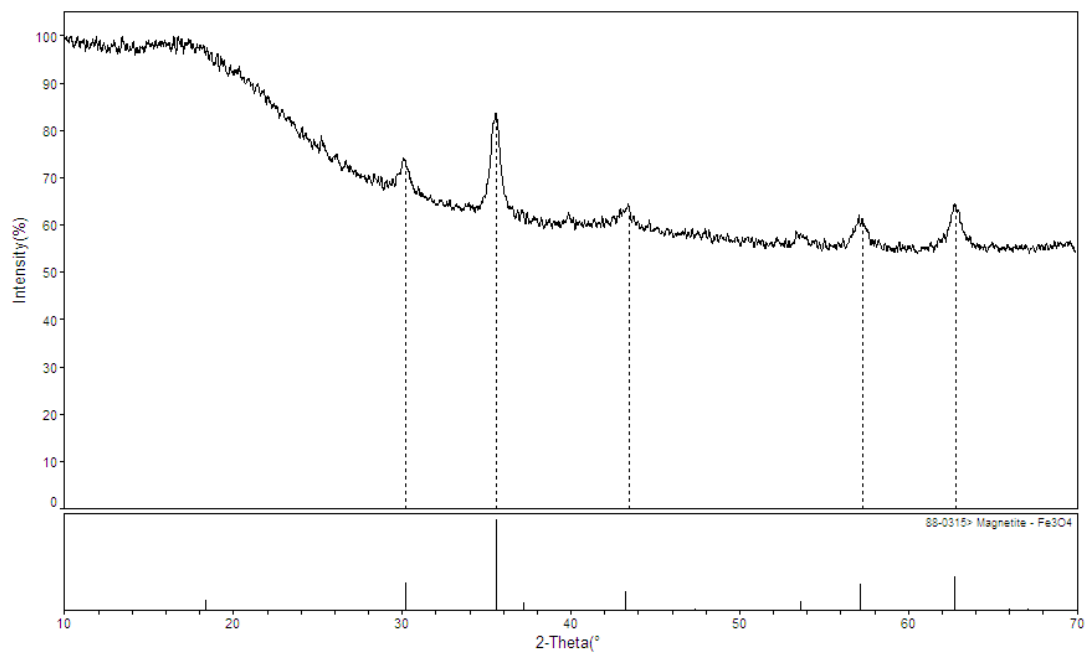


Figure 3.9 XRD pattern of magnetic nano-sized crystals in the PMAA coated ferrofluid.

The magnetite content of the dried PMAA coated ferrofluid (25.403 mg) was evaluated with a thermogravimetric analyzer. The resulting weight loss curve in Fig. 3.10 shows two degradation stages. In the first, which is due to dehydration and decarboxylation of the carboxylic groups of the PMAA, 7.28% of the original mass is lost.

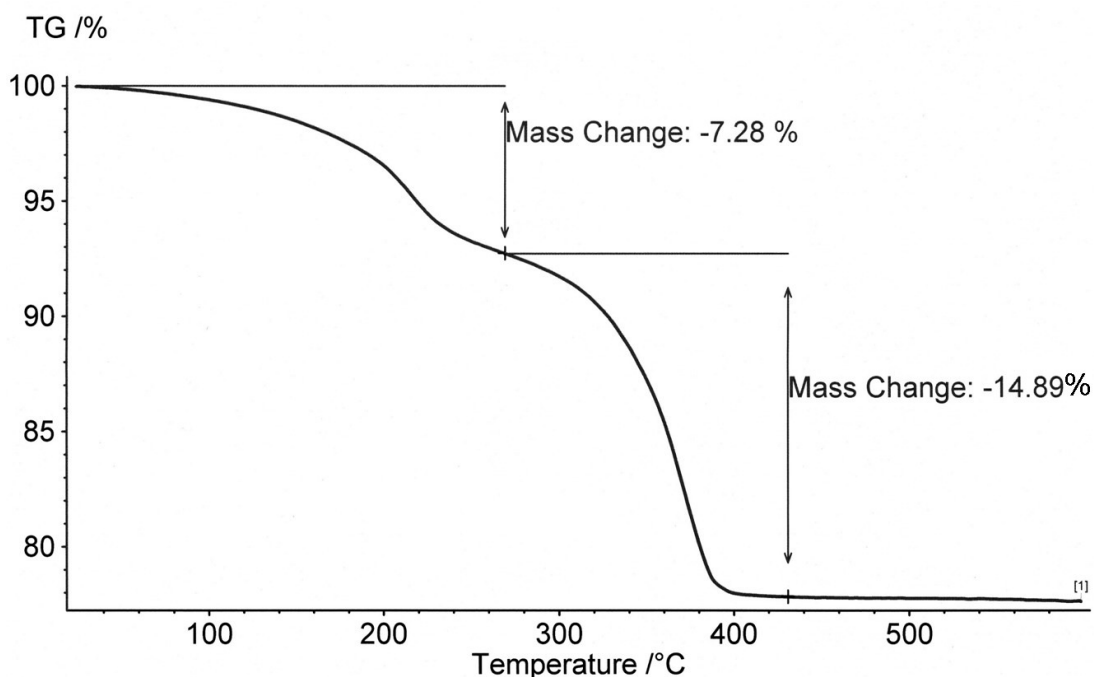


Figure 3.10 Thermogravimetric weight loss curve for the PMAA coated ferrofluid prepared in this work.

In the second phase (14.89% mass loss), the polymer is burned out and Fe_3O_4 is oxidized to Fe_2O_3 according to the reaction: $2\text{Fe}_3\text{O}_4 + \frac{1}{2}\text{O}_2 \rightarrow 3\text{Fe}_2\text{O}_3$

The magnetite content of the PMAA coated ferrofluid can be calculated as follows:

- The final amount of Fe_2O_3 = $25.403 \text{ mg} \times (100 - 22.17)\% = \underline{19.771 \text{ mg}}$; or
 $0.019771 \text{ g} \div 159.687 \text{ g mol}^{-1} = \underline{123.81 \text{ } \mu\text{mol}}$.
- In the reaction 2 moles of Fe_3O_4 are oxidized to 3 moles of Fe_2O_3 .
- Thus the amount of Fe_3O_4 in the original sample = $\frac{2}{3} \times 123.81 = \underline{82.54 \text{ } \mu\text{mol}}$; or
 $82.54 \text{ } \mu\text{mol} \times 231.531 \text{ g mol}^{-1} = 0.01911 \text{ g} = \underline{19.110 \text{ mg}}$.
- The magnetite content of the PMAA coated ferrofluid is thus simply = $(19.110 \div 25.403) \times 100\% = \underline{75.23\%}$.

The bulk magnetic properties of the PMAA coated ferrofluid were examined at room temperature in a vibrating sample magnetometer across ± 2.0 Tesla of externally applied magnetic field. The resulting VSM loop (Fig. 3.11) is completely closed, crosses the origin point and illustrates classical superparamagnetism, i.e. a complete absence of magnetic memory. The saturation magnetization (M_s) of the dried PMAA coated ferrofluid was determined as $57.6 \text{ Am}^2 \text{ kg}^{-1}$. Assuming the magnetite content of 75.2% determined by TGA, the M_s of the magnetite crystal component of the PMAA coated ferrofluid can be calculated as $76.6 \text{ Am}^2 \text{ kg}^{-1}$. This value for magnetite in the ferrofluid is lower than widely cited M_s for bulk magnetite of $92 \text{ Am}^2 \text{ kg}^{-1}$ (Harris *et al.*, 2003). Lower M_s values for pure magnetite in coated ferrofluids *cf.* bulk magnetite have been reported by others (Moralesy *et al.*, 1997; Varanda *et al.*, 2002). According to these authors the high surface curvature of tiny nano-sized magnetite crystals in coated ferrofluids disorders the crystal orientation at their surfaces, causing magnetic moment canting which results in significant reduced saturation magnetization in nanoparticles.

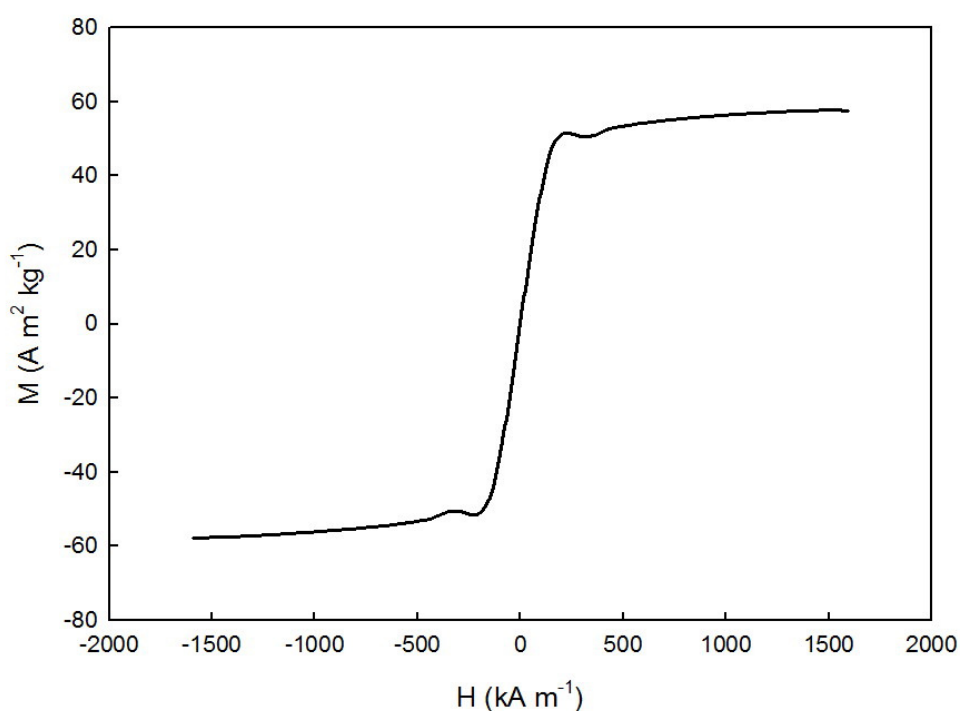


Figure 3.11 VSM curve for the PMAA coated ferrofluid prepared in this work. The full magnetic hysteresis loop of the dried ferrofluid was recorded at room temperature, sweeping the external field between ± 2.0 Tesla.

The particle size distribution of the PMAA coated ferrofluid was measured by dynamic light scattering (DLS) technique, the results are presented in Fig. 3.12. More than 95% of particles in the preparation are smaller than 30 nm, but none are less than 10 nm diameter.

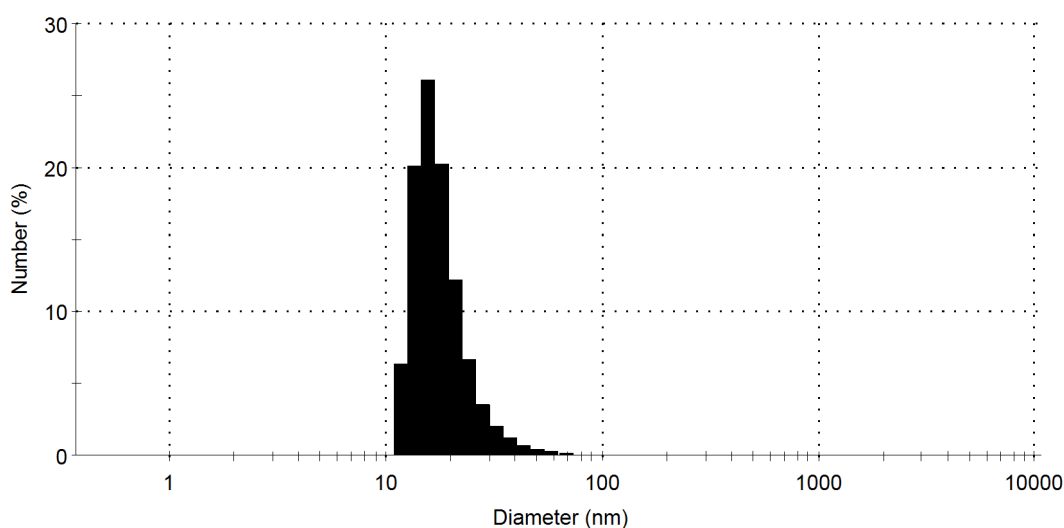


Figure 3.12 DLS particle size distribution of the PMAA coated ferrofluid prepared in this work.

Examination of the PMAA coated ferrofluid by transmission electron microscopy (Fig.3.13) revealed irregularly shaped particles of 10-30 nm in good agreement with the DLS number percent size distribution (Fig. 3.12). Further, it is noticeable that most of the particles in the ferrofluid are singly dispersed and non-coalescent; the small loose cluster-like area in the centre of the image is likely the result of sample preparation. Taken collectively, the XRD, TGA, VSM, DLS and TEM data presented here (Figs. 3.8 – 3.13) indicate that the PMAA coated ferrofluid prepared is stably coated and potentially represents a superior magnetic material *cf.* naked magnetite powder, oleic acid and poly(acrylic acid) coated ferrofluids, for rendering poly(acrylamide-*co*-ethylenebisacrylamide) beads magnetically susceptible.

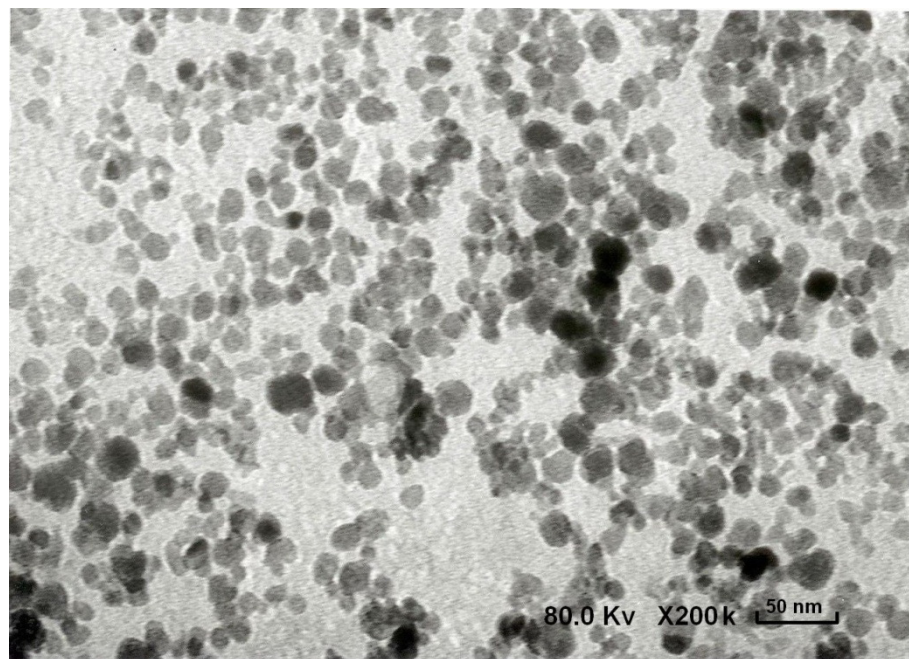


Figure 3.13 TEM image of the PMAA coated ferrofluid prepared in this work.

3.4.4 Preparation of magnetic poly(acrylamide-co-ethylenebisacrylamide) composite supports using PMAA-coated ferrofluids

3.4.4.1 Comparison of ‘initiator + continuous phase’ combinations: ‘APS/TEMED + Arlcel® 83/ Isopar M’ vs. ‘ABCN + Arlcel® 83/ cyclohexane’

The results of a head to head comparison of two different combinations of initiator and continuous phase on the preparation and subsequent characterization of magnetic poly(acrylamide-co-ethylenebisacrylamide) supports prepared using PMAA coated ferrofluid are presented in Figs 3.14 – 3.16 and Table 3.6. The VSM plots (Fig. 3.14) confirm both materials as superparamagnetic and exhibiting similar M_s values, i.e. 10.1 and 8.9 Am² kg⁻¹ for batch #1 and #2 respectively.

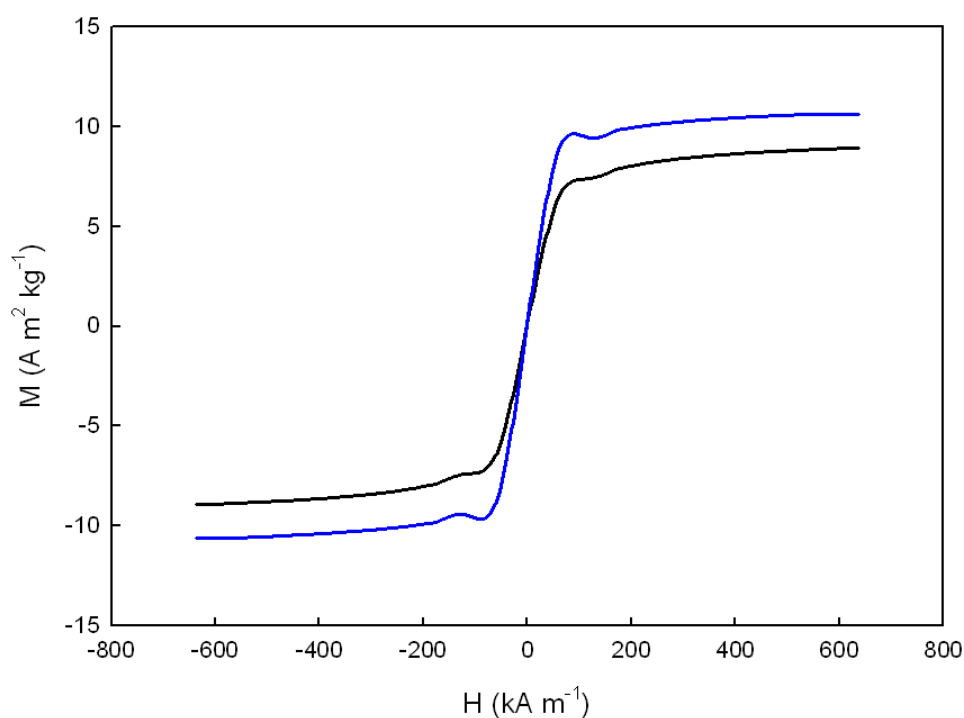


Figure 3.14 VSM curves for magnetic poly(acrylamide-co-ethylenebisacrylamide) supports prepared using PMAA coated ferrofluid (Batch #1 – blue trace and batch #2 – black trace; Table 3.3). The full magnetic hysteresis loops were recorded at room temperature, sweeping the external field between ± 0.8 Tesla.

The low angle scattering derived particle size distributions indicate that the magnetic poly(acrylamide-co-ethylenebisacrylamide) supports produced using the ‘ABCN + Arlacel® 83/ cyclohexane’ combination (batch #2) are larger, for example the Sauter mean diameters is $7.6 \mu\text{m}$ for batch #2 *cf.* $5.7 \mu\text{m}$ for batch #1. This size difference can be attributed to the differences in the efficiency of breakage and coalescence of monomer droplets during emulsification between the two continuous phases, Isopar M and cyclohexane.

Table 3.6 Summary of magnetic properties, refraction index and particle sizing data for magnetic poly(acrylamide-co-ethylenebisacrylamide) supports synthesized using PMAA coated ferrofluid.

Batch ID#		#1	#2
Initiator system		APS/TEMED	ABCN
Continuous phase solvent		Isopar M	Cyclohexane
Phase initiator dissolved in:		Dispersion	Continuous
M_s ($\text{Am}^2 \text{kg}^{-1}$)		10.1	8.9
Fe_3O_4 content (% w/w)		13.2%	11.7%
Refractive index		1.613	1.599
Particle size distribution (μm)	D(10)	3.7	4.4
	D(50)	6.1	9.3
	D(90)	9.9	14.5
Sauter diameter (μm)		5.7	7.6

Analysis of TEM images of thin cross-sections of magnetic poly(acrylamide-co-ethylenebisacrylamide) support batches #1 and #2 and the corresponding EDAX spectra are shown in Figs 3.15 and 3.16 respectively.

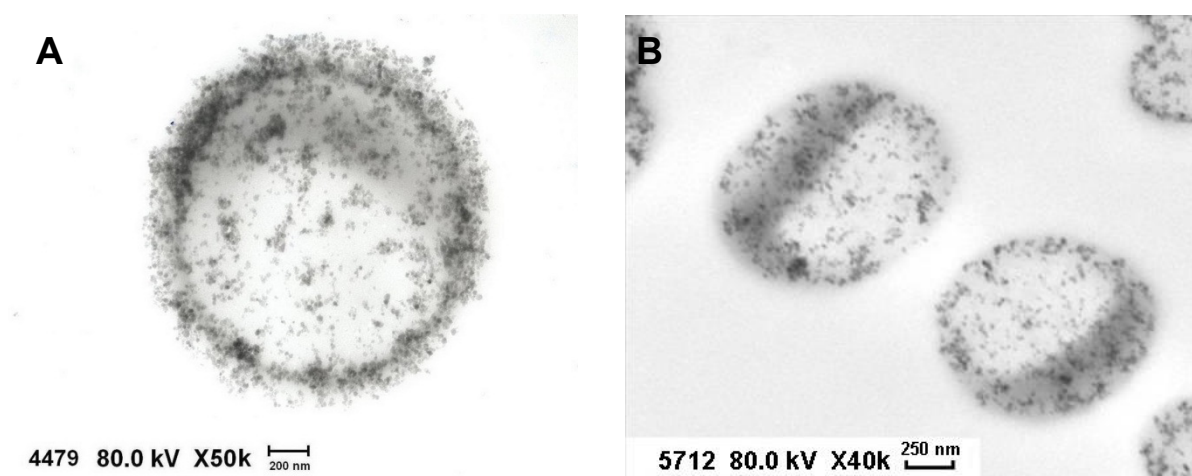


Figure 3.15 Transmission electron micrographs of cross-sections through (A) batch #1 (50k \times magnification) and (B) batch #2 (40k \times magnification) magnetic polymeric supports prepared using PMAA coated ferrofluid (see Table 3.3).

In stark contrast to TEM images of magnetic poly(acrylamide-co-ethylenebisacrylamide) prepared using poly(acrylic acid) coated ferrofluid (see Fig. 3.6), where large clusters of electron dense magnetic material unevenly distributed throughout the polymer matrix were observed, the TEM images for magnetic poly(acrylamide-co-ethylenebisacrylamide) supports fabricated using the PMAA ferrofluid prepared in this work show comparatively little clustering and much more uniform distribution throughout. This said, it should be noted that electron dense material within the batch #1 support appears more concentrated at the bead periphery (Fig. 3.15A). By comparison the distribution of electron dense grains within batch #2 appears much more uniform (Fig. 3.15B) with no evidence of a greater concentration of elements at the support's exterior. In common with earlier findings for magnetic poly(acrylamide-co-ethylenebisacrylamide) support batch 'C' prepared using the poly(acrylic acid) coated ferrofluid, the EDAX spectra of TEM images of support batches #1 and #2 confirmed the identity of the dark grainy materials (Fig. 3.16A & C) and pale grain devoid areas (Fig. 3.16B & D) as magnetite and polymer matrix respectively.

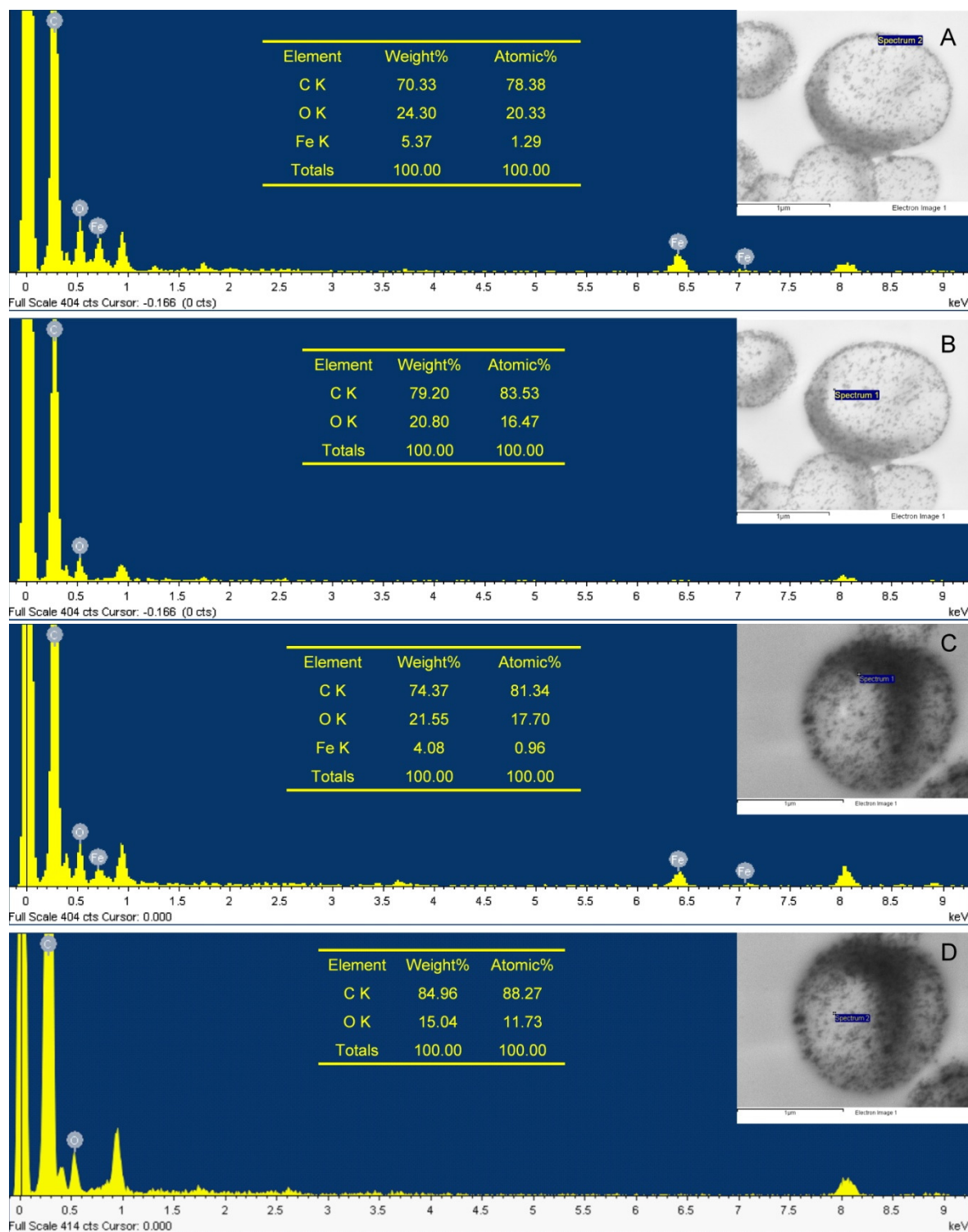


Figure 3.16 Representative EDAX spectra and corresponding elemental compositions of dark (grainy) and pale (grain devoid) areas within batch #1 (A -dark & B - pale) and batch #2 (C - dark & D - pale) magnetic poly(acrylamide-co-ethylenebisacrylamide) support particles prepared using PMAA coated ferrofluid (Table 3.2).

In conclusion, the magnetic poly(acrylamide-co-ethylenebisacrylamide) support fashioned out using the 'ABCN + Arlacel[®] 83/ cyclohexane' combination (batch #2) must be judged superior to the original 'APS/TEMED + Arlacel[®] 83/ Isopar M' (batch #1). Although batch #1 exhibited a slightly higher M_s (10.1 *cf.* 8.9 Am² kg⁻¹) and smaller particle size (e.g. SMD of 5.7 *cf.* 7.6 μm) TEM revealed much more uniform distribution of magnetic elements throughout the support with no evidence of a higher concentration at/near the surface. An important consequence of the uniform distribution is that loss of magnetic elements into the bulk liquid phase during operation and long term storage via mechanical abrasion/sloughing and leaching mechanisms is much less likely to occur. Further, the presence of high numbers of magnetite crystals at the exterior surfaces may diminish the available surface for subsequent modification (such as functionalisation with various ligands by conventional staged activation and coupling and graft polymerization methods) and binding of target species.

A possible reason for the difference in distribution of PMAA coated crystals within support batches #1 and #2 relating to electrostatic interactions of stabilized magnetic crystals with APS is offered here. Under alkaline conditions both the PMAA coated magnetite and peroxydisulphate ions of the APS initiator are negatively charged, and repel one another. However, the magnitude of this repulsion is not large enough to

partition the coated magnetic crystals from the dispersion droplet into the hydrophobic Isopar M continuous phase, thus the magnetic elements concentrate at the inner surface of the droplet. ABCN by contrast exhibits good solubility in the cyclohexane continuous phase, and as it is uncharged it doesn't influence the location of the PMAA coated ferrofluid within the dispersion droplet.

3.4.4.2 Influence of agitation speed during emulsification on the preparation of magnetic poly(acrylamide-co-ethylenebisacrylamide) supports using ABCN + Arlcel[®] 83/ cyclohexane + PMAA-coated ferrofluid

Magnetic poly(acrylamide-co-ethylenebisacrylamide) composite supports were synthesized via inverse phase emulsion polymerization using ABCN as initiator, 'Arlcel[®] 83/ cyclohexane' as the continuous phase and PMAA coated ferrofluid as the magnetic 'seeding' element. Three preparations (Batches #2, #3 & #4; Table 3.3) were made under different agitation conditions during emulsification (3000 rpm, 4000rpm and 5000 rpm), and the resulting magnetic supports were subjected to VSM, particle sizing, BET analysis, SEM and TEM examination.

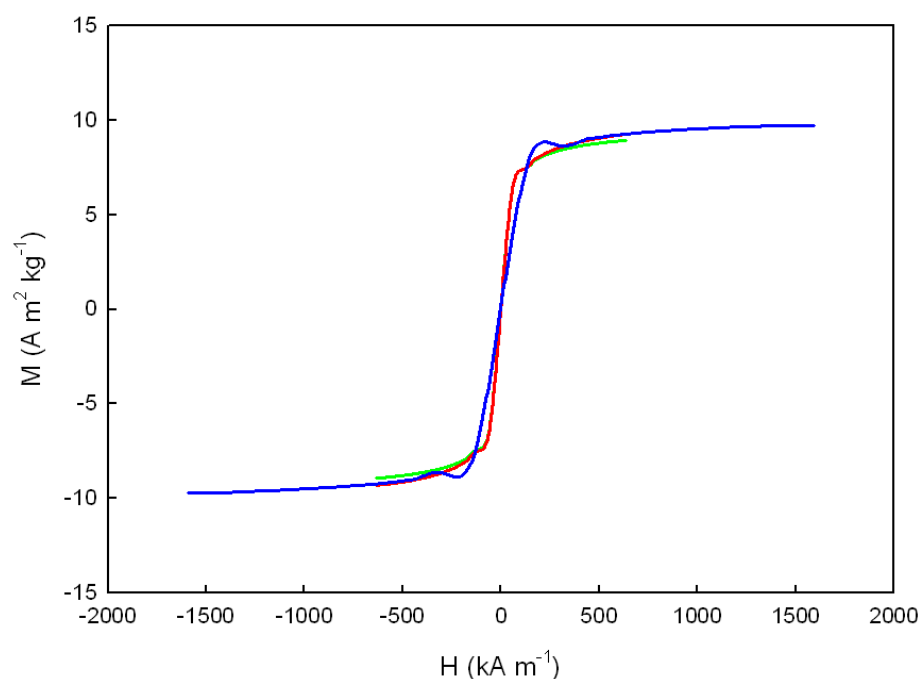


Figure 3.17 VSM curves for magnetic poly(acrylamide-co-ethylenebisacrylamide) supports prepared using ABCN + Arlacen[®] 83/ cyclohexane + PMAA-coated ferrofluid at agitation rates of 3000 rpm (batch #2 – green trace); 4000 rpm (batch #3 – red trace) and 5000 rpm (batch #4 – blue trace). The full magnetic hysteresis loops were recorded at room temperature, sweeping the external field between ± 0.8 or ± 2.0 Tesla.

The VSM curves for magnetic poly(acrylamide-co-ethylenebisacrylamide) support batches #2 to #4 (Fig. 3.17) are completely closed consistent with superparamagnetic behaviour. The M_s values were observed to increase only very slightly from 8.9 to 9.7 $\text{Am}^2 \text{kg}^{-1}$ as the agitation rate during emulsification was raised from 3000 to 5000 rpm (Fig. 3.17 & Table 3.6)⁵. In contrast, raising the agitation rate was accompanied by significant reductions in particle size of the magnetic

⁵ It should be noted that the magnetization curve for batch 4 (5000 rpm) was swept over a larger range of magnetic flux, i.e. ± 2.0 Tesla *cf.* ± 0.8 Tesla.

poly(acrylamide-co-ethylenebisacrylamide) supports (Table 3.7).

Table 3.7 Summary of magnetic properties, refraction index, particle sizing and specific surface area data for magnetic poly(acrylamide-co-ethylenebisacrylamide) supports prepared using ABCN + Arlcel[®] 83/ cyclohexane + PMAA-coated ferrofluid at three different agitation rates (Batches #2, #3 & #4; Table 3.3).

Batch ID#		#2	#3	#4
Agitation speed (rpm)		3000	4000	5000
PMAA coated ferrofluid loading (mg)		500	500	500
Arlcel [®] 83 surfactant (mg)		400	400	400
M_s ($\text{Am}^2 \text{kg}^{-1}$)		8.9	9.3	9.7
Fe_3O_4 content (% w/w)		11.7%	12.1%	12.7%
Refractive index		1.599	1.603	1.608
Particle size distribution (μm)	D(10)	4.4	3.4	2.9
	D(50)	9.3	7.5	4.7
	D(90)	14.5	16.1	11.7
Sauter diameter (μm)		7.6	6.2	4.4
Specific surface area ($\text{m}^2 \text{g}^{-1}$)		1.5	7.1	6.2

For example, the Sauter mean diameter fell from 7.6 μm at 3000 rpm, through 6.2 μm at 4000 rpm, to 4.4 μm at 5000 rpm (which is close to the maximum possible under full load of 6000 rpm; Silverson Machines Ltd., 2010).⁶ The BET surface area increased nearly 5-fold from 1.5 $\text{m}^2 \text{g}^{-1}$ to 7.1 $\text{m}^2 \text{g}^{-1}$ on raising the agitation rate from 3000 to

⁶ As has been described in section 2.3.4, increasing the agitation speed puts more mechanical energy into the system. As monomer droplets pass through the workhead they are subjected to milling and hydrodynamic shear forces which cause them to break. However, provided that there is sufficient surfactant in the system to prevent the newly created droplets from coalescing/agglomerating with one another, breakage of the monomer droplets will dominate over coalescence/agglomeration. With this in mind the effects of surfactant concentration were subsequently examined (see later) at the highest agitation rate possible with the Silverson L5 M high shear mixer employed in this study, i.e. 5000 rpm.

4000 rpm, but a further increase to 5000 rpm caused a slight drop to $6.2 \text{ m}^2 \text{ g}^{-1}$ (Table 3.6). This reduction of specific surface area following the preparation under the 5000 rpm agitation speed can be attributed to aggregations of particles during drying process. Some dried particles stick to clusters and create dead zone in these clusters. Octane cannot diffuse into the dead zones and thus cannot adsorb onto the particle surface. However, these dead zone contained clusters don't provide total surface area to the calculation but provide its weight, thus it results in measured specific surface area decline. Under SEM, in stark contrast to the batch C magnetic support material (see Fig. 3.5) magnetic support batches #2 – #4 all appeared as spherical beads with little surface roughness (Fig. 3.18).

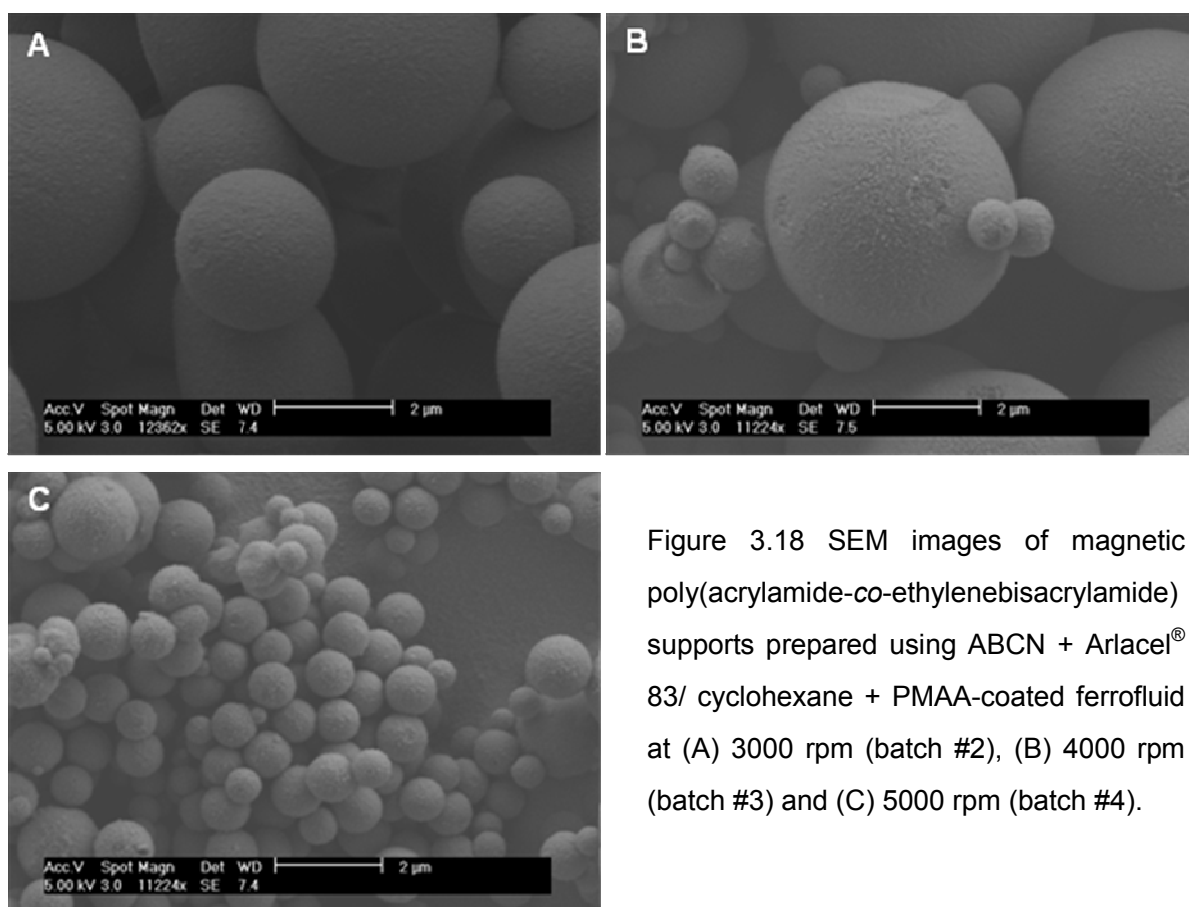


Figure 3.18 SEM images of magnetic poly(acrylamide-co-ethylenebisacrylamide) supports prepared using ABCN + Arlacel® 83/ cyclohexane + PMAA-coated ferrofluid at (A) 3000 rpm (batch #2), (B) 4000 rpm (batch #3) and (C) 5000 rpm (batch #4).

Comparison of TEM images of cross-sections of magnetic supports prepared at 3000 rpm and the highest agitation rate of 5000 rpm (Fig. 3.19) confirmed that the uniformity of distribution of PMAA coated crystals was had been retained.

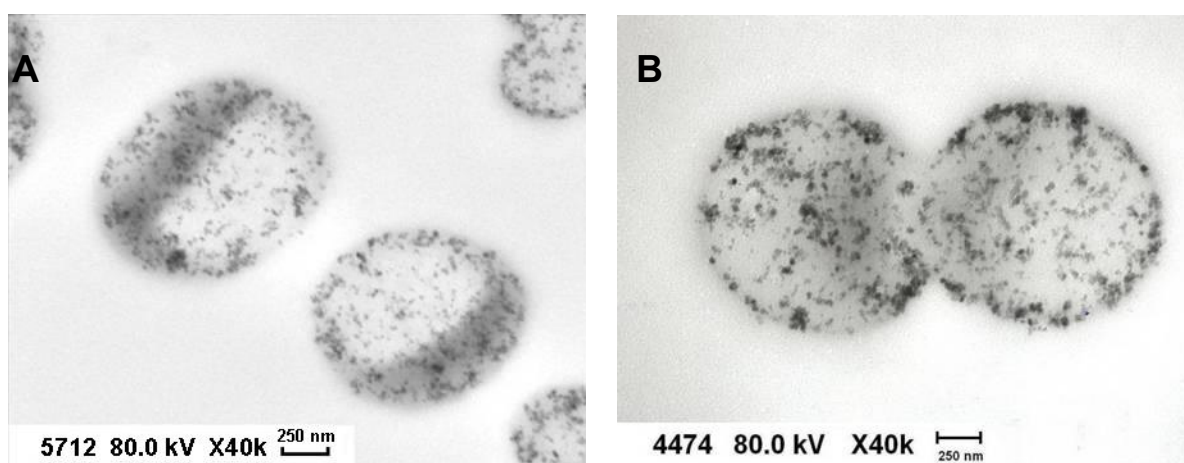


Figure 3.19 Transmission electron micrographs (40,000 \times magnification) of cross-sections through magnetic poly(acrylamide-co-ethylenebisacrylamide) supports produced at (A) 3000 rpm (batch # 2) and (B) 5000 rpm (batch #4) prepared using ABCN + Arlcel[®] 83/ cyclohexane + PMAA-coated ferrofluid (see Table 3.3).

3.4.4.3 Influence of PMAA ferrofluid loading on the preparation of magnetic poly(acrylamide-co-ethylenebisacrylamide) supports using ABCN + Arlcel[®] 83/ cyclohexane + PMAA-coated ferrofluid

Fast separation of product-loaded magnetic adsorbents is dependent not only on the use of an appropriate intensity of externally applied magnetic field, but also on successful incorporation of adequate quantities of a sufficiently magnetically susceptible material. In the preparation of magnetic

poly(acrylamide-co-ethylenebisacrylamide) supports prepared using coated ferrofluids, a 500 mg loading has been employed. These results in magnetic supports with M_s values of $\sim 10 \text{ Am}^2 \text{ kg}^{-1}$ regardless of other process variables. In an attempt to increase the M_s of magnetic poly(acrylamide-co-ethylenebisacrylamide) supports, whilst retaining the smallest possible particle size new batches of supports were made using PMAA coated ferrofluid loadings of 500, 1000 and 1500 mg at a constant agitation speed of 5000 rpm. Additional experiments were performed in which higher quantities of Arlacel[®] 83 surfactant were incorporated in the cyclohexane continuous phase to mitigate support agglomeration issues noted midway through conducting this experimental series. The resulting support materials were analysed by VSM, low angle light scattering, and BET analysis, SEM and TEM.

Simultaneously increasing the amounts of ferrofluid and surfactant whilst keep the ratio of the two constant was accompanied by parallel increases in M_s without compromising their superparamagnetic behaviour (Fig. 3.20). For example, doubling the ferrofluid and surfactant contents (from 500 mg and 400 mg to 1000 mg and 800 mg) more than tripled the M_s value (i.e. rising from 9.7 to $34.0 \text{ Am}^2 \text{ kg}^{-1}$), while a further increase in ferrofluid and surfactant loadings to 1500 mg and 1200 mg respectively pushed the M_s to $42.2 \text{ A m}^2 \text{ kg}^{-1}$ (equating to high magnetite loading of >55% w/w; Table 3.8).

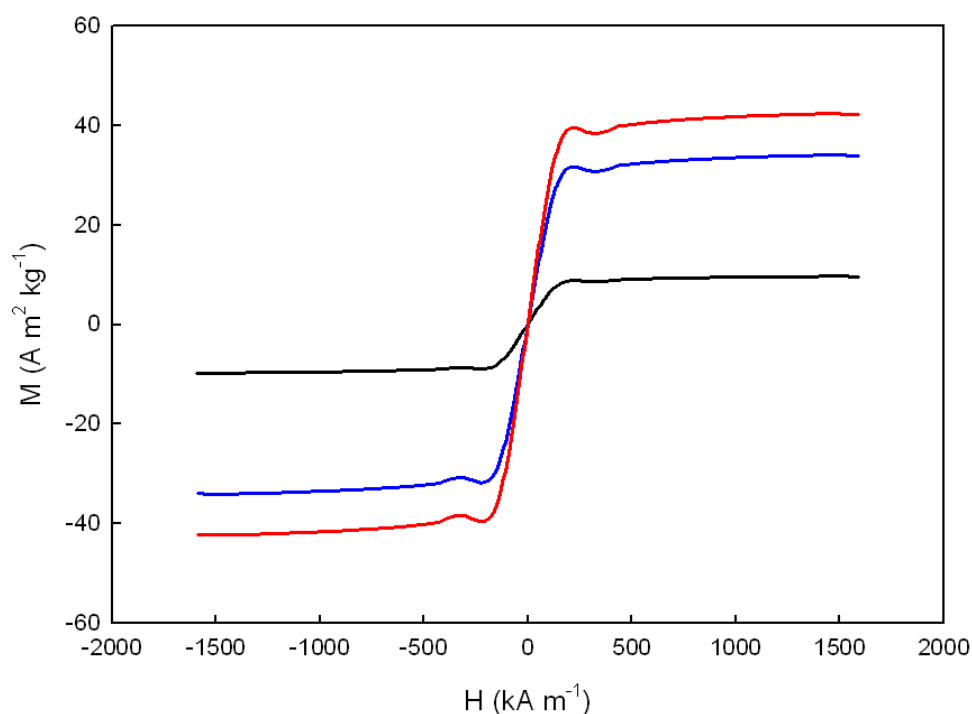


Figure 3.20 VSM curves for magnetic poly(acrylamide-co-ethylenebisacrylamide) supports prepared using ABCN + Arlancel[®] 83/ cyclohexane + PMAA-coated ferrofluid at 5000 rpm and various combinations of ferrofluid and surfactant. Key: 500 mg PMAA-ferrofluid + 400 mg Arlancel[®] 83 (batch #4 – black trace); 1000 mg PMAA-ferrofluid + 800 mg Arlancel[®] 83 (batch #7 – blue trace); 1500 mg PMAA-ferrofluid + 1200 mg Arlancel[®] 83 (batch #9 – red trace). The full magnetic hysteresis loops were recorded at room temperature, sweeping the external field between ± 2.0 Tesla.

Changing the amount of ferrofluid and surfactant profoundly affects the particle size (Table 3.8) and morphology (Figs 3.21 & 3.22) of magnetic poly(acrylamide-co-ethylenebisacrylamide) preparations. Others (Kondo *et al.*, 1994; Xie *et al.*, 2003; Xu *et al.*, 2004) have reported on this previously. SEM micrographs of support batches #4, #7 and #9 corresponding to the VSM plots in Fig. 3.20 are shown in Fig. 3.21. These supports were prepared using varying loadings of ferrofluid and

surfactant, but importantly the surfactant/ferrofluid ratio was maintained at 0.8 mg/mg. With increasing loading of ferrofluid the support particles become much smaller and much rougher⁷ and not surprisingly the BET surface area also increases. Importantly, however, distinct supports appear have been produced in all three batches. It should be noted however, that particle size of batch #9 under SEM (Fig. 3.21C) is very much smaller than that measured by low angle light scattering. For example, SEM shows that all particles are much smaller than 1 μm , whereas the Sauter mean diameter indicates a size of 1.9 μm . Other than this however, there are few signs of serious particle agglomeration.

⁷ The increased surface roughness comes from the increased concentration of coated magnetite crystals at the support surface.

Table 3.8 Summary of magnetic properties, refraction index, particle sizing and specific surface area data for magnetic poly(acrylamide-co-ethylenebisacrylamide) supports prepared using ABCN + Arlcel[®] 83/ cyclohexane + PMAA-coated ferrofluid at 5000 rpm and various combinations of ferrofluid and surfactant.

Batch ID#		#4	#5	#6	#7	#8	#9
Agitation speed (rpm)		5000	5000	5000	5000	5000	5000
PMAA coated ferrofluid loading (mg)		500	1000	1000	1000	1500	1500
Arlcel 83 surfactant (mg)		400	400	600	800	800	1200
Surfactant to ferrofluid ratio (mg/mg)		0.80	0.40	0.60	0.80	0.53	0.80
M_s (Am ² kg ⁻¹)		9.7	nd	nd	34.0	44.5	42.2
Fe ₃ O ₄ content (% w/w)		12.7	nd	nd	44.3	58.1	55.1
Refractive index		1.608	nd	nd	1.903	2.030	2.002
Particle size distribution (μm)	D(10)	2.9	nd	nd	2.1	2.4	1.3
	D(50)	4.7	nd	nd	3.1	15.8	1.8
	D(90)	11.7	nd	nd	4.3	49	4.5
Sauter diameter (μm)		4.4	nd	nd	3	6.8	1.9
Specific surface area (m ² g ⁻¹)		6.2	nd	nd	6.4	nd	8.5

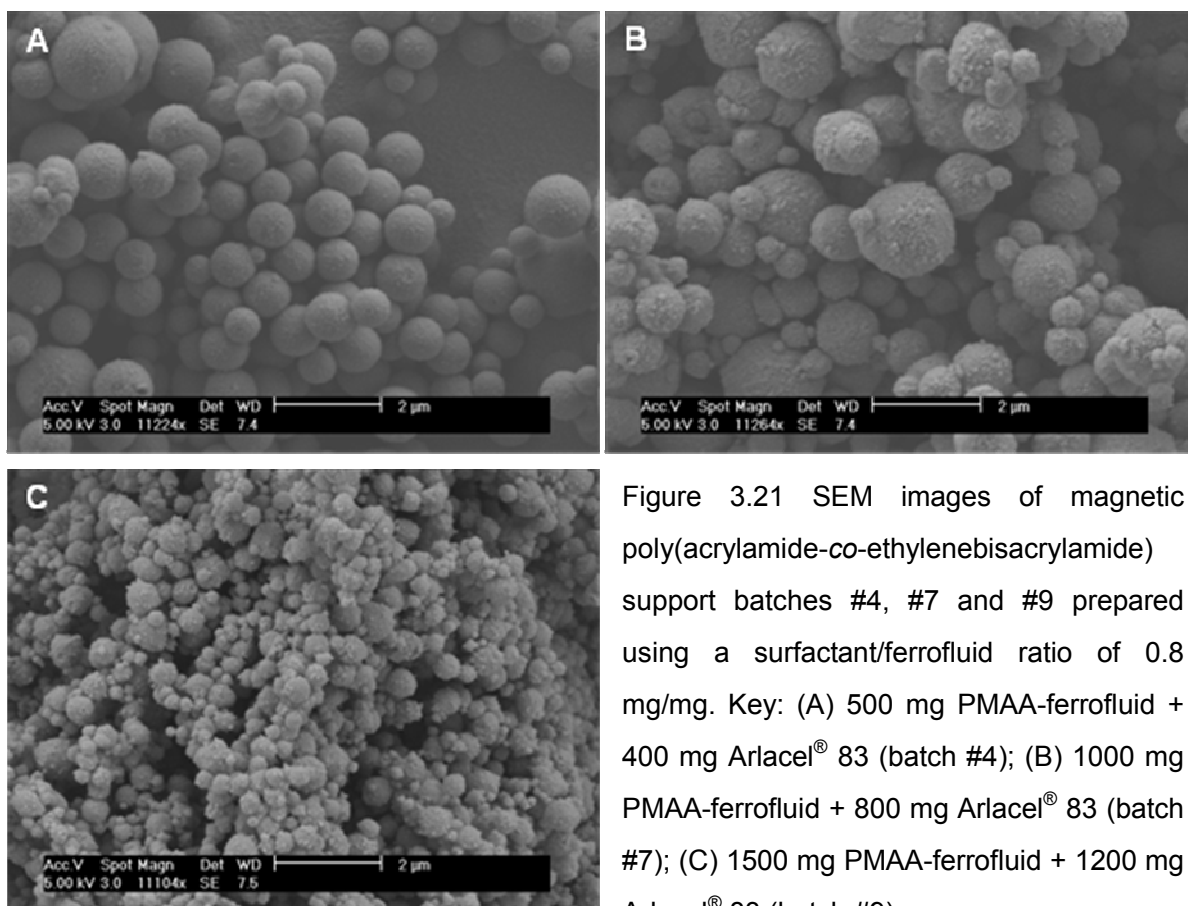


Figure 3.21 SEM images of magnetic poly(acrylamide-co-ethylenebisacrylamide) support batches #4, #7 and #9 prepared using a surfactant/ferrofluid ratio of 0.8 mg/mg. Key: (A) 500 mg PMAA-ferrofluid + 400 mg Arlancel[®] 83 (batch #4); (B) 1000 mg PMAA-ferrofluid + 800 mg Arlancel[®] 83 (batch #7); (C) 1500 mg PMAA-ferrofluid + 1200 mg Arlancel[®] 83 (batch #9).

In stark contrast, at low surfactant/ferrofluid ratios (Fig. 3.22) the support particles have lost much of their spherical shape (see e.g. Fig. 3.22A) and severe support agglomeration is manifest (especially in Figs 3.22A & B).

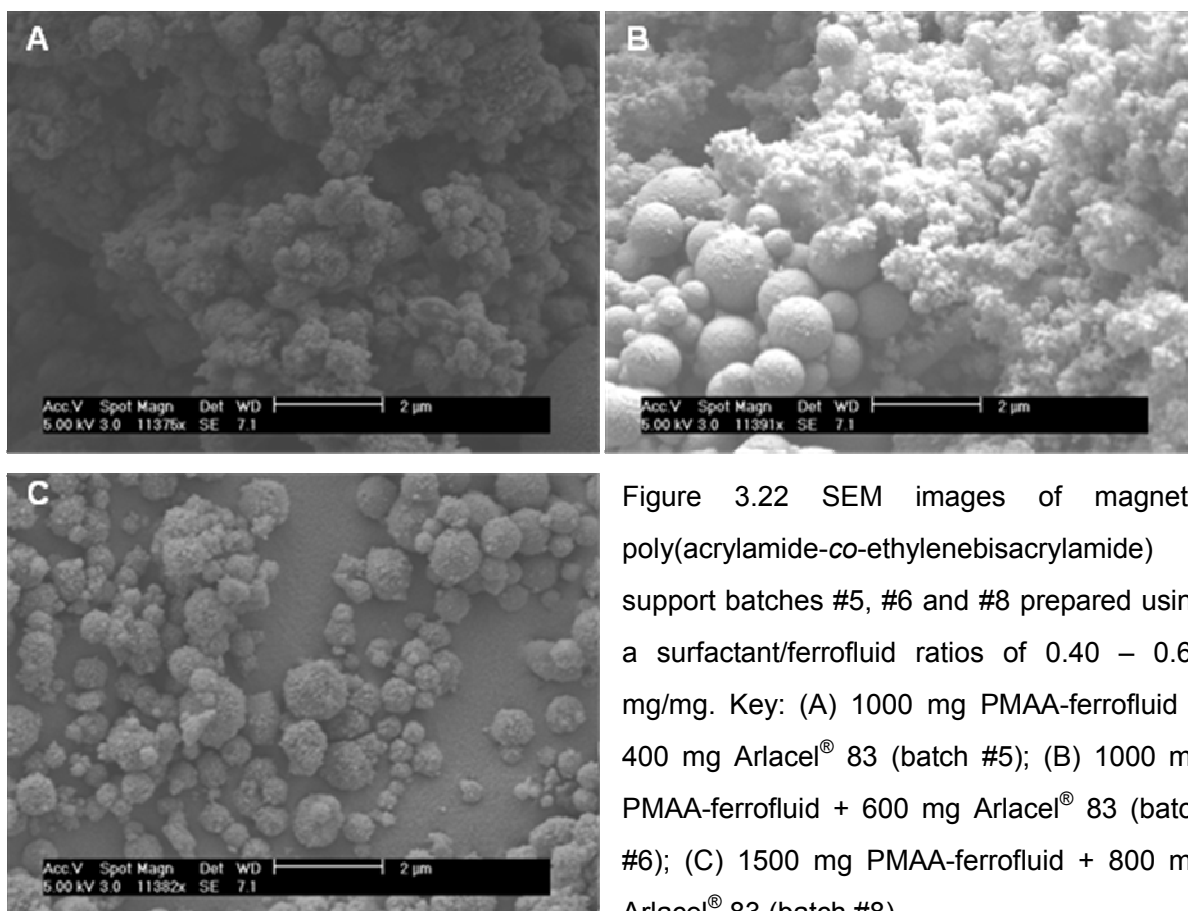


Figure 3.22 SEM images of magnetic poly(acrylamide-co-ethylenebisacrylamide) support batches #5, #6 and #8 prepared using a surfactant/ferrofluid ratios of 0.40 – 0.60 mg/mg. Key: (A) 1000 mg PMAA-ferrofluid + 400 mg Arlacel® 83 (batch #5); (B) 1000 mg PMAA-ferrofluid + 600 mg Arlacel® 83 (batch #6); (C) 1500 mg PMAA-ferrofluid + 800 mg Arlacel® 83 (batch #8).

TEM performed on thin sections of LR White resin fixed magnetic poly(acrylamide-co-ethylenebisacrylamide) batch #4 (Fig. 3.23A) and #7 (Fig. 3.23B) revealed that the uniformity of distribution of coated magnetite crystals within poly(acrylamide-co-ethylene) beads was unaffected by the greater than 3 fold increase in magnetic material (see Table 3.7). Numerous issues were experienced in the preparation of batch #9 supports for TEM analysis which could not be solved within the time available. White areas indicated poor penetration of LR White resin into the batch #9 support sample, and large numbers of non-encapsulated magnetite crystals and evidence of damaged support beads (Fig. 3.22C) resulted during

ultramicrotome sectioning.

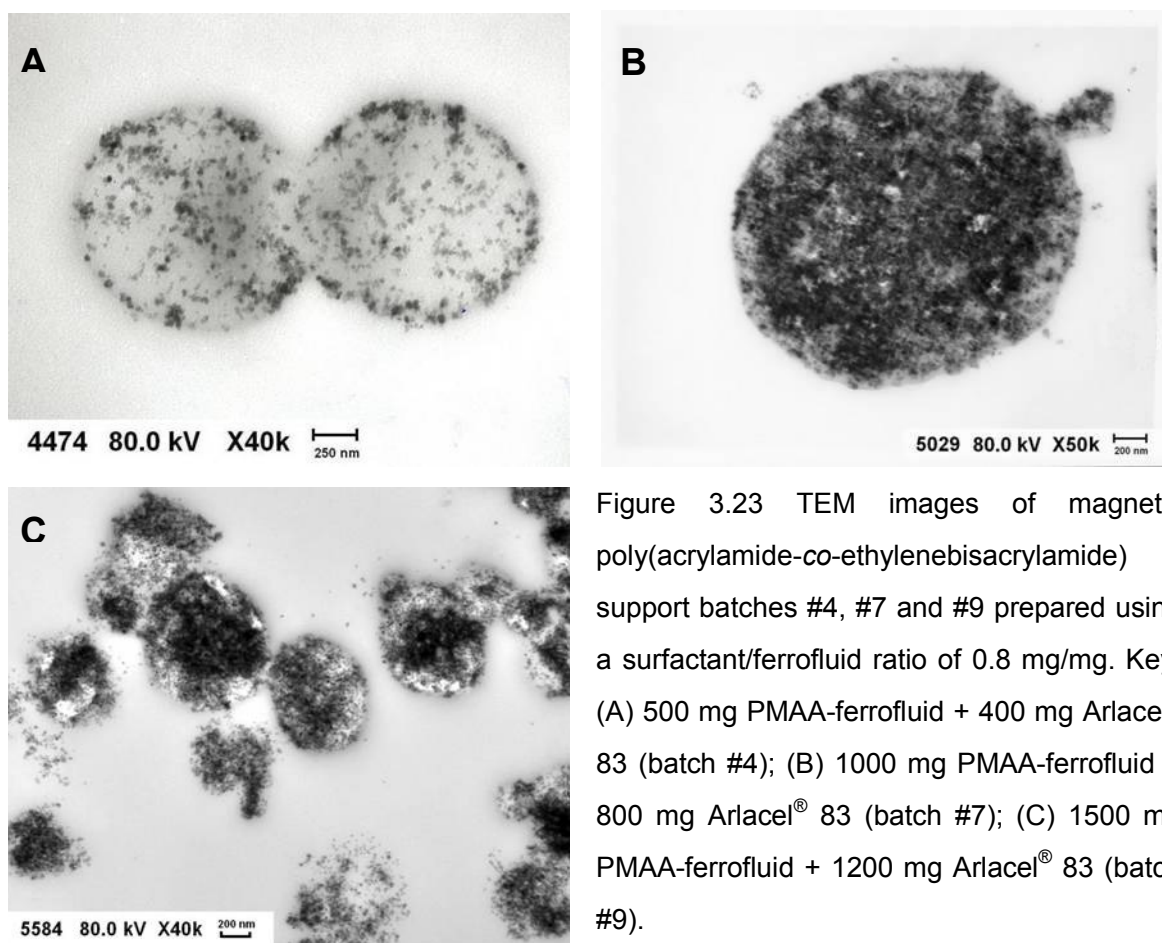


Figure 3.23 TEM images of magnetic poly(acrylamide-co-ethylenebisacrylamide) support batches #4, #7 and #9 prepared using a surfactant/ferrofluid ratio of 0.8 mg/mg. Key: (A) 500 mg PMAA-ferrofluid + 400 mg Arlcel[®] 83 (batch #4); (B) 1000 mg PMAA-ferrofluid + 800 mg Arlcel[®] 83 (batch #7); (C) 1500 mg PMAA-ferrofluid + 1200 mg Arlcel[®] 83 (batch #9).

3.4.4.4 Influence of surfactant content (Arlcel[®] 83) on the preparation of magnetic poly(acrylamide-co-ethylenebisacrylamide) supports using ABCN + Arlcel[®] 83/ cyclohexane + PMAA-coated ferrofluid

The importance of providing sufficient surfactant to prevent particle coalescence and agglomeration was identified in Figs 3.22 and 3.23. The influence of increasing surfactant loading on the preparation of magnetic poly(acrylamide-co-ethylenebisacrylamide) supports was examined further at two

fixed magnetite loadings (500 and 1000 mg) at an agitation speed of 5000 rpm (Table 3.9 & Figs 3.24 – 3.26). At both ferrofluid loadings doubling the surfactant loading exerted little if any influence on the M_s values of the resulting superparamagnetic poly(acrylamide-co-ethylenebisacrylamide) supports (Fig. 3.24 & Table 3.9), and only slight reductions in particle size (Table 3.9).

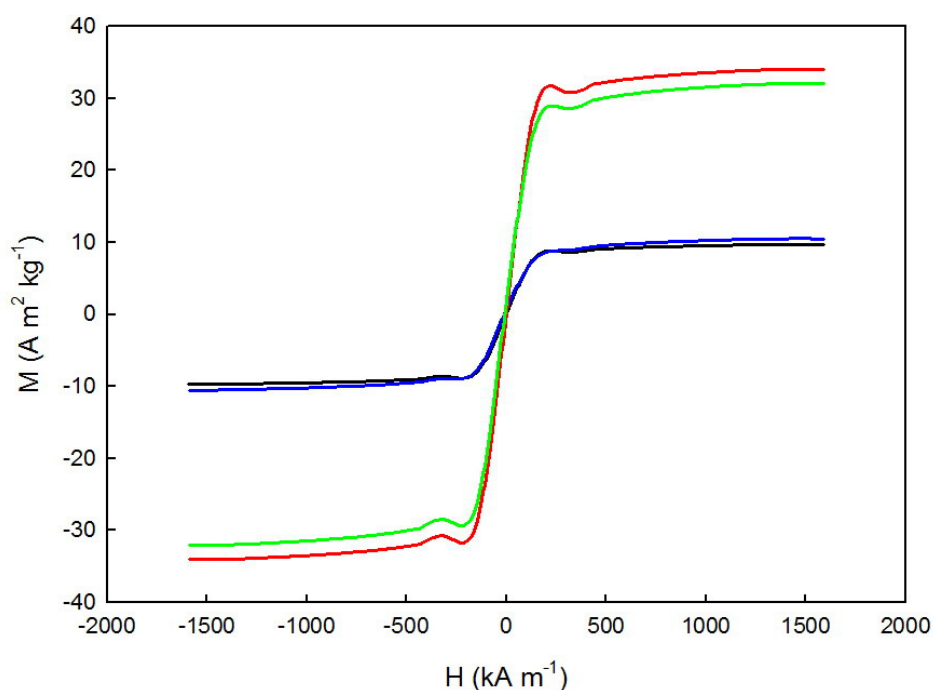


Figure 3.24 VSM curves for magnetic poly(acrylamide-co-ethylenebisacrylamide) support batches #4 (500 mg PMAA-ferrofluid + 400 mg Arlacel[®] 83 – black trace), #11 (500 mg PMAA-ferrofluid + 800 mg Arlacel[®] 83 – blue trace), #7 (1000 mg PMAA-ferrofluid + 800 mg Arlacel[®] 83 – red trace) and #12 (1000 mg PMAA-ferrofluid + 1200 mg Arlacel[®] 83 – green trace). The full magnetic hysteresis loops were recorded at room temperature, sweeping the external field between ± 2.0 Tesla.

Table 3.9 Summary of magnetic properties, refraction index and particle sizing data for magnetic poly(acrylamide-co-ethylenebisacrylamide) supports batches prepared at 500 and 1000 mg loadings of PMAA coated ferrofluid and various Arlcel® 83 loadings.

Batch ID#		#10	#4	#11	#5	#7	#12
Agitation speed (rpm)		5000	5000	5000	5000	5000	5000
PMAA coated ferrofluid loading (mg)		500	500	500	1000	1000	1000
Arlcel 83 surfactant (mg)		200	400	800	400	800	1200
Surfactant: ferrofluid ratio (mg/mg)		0.40	0.80	1.60	0.40	0.80	1.20
M_s ($\text{Am}^2 \text{kg}^{-1}$)		nd	9.7	10.5	nd	34.0	32.1
Fe_3O_4 content (% w/w)		nd	12.7	13.7	nd	44.3	41.9
Refractive index		nd	1.608	1.617	nd	1.903	1.880
Particle size distribution (μm)	D(10)	nd	2.9	2.8	nd	2.1	1.8
	D(50)	nd	4.7	4.4	nd	3.1	2.8
	D(90)	nd	11.7	11.3	nd	4.3	10.2
Sauter diameter (μm)		nd	4.4	4.4	nd	3.0	2.9

By contrast, reducing the surfactant/ferrofluid loading ratio from 0.8 mg/mg to 0.4 mg/mg was accompanied by serious agglomeration of the support particles. This is clearly seen when one compares for example the SEM images in Figs 3.25B & C with Fig. 3.25A, and Figs 3.26B & C with Fig. 3.26.

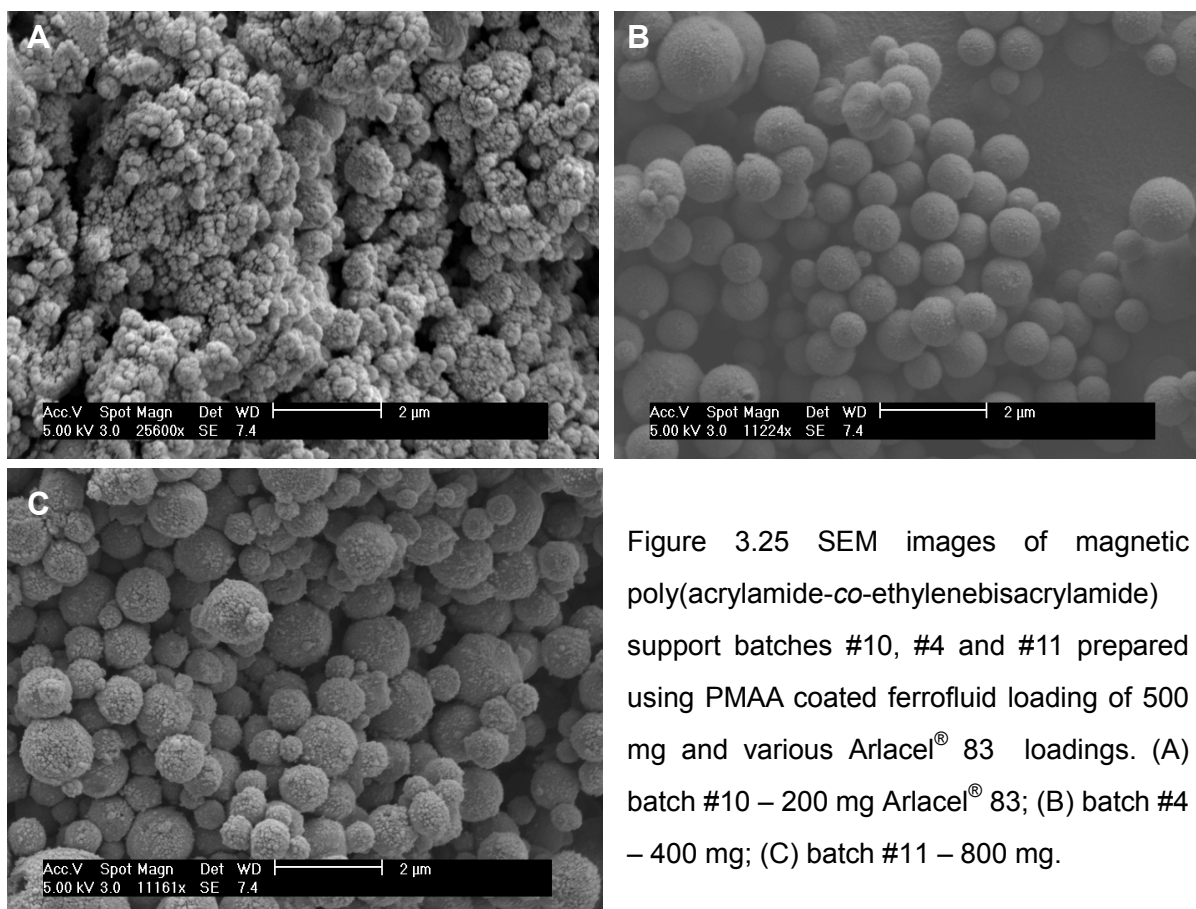


Figure 3.25 SEM images of magnetic poly(acrylamide-co-ethylenebisacrylamide) support batches #10, #4 and #11 prepared using PMAA coated ferrofluid loading of 500 mg and various Arlacel® 83 loadings. (A) batch #10 – 200 mg Arlacel® 83; (B) batch #4 – 400 mg; (C) batch #11 – 800 mg.

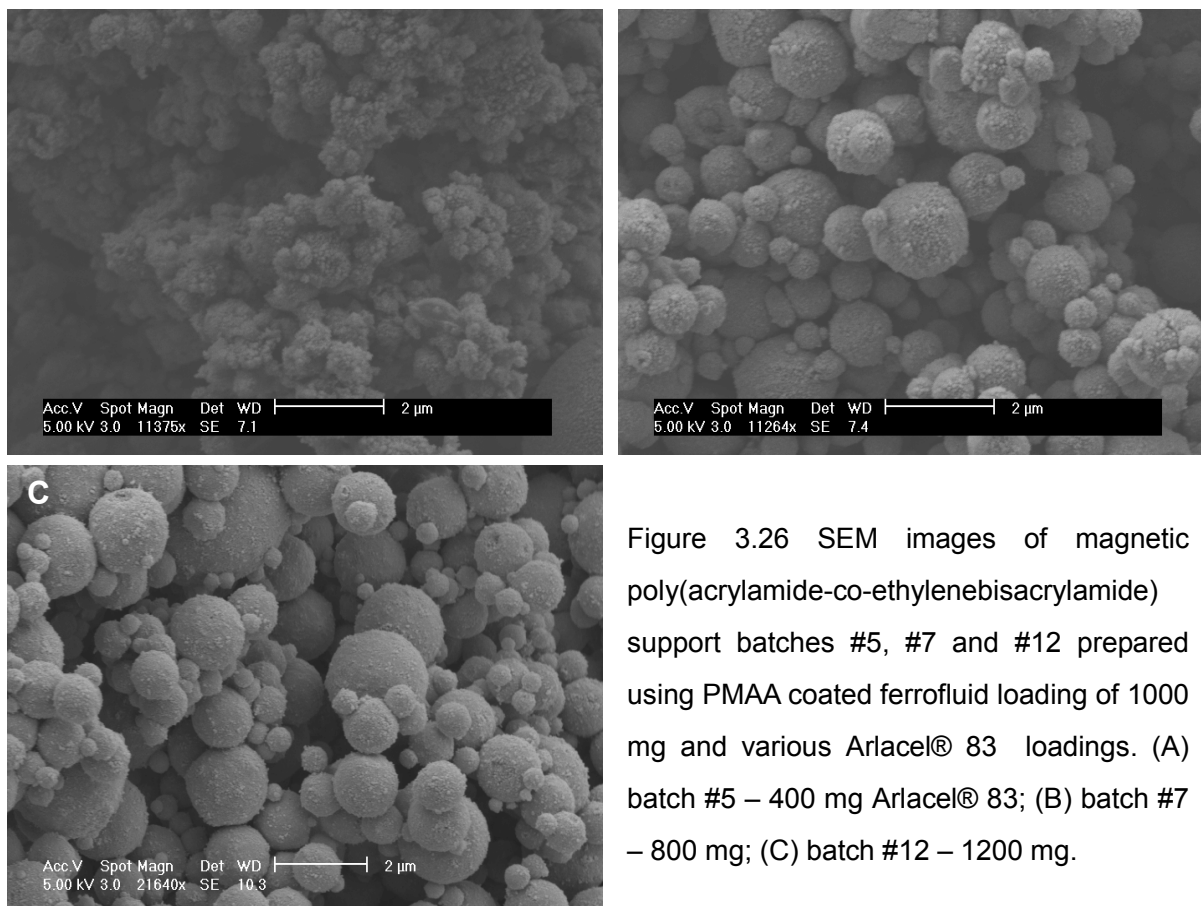


Figure 3.26 SEM images of magnetic poly(acrylamide-co-ethylenebisacrylamide) support batches #5, #7 and #12 prepared using PMAA coated ferrofluid loading of 1000 mg and various Arlacel® 83 loadings. (A) batch #5 – 400 mg Arlacel® 83; (B) batch #7 – 800 mg; (C) batch #12 – 1200 mg.

These results highlight the key role that surfactant plays in the production of magnetic poly(acrylamide-co-ethylenebisacrylamide) supports using inverse liquid-liquid two phase emulsion polymerization systems. The surfactant stabilizes the system, by adsorbing onto newly created surfaces of monomer droplets as undergo shear induced break-up, and keeping their shape and preventing particles coalescing with one another and from agglomerating together during polymer chain growth.

3.5 Conclusions

In this chapter the systematic adaptation of inverse liquid-liquid two phase emulsion

polymerization advanced in Chapter 2 into a 'one-pot' manufacturing route for the rapid production of small non-porous beaded magnetic polymer composites is described. Initially various elements (naked magnetite and ferrofluids coated with oleic acid and poly(acrylic acid)) were screened for their ability to render poly(acrylamide-co-ethylenebisacrylamide) preparations magnetically responsive, but none of these proved ideal. Naked magnetite powders exhibited strong aggregation tendencies, poor dispersibility within monomer droplets and low entrapment efficiency. The oleic acid coated ferrofluid was unable to confer magnetic susceptibility; likely caused by progressive oxidation of the magnetic iron oxide components to weakly paramagnetic forms. Although magnetic poly(acrylamide-co-ethylenebisacrylamide) supports prepared using the poly(acrylic acid) coated ferrofluid possessed superparamagnetic properties, their long-term storage prospects are questionable. A new ferrofluid coated with poly(methacrylic acid) was synthesized and was subsequently shown to be an ideal magnetic material to employ for the purposes of magnetizing poly(acrylamide-co-ethylenebisacrylamide) beads. The choice of ABCN as the favoured initiator over the APS/TEMED system employed in Chapter 2, is based on the finding that unlike the peroxydisulphate ions of APS ABCN does not appear to influence the location of the negatively charged PMAA coated ferrofluid with the monomer dispersion droplet, thus uniform distribution of the ferrofluid throughout the support is assured.

Following selection of ABCN as initiator of choice for the 'one-pot' manufacture of magnetic polymer composite supports, attempts to optimize key support features, i.e. minimize the size, maximize the magnetite loading and resulting M_s , and increase the surface area, were undertaken and conditions for fabrication of small highly magnetic beaded supports with roughened surfaces were found simply by systematically varying agitation speed, ferrofluid and surfactant loading. It is apparent that incorporating increasing amounts of magnetic material into the mix requires parallel increases in surfactant. Increasing the magnetite loading seems to promote the break-up of monomer droplets and exerts a powerful effect on the size of resulting magnetic polymer particles, while surfactant plays a crucial stabilizing role in maintaining particle shape, and thwarting coalescence and agglomeration.

4. 'One-pot' synthesis of beaded magnetic ion exchange adsorbents by inverse phase emulsion polymerization routes

Abstract

The 'one-pot' manufacture procedure described in previous work was employed to produce magnetic ion exchange adsorbents. Magnetic anion exchangers created using 2-(diethylamino)ethyl methacrylate as the functional monomer, generated distinct spherical particles, with successful magnetic core material encapsulation, exhibiting classical superparamagnetic behaviour and multilayer protein binding ($Q_{\max} = 46.1 \text{ mg g}^{-1}$ adsorbents and $K_d = 2.52 \text{ }\mu\text{M}$) with complete protein recovery. During the preparation of magnetic cation exchange adsorbents, poly(methacrylic acid) coated ferrofluid could not be incorporated in the monomer droplets, due to the electrostatic repulsion between the negatively charged magnetite crystals and the same negatively charged functional monomer. When the positively charged tetramethylammonium hydroxide (TMAOH) coated ferrofluid was employed instead in the manufacture of magnetic cation exchangers, poor magnetic particle encapsulation endowed adsorbents with insufficient magnetic susceptibility.

4.1 Introduction


Since their introduction in the middle of 1970s, magnetic adsorbents have been extensively researched and employed in various biotechnological applications (Ma *et al.*, 2007), because they can deliver rapid and highly selective protein recovery from crude feedstocks (Franzreb *et al.*, 2006). In most cases, these magnetic adsorbents are: nonporous to minimise biological fouling (Ma *et al.*, 2005); measure 50 nm to 10 μm in size, to achieve a comparable surface area to porous adsorbents (Safarik and Safarikova, 2004); and possess superparamagnetic properties, to avoid undesirable adsorbent agglomeration in the presence of an externally applied magnetic field (Franzreb *et al.*, 2006). Commercially available adsorbents contain affinity ligands (i.e. streptavidin, antibodies, protein A and protein G), to allow highly selective isolation of the target proteins and peptides (Safarik and Safarikova, 2004). In addition, magnetic carriers with functional groups (e.g. $-\text{COOH}$, $-\text{OH}$ and $-\text{NH}_2$) can be obtained from both commercial available and laboratory made supports, on which further functionalisation can be achieved using a wide range of ligands after surface modifications (e.g. tosyl-activation, epoxy-activation and silanization); and finally adapt in various biologic product adsorptions (Safarik and Safarikova, 2004).

The early researches were first focused on the applications of magnetic affinity adsorbents in biologic products recovery. Examples that have been reported in the literature include: Cu^{2+} -IDA ligand metal affinity adsorption of haem proteins (O'Brien

et al., 1996, 1997); alcohol dehydrogenase recovery using cibacron blue coupled magnetic support (Tong *et al.*, 2001); benzamidine-linked affinity magnetic supports for trypsin capture (Hubbuch and Thomas, 2002; Heebøll-Nielsen, 2002); and Cu^{2+} -IDA ligand metal affinity adsorption of bovine haemoglobin (Ma *et al.*, 2005; Liu *et al.*, 2005). However, little research had been carried out on magnetic ion exchangers, until Xue and Sun (2002) reported the recovery of bovine serum albumin (BSA) employing diethylamine immobilized magnetic anion exchange adsorbents (Heebøll-Nielsen, 2002).

Proteins carry positively or negatively charged groups on their surface. Therefore, they can be selectively isolated by electrostatic interactions between charged surface groups on proteins and opposite charge groups (see Table 4.1) carried on ion exchange adsorbents. Protein recovery can be then achieved through elution with reversing pH or increasing the salt concentration of surrounding buffer to break the static interacting between protein and adsorbents.

Table 4.1 Examples of ion exchange groups used in protein purification (taken from Pitfield, 1992)

Name		Abbr.	Structure
Anion exchangers	Diethyl aminoethyl	DEAE	$-\text{OCH}_2\text{CH}_2\text{N}(\text{C}_2\text{H}_5)_2$
	Dimethyl aminoethyl	DMAE	Polymerized $\text{CH}_2=\text{CHCONHCH}_2\text{CH}_2\text{N}(\text{CH}_3)_2$
	Trimethyl hydroxypropyl	QA	$-\text{OCH}_2\text{CH}(\text{OH})\text{N}^+(\text{CH}_3)_3$
	Trimethyl aminoethyl	TMEA	Polymerized $\text{CH}_2=\text{CHCONHCH}_2\text{CH}_2\text{N}^+(\text{CH}_3)_3$
	Quaternary aminomethyl	QAM	$-\text{OCH}_2\text{N}^+(\text{CH}_3)_3$
	Poly(ethylene imine)	PEI	
Cation exchangers	Acrylate	COO^-	Polymerized $\text{CH}_2=\text{CHCOOH}$
	Carboxymethyl	CM	$-\text{OCH}_2\text{COOH}$
	Sulphonate	SO_3^-	Polymerized $\text{CH}_2=\text{CHCONHC}(\text{CH}_3)_2\text{CH}_2\text{SO}_3\text{H}$
	Sulphopropyl	SP	$-\text{OCH}_2\text{CH}_2\text{CH}_2\text{SO}_3\text{H}$

Early on, functional polymers, such as poly(acrylic acid) or poly(ethylene oxide), were either used directly to coat magnetite crystals (Liao and Chen, 2002) or added onto polymer preassembled magnetite clusters (Ditsch *et al.*, 2006). However, very little amount of magnetic core material was encased in each adsorbent, thereby producing supports with insufficient magnetic susceptibility and resulting in slow magnetic separation. In addition, due to the relative small size of these adsorbents, protein molecules could act as cross-linking agents during adsorption, leading to particle aggregation (Ditsch *et al.*, 2006). Heebøll-Nielsen *et al.* (2004) prepared a series of

magnetic anion exchange supports with various ligands (i.e. DEAE, TMA and PEI) by graft polymerization (see Fig. 1.9) and tested them in the fractionation of bovine whey proteins. Of these, a PEI-linked absorbent reached maximum BSA binding capacity of 337 mg g^{-1} combined with a dissociation constant of $0.0042 \text{ }\mu\text{M}$. Hickstein and Peuker (2008) and K  ppler *et al.* (2008) introduced a ‘step by step’ synthesis of magnetic ion exchangers, in which magnetic core materials and ion exchangers were prepared separately, and then mixed together and spray dried. During protein adsorption experiments using the above absorbents, binding capacities of 192 mg of lysozyme per gram of sulfonated polystyrene magnetic cation exchangers (Hickstein and Peuker, 2008) and 85 mg of BSA per gram of aminated poly(methyl methacrylate) magnetic anion exchangers were achieved (K  ppler *et al.*, 2008).

Since its introduction in 2000 (Hubbuch, 2000; Hubbuch *et al.*, 2001 and Hubbuch and Thomas, 2002), High Gradient Magnetic Fishing (HGMF) has gained momentum in the field of Bioseparations, with the first small pilot-scale HGMF device being already in production (Franzreb *et al.*, 2006). Furthermore, additional hybrid processes, such as magnetic field enhanced press filtration (Stolarski *et al.*, 2006) and centrifugation (Lindner *et al.*, 2010) have been successfully introduced in the purification of biopharmaceutical products. However, the major stumbling block in the scale-up of magnetic based bioprocesses is the lack of a robust and easy to implement method to

create large quantities of cheap functionalized magnetic materials⁸ (Franzreb *et al.*, 2006).

This chapter describes the manufacturing of magnetic ion exchange adsorbents using a simple, fast, scalable and low cost ‘one-pot’ procedure. These magnetic adsorbents are first characterized in terms of their size distribution, specific surface area, magnetic properties, magnetite encapsulation efficiency and support morphology, and then subsequently used for the recovery of human serum albumin during batch binding and elution studies.

4.2 Materials

Table 4.2 List of chemicals involved in this chapter

Chemical Name	Abbr.	Supplier	Description
Acrylamide	AM	Sigma-Aldrich	Neutral monomer
2-(diethylamino)ethyl methacrylate	DEAE	Sigma-Aldrich	Anion exchanger monomer
acrylic acid	AA	Sigma-Aldrich	Cation exchange monomer
2-acrylamido-2-methyl-1-propanesulfonic acid	SP	Sigma-Aldrich	Cation exchange monomer
N,N'-ethylenebisacrylamide	EBA	Sigma-Aldrich	Cross linker
cyclohexane	N.A.	Fisher Scientific	Continuous phase solvent
sorbitan sesquioleate (Arlacel [®] 83)	N.A.	Sigma-Aldrich	Surfactant
1,1'-azobis(cyclohexanecarbonitrile)	ABCN	Sigma-Aldrich	Initiator
Human serum albumin	HSA	Sigma-Aldrich	Binding modeling protein; Mw: 66.5k Da
Sodium chloride	N.A.	Sigma-Aldrich	Elution chemical
Sodium hydroxide	N.A.	Sigma-Aldrich	Strip chemical
Trizma [®] hydrochloride	N.A.	Sigma-Aldrich	Binding buffer chemical
Trizma [®] base	N.A.	Sigma-Aldrich	Binding buffer chemical
Nitric acid	N.A.	Sigma-Aldrich	Solvent for ammonium iron ^{III} sulfate dodecahydrate

⁸ In general, prices for 1 gram of simple surface modified commercial magnetic adsorbents is approximately € 400 to several thousands euros per gram in the case of those carrying attached bioaffinity ligands (Franzreb *et al.*, 2006).

Table 4.2 List of chemicals involved in this chapter (continued)

Ammonium iron ^{III} sulfate dodecahydrate	N.A.	Sigma-Aldrich	Ionic capacity assay reagent
mercury ^{II} thiocyanate	N.A.	Sigma-Aldrich	Ionic capacity assay reagent
poly(methacrylic acid, sodium salt) solution	PMAA	Sigma-Aldrich	Ferrofluid stabilizer; Mw: 4000-6000, 40 wt. % in H ₂ O
Iron ^{II} chloride tetrahydrate	N.A.	Sigma-Aldrich	Production of magnetite
Iron ^{III} chloride hexahydrate	N.A.	Sigma-Aldrich	Production of magnetite
Ammonium hydroxide	N.A.	Sigma-Aldrich	Production of magnetite
Hydrochloric acid	N.A.	Sigma-Aldrich	pH adjuster
Ethanol	N.A.	Fisher Scientific	Wash resulting particles

Tetramethylammonium hydroxide (TMAOH) stabilized ferrofluid (97 mg mL⁻¹) was received as a gift from Dr. Bolle and Prof. Franzreb (KIT, Karlsruhe, Germany). The double distilled water used in this work was generated from a Hamilton water boiler (Hamilton Laboratory glass Ltd., Margate, UK). Nitrogen was supplied by the BOC Group (Dudley, UK).

4.3 Experimental methods

4.3.1 'One-pot' synthesis of magnetic anion exchange DEAE adsorbents

DEAE (2.814 mL) was mixed with 1.451 mL of N-hydroxyethyl acrylamide (HEA), 0.34 g of N,N'-ethylenebisacrylamide (EBA), PMAA coated ferrofluid containing 500 mg of magnetite crystals and double distilled water to create 10 mL of dispersion phase, which was then purged with nitrogen for 30 minutes. Arlacel[®] 83 (400 mg) was mixed with 40 mL of cyclohexane to create the continuous phase, which was also purged with nitrogen for 30 minutes. The two phases were then mixed and emulsified with a Silverson L5 M high shear mixer at 5000 rpm for 12 minutes. Subsequently, 150 mg of

ABCN was added into the mixture, and the reaction was left to proceed at 67°C with continuous mixing for another 36 minutes. The magnetic anion exchange adsorbents were then collected with the aid of a Chemagic Stand 50k magnetic rack (chemagen Biopolymer-Technologie AG, Baesweiler, Germany) and washed once with ethanol and three times with double distilled water. The washed adsorbents were then characterized for particle size distribution, specific surface area, magnetic properties, and morphology. A batch of unfunctionalized particles was also prepared in the same manner to act as control (the functional monomer DEAE and co-monomer HEA were replaced by 2 g of acrylamide).

4.3.2 'One-pot' synthesis of magnetic cation exchange adsorbents

4.3.2.1 Synthesis of magnetic cation exchange adsorbents with PMAA coated ferrofluid

Various cation functional monomers (1.92 mL of acrylic acid or 5.803 g of 2-acrylamido-2-methyl-1-propanesulfonic acid) were respectively mixed with 0.34 g of N,N'-ethylenebisacrylamide, PMAA coated ferrofluid containing 500 mg of magnetite and double distilled water to create 10 mL of dispersion phase. This solution was then purged with nitrogen for 30 minutes. Arlacel[®] 83 (400 mg) was mixed with 40 mL of cyclohexane to create the continuous phase, which was purged with nitrogen for 30 minutes. Then the emulsification, polymerization and following washing steps were carried out as described in section 4.3.1.

4.3.2.2 Synthesis of magnetic cation exchange adsorbents with TMAOH coated ferrofluid

Various cation functional monomers (1.92 mL of acrylic acid or 5.803 g of 2-acrylamido-2-methyl-1-propanesulfonic acid) were respectively mixed with 0.34 g of N,N'-ethylenebisacrylamide, TMAOH coated ferrofluid containing 500 mg of magnetite and double distilled water to create 10 mL of dispersion phase. The solution was purged with nitrogen for 30 minutes. Arlacel[®] 83 (400 mg) was mixed with 40 mL of cyclohexane to create the continuous phase, and the solution was purged with nitrogen for 30 minutes. Then the emulsification and polymerization steps were carried out as described in section 4.3.1. The magnetic cation exchange adsorbents were magnetically separated from the continuous phase and washed with various solvents (see Table 4.3). The results are characterized with their particle size distribution, magnetic property, morphology with SEM and images of TEM.

Table 4.3 Solvents used to wash the magnetic adsorbents prepared in this section.

Wash step No.	1	2	3	4	5	6
Cyclohexane	75%	25%	—	—	—	—
Ethanol	25%	75%	100%	75%	25%	—
Double distilled water	—	—	—	25%	75%	100%

4.3.3 Human serum albumin binding and elution study

Trizma[®] hydrochloride (3.175 g) and 0.59 g of Trizma[®] base were dissolved in double

distilled water to create 500 mL of 50 mM Tris-HCl buffer pH 7.5. A series of HSA concentrations ($10\ \mu\text{g mL}^{-1}$, $20\ \mu\text{g mL}^{-1}$, $50\ \mu\text{g mL}^{-1}$, $100\ \mu\text{g mL}^{-1}$, $200\ \mu\text{g mL}^{-1}$, $500\ \mu\text{g mL}^{-1}$ and $1000\ \mu\text{g mL}^{-1}$) were prepared by series dilution of $2000\ \mu\text{g mL}^{-1}$ of HSA solution with 50 mM Tris-HCl buffer pH 7.5 and a calibration curve was constructed by measuring the absorbance at 280 nm using a Uvikon 922 Spectrophotometer.

Twenty milligrams of magnetic anion exchanger DEAE or unfunctionalized adsorbents were equilibrated twice with 1.5 mL of Tris-HCl buffer pH 7.5 for 30 minutes. The adsorbents were magnetically collected, transferred into 1 mL of $10\ \mu\text{g mL}^{-1}$ HSA solution and incubated at room temperature in an Eppendorf Thermomixer comfort (Eppendorf UK Ltd., Cambridge, UK) at 2000 rpm. After 30 minutes, the supernatant was separated from the support with the aid of a magnetic rack Chemagic Stand 50k magnetic rack (Chemagen Biopolymer-Technologie AG, Baesweiler, Germany) and the unbound HSA was calculated by measuring the absorbance at 280 nm using an Uvikon 922 Spectrophotometer and comparing to pre-prepared standard curves. Then, the above HSA binding procedure was repeated sequentially using each following HSA concentration: $10\ \mu\text{g mL}^{-1}$, $20\ \mu\text{g mL}^{-1}$, $20\ \mu\text{g mL}^{-1}$, $50\ \mu\text{g mL}^{-1}$, $50\ \mu\text{g mL}^{-1}$, $100\ \mu\text{g mL}^{-1}$, $100\ \mu\text{g mL}^{-1}$, $200\ \mu\text{g mL}^{-1}$, $200\ \mu\text{g mL}^{-1}$, $500\ \mu\text{g mL}^{-1}$, $500\ \mu\text{g mL}^{-1}$, $1000\ \mu\text{g mL}^{-1}$, $1000\ \mu\text{g mL}^{-1}$ and $2000\ \mu\text{g mL}^{-1}$.

Following incubation with $2000\ \mu\text{g mL}^{-1}$ HSA solution, the protein loaded adsorbents

were washed once with equilibration buffer and then eluted with 1.2 mL of elution buffer (composed of 50 mM Tris-HCl buffer pH 7.5 containing 1M NaCl) for 30 minutes. The adsorbents were magnetically separated from the supernatant and the concentration of HSA eluted from the adsorbents was determined as above. Elution was repeated for a further three times before the adsorbents were striped twice with 1.2 mL of 50 mM Tris-HCl buffer pH 7.5 containing 1M NaOH. The concentration of HSA striped from the adsorbents was determined as above.

The binding isotherms were fitted to the Langmuir model (see equation 4.2) using the Sigma Plot version 11.0 software (Systat Software Inc, CA, USA).

$$Q^* = Q_{\max} \frac{C^*}{K_d + C^*} \quad (4.2)$$

where, Q^* is the amount of protein adsorbed on per gram of adsorbents; Q_{\max} is the maximum binding capacity. C^* is the liquid phase protein concentration at equilibrium condition and K_d is dissociation constant.

4.3.4 Analytical techniques

4.3.4.1 Particle sizing techniques

4.3.4.1.1 Dynamic light scattering (DLS)

The particle size of magnetic iron oxide crystals in ferrofluids was analyzed as described in section 3.3.3.1.1.

4.3.4.1.2 Low angle light scattering technique

Particle size distributions of magnetic ion exchange adsorbents and unfunctionalized magnetic particles were measured with a Mastersizer 2000 (Malvern Instruments Ltd, Malvern, UK) in the same manner as it has been introduced in section 3.3.3.1.2. The refractive index of water and magnetite were set at 1.33 (Polyanskiy, 2011) and 2.42 (Steitz *et al.*, 2007) respectively. Refractive index of 1.49 was assumed for the anion exchanger DEAE polymer matrix⁹. Therefore, the refractive indexes of magnetic anion exchanger DEAE and unfunctionalized adsorbents could be set as the calculation according to the equation 3.2 in Chapter 3.

4.3.4.2 Specific surface area measurement

Magnetic ion exchange adsorbents and unfunctionalized magnetic particles were critical point dried (see 3.3.3.2.2) prior to being analyzed for their specific surface area as described in section 3.3.3.3.

4.3.4.3 Vibrating Sample Magnetometry (VSM)

The magnetic properties of TMAOH coated ferrofluid, the magnetic ion exchange adsorbents and unfunctionalized magnetic particles were measured as described in

¹⁰ No value for this specific polymer could be found from available databases. However, the refractive indexes of most transparent plastic/polymer materials fall within a narrow range of 1.47-1.57 with most lying between 1.48-1.52 (Polyanskiy, 2011). Therefore, the refractive index of 1.49 set for poly(acrylamide-co-ethylenebisacrylamide) was employed here.

section 3.3.3.6.

4.3.4.4 Scanning Electron Microscopy (SEM)

The magnetic ion exchange adsorbents were prepared and imaged as described in section 3.3.3.7.

4.3.4.5 Transmission Electron Microscopy (TEM)

The cross-sections of magnetic ion exchange adsorbents were prepared and imaged as described in section 3.3.3.8. Samples of TMAOH coated ferrofluid were also imaged by TEM in the same manner after drying at room temperature for 30 minutes.

4.3.4.6 Determination of ionic capacity of magnetic anion exchange adsorbents

The method used to determine the total ionic exchange capacity of the supports used in this study, was taken from Theodossiou and Thomas (2002). Routinely, 2 mL (settled volume) of magnetic anion exchanger DEAE, StreamlineTM QXL (Amersham Pharmacia Biotech, Uppsala, Sweden) and unfunctionalized adsorbents were respectively incubated with 50 mL of 2 M NaCl for 90 minutes and then washed three times on a glass sinter with 50 mL double distilled water, before transferring the drained materials to 100 mL plastic bottles containing 50 mL of 0.1 M NaOH and mixing at 150 rpm for 24 h on an orbital shaker (IKA[®]-Werke GmbH, Staufen, Germany). The adsorbents were magnetically settled (gravitationally settled for

Streamline™ QXL) and then, 1 mL of the liquid phase from each sample was taken for chloride ion content determination using the assay described by Vogel (1989). The assay for the concentration of Cl⁻ ions present in the sample is based on following reaction:



The displacement of thiocyanate ions from mercury thiocyanate by Cl⁻ ions in samples in the presence of ferric ions forms iron^{III} thiocyanate complex, which yields intense yellow colored solution. The assay was performed as following: a standard curve was prepared by dilution of 10 mM NaCl stock solution to produce 1 mL of various concentrations (0, 0.1, 0.2, 0.4, 0.6, 0.8 and 1.0 mM) of NaCl. One milliliter of the liquid phase of each sample and 1 mL of the various NaCl concentrations were added in 2 mL plastic screw-capped vials. One hundred microlitres of 0.25 M ammonium iron^{III} sulphate in 9 M HNO₃ and 100 µL of a saturated solution of mercury^I thiocyanate in 96% ethanol were added into each vial. Following vigorous mixing on an Eppendorf Thermomixer comfort (Eppendorf UK Ltd., Cambridge, UK) at 2000 rpm for 10 minutes at room temperature, the chloride ion contents in the liquid phases were determined from absorbance measurements at 460 nm conducted in an Uvikon 922 Spectrophotometer (Kontron Instruments, Bletchley, UK).

4.4 Results and discussion

4.4.1 'One-pot' synthesis of magnetic anion exchange DEAE adsorbents

4.4.1.1 Magnetic properties

The magnetic properties of the anion exchange DEAE and unfunctionalized adsorbents were evaluated with a Vibrating Sample Magnetometer and saturation magnetization values of $13.8 \text{ A m}^{-2} \text{ kg}^{-1}$ and $11.9 \text{ A m}^{-2} \text{ kg}^{-1}$ were recorded respectively, when samples were magnetized between ± 2.0 Tesla under an externally applied magnetic field at room temperature. The magnetite contents for both anion exchange and unfunctionalized adsorbents are approximately equal (18% and 15.5% (w/w) respectively¹⁰). Furthermore, both batches exhibited superparamagnetic behaviour, because neither magnetic remanence nor magnetic coercivity could be detected during support magnetization (see Fig. 4.1).

³ The saturation magnetization of the pure magnetite in nanosized crystal form is $76.6 \text{ A m}^{-2} \text{ kg}^{-1}$ (see section 3.4.3).

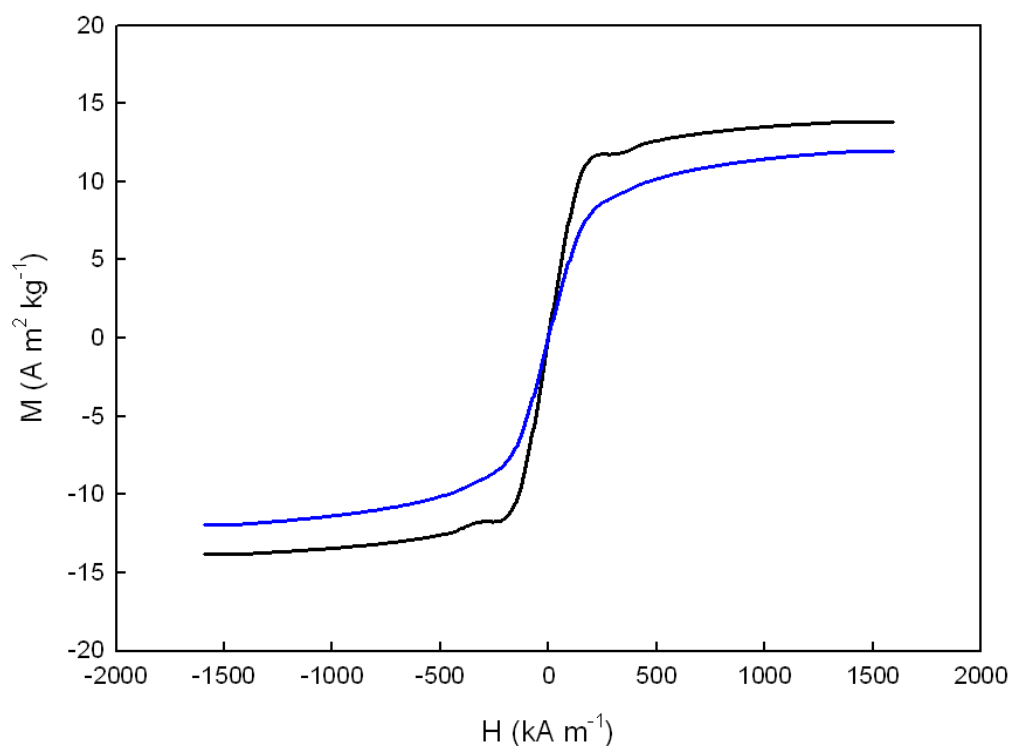


Figure 4.1 Hysteresis curves of magnetic adsorbents (blue curve: unfunctionalized adsorbents; black curve: magnetic anion exchanger).

4.4.1.2 Particle size distribution and specific surface area

Particle size distribution of the anion exchange and unfunctionalized adsorbents was carried out with Malvern Mastersizer 2000. The results of the particle size distribution and the specific surface areas of the anion exchange and unfunctionalized adsorbents are presented in Table 4.4.

Table 4.4 Results of particle size distribution and specific surface area for anion exchange and unfunctionalized magnetic adsorbents.

Type of adsorbent		Anion exchange	Unfunctionalized
Agitation speed (rpm)		5000	5000
Monomer		DEAE/HEA (1/1; mol/mol)	AM
Magnetite loading (mg)		500	500
Arlacel [®] 83 surfactant (mg)		400	400
M_s ($\text{Am}^2 \text{ kg}^{-1}$)		13.8	11.9
Magnetic content		18%	15.5%
Refractive Index		1.6574	1.6342
Particle size distribution (μm)	d(10)	2.5	2.6
	d(50)	3	3.7
	d(90)	3.7	8.4
Sauter diameter (μm)		3	3.7
Specific surface area ($\text{m}^2 \text{ g}^{-1}$)		4	2.5

4.4.1.3 Particle morphology study

The morphology of the anion exchange adsorbents and their unfunctionalized counterparts were studied with SEM at 5 kV and as can be seen from Fig. 4.2, spherical particles with relatively rough surfaces were created in both cases. Furthermore, the cross-sectional area of the supports was visualized under TEM at 80 kV (Fig. 4.3) to ensure that a uniform distribution of the magnetic crystals was achieved within the particles.

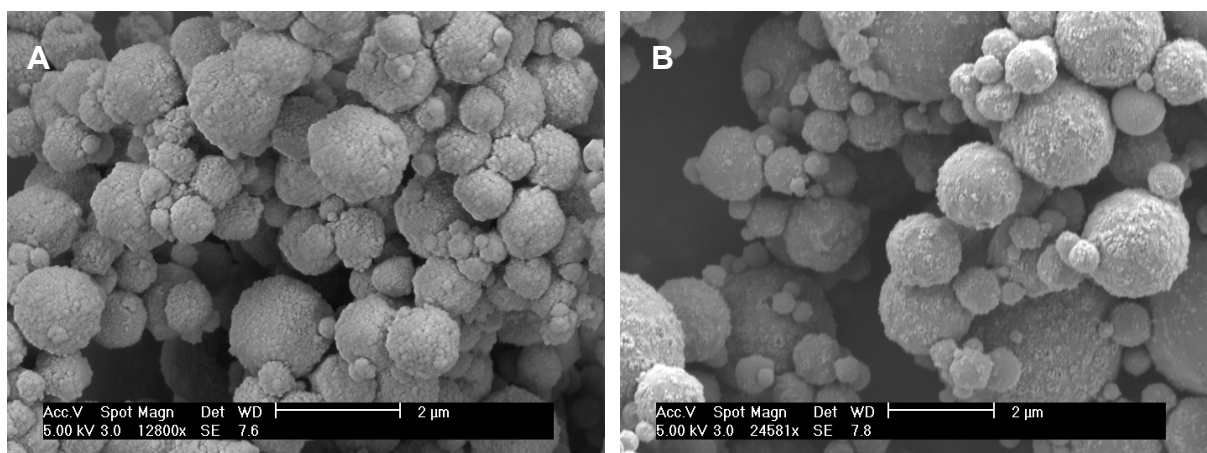


Figure 4.2 Electron micrographs of the magnetic particles following sputter coating of the samples with platinum (A: magnetic anion exchangers; B: unfunctionalized).

Although magnetic crystals seem to be present throughout the supports, there seems to be a certain extent of agglomeration within both adsorbents. This could be attributed to the removal of the surfactant during the long-term storage of the ferrofluid used. Following the same mechanism as the poly(acrylic acid) coated ferrofluid described in Chapter 3, the carboxylic part of the poly(methacrylic acid) can interact strongly with both hydroxyl groups on the magnetite surface and also the aqueous carrier liquid. Over long periods of time, the carrier liquid can diffuse through the hydrophobic layer and interact with magnetite surface hydroxyl groups interacted carboxyl groups. This thus results in the removal of the poly(methacrylic acid) from the magnetite and exposing a naked surface. These naked magnetite surfaces tend to agglomerate and form clusters; which are subsequently poorly dispersed within the monomer droplets leading to partially uneven distribution in the final adsorbents.

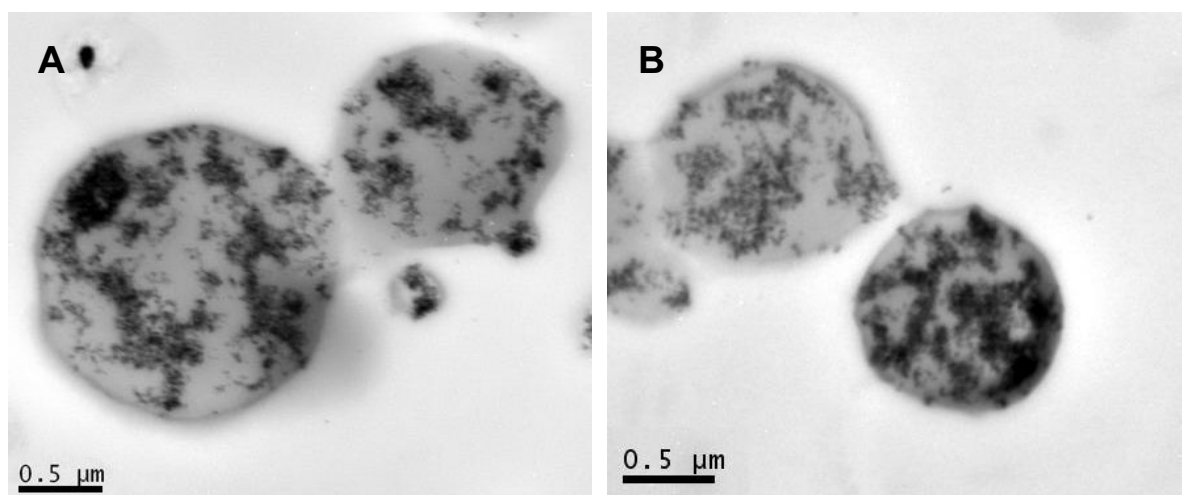


Figure 4.3 Cross section TEM images of the magnetic adsorbents (A: anion exchangers; B: unfunctionalized).

4.4.1.4 Ionic capacity of the magnetic anion exchange adsorbents

The ionic capacity of the, DEAE anion exchangers was determined using Streamline™ QXL and unfunctionalized supports as positive and negative controls respectively. All three types of adsorbents were first washed with NaCl to convert them into the hydrochloride salt or quaternary alkyl ammonium chloride form, and then incubated with excess NaOH, to displace their chloride ions (see Fig. 4.4; Harris and Angael, 1989). The displaced chloride ions content was determined using the assay described by Vogel (1989), and the standard curve is presented in Appendix 6.2

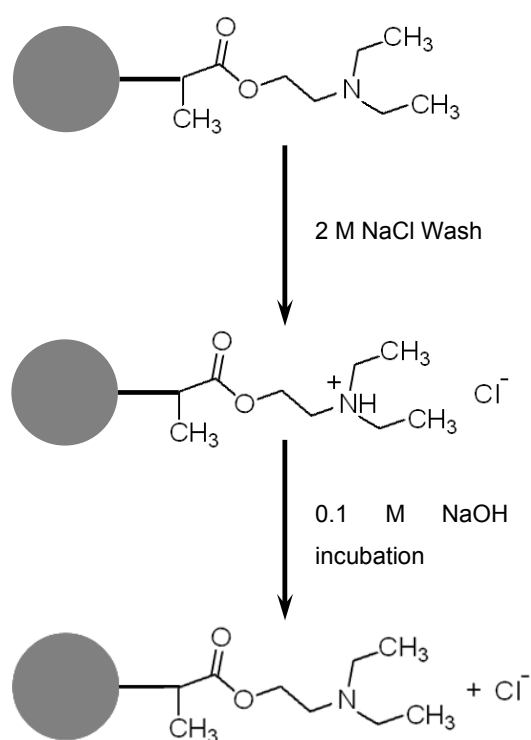


Figure 4.4 Schematic diagram of determination of anionic exchange capacity (reproduced from Pitfield, 1992).

The measured ionic capacity of the Streamline™ QXL was $239.6 \mu\text{mol Cl}^- \text{ mL}^{-1}$ adsorbent, which falls within the range quoted in the Product Certificate of Analysis ($230\text{--}330 \mu\text{mol Cl}^- \text{ mL}^{-1}$ adsorbent; Amersham Pharmacia Biotech, 1999). The magnetic anion exchanger DEAE had an ionic capacity of $33.9 \mu\text{mol Cl}^- \text{ g}^{-1}$ adsorbent compared to $2.8 \mu\text{mol Cl}^-$ per gram of the unfunctionalized adsorbent (see Table 4.5). The small amount of Cl⁻ ions detected on the unfunctionalized adsorbent could be attributed to experimental error.

Table 4.5 Ionic exchange capacities of the Streamline™ QXL; the magnetic anion exchanger DEAE and the unfunctionalized adsorbent.

Adsorbents	Density (mg mL ⁻¹)	μmol Cl ⁻ mL ⁻¹ adsorbents	μmol Cl ⁻ g ⁻¹ adsorbents
Streamline™ QXL	230.8	239.6	1038.2
Magnetic DEAE	41.5	1.4	33.9
Unfunctionalized	74.3	0.2	2.8

4.4.1.5 Human serum albumin binding and elution study

Protein binding and elution studies were carried out using anion exchange and unfunctionalized magnetic adsorbents and human serum albumin in Tris-HCl binding buffer, pH 7.5, as the target molecule. HSA was chosen because not only is a widely employed model protein but it is also acidic with an isoelectric point (pI) of 4.7 (Ortega-Vinuesa and Lundström, 1998; Nayak and Shin, 2008), and carries an overall negative charge in the above binding conditions.

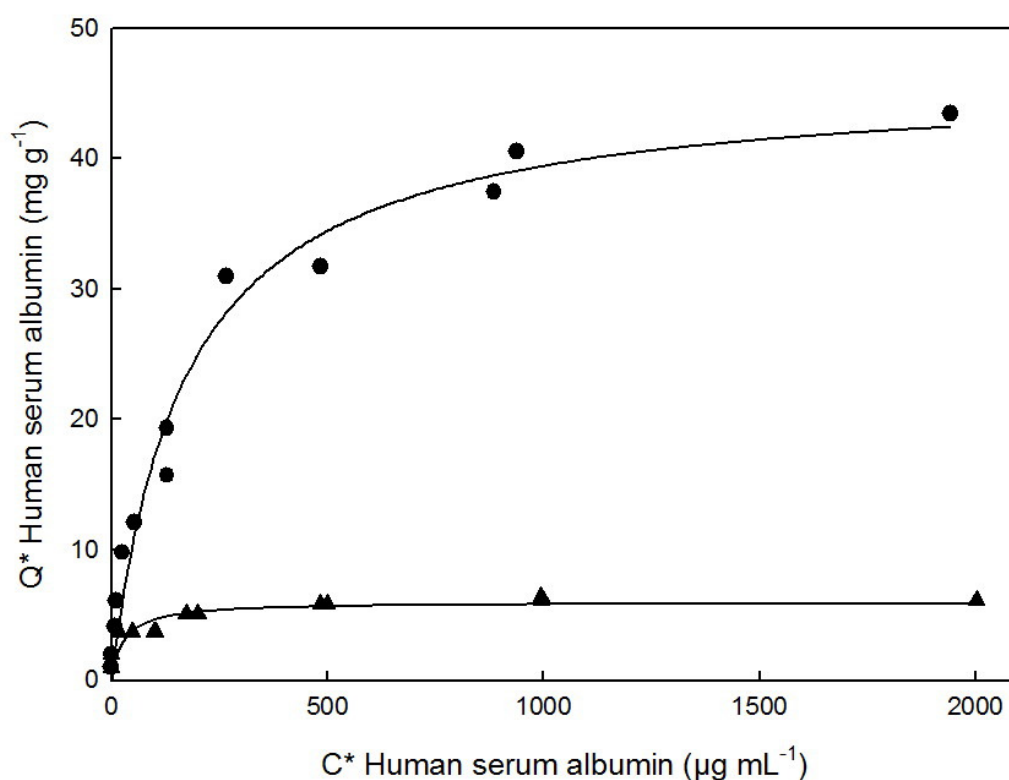


Figure 4.5 Equilibrium binding isotherms for HSA to magnetic anion exchange DEAE and unfunctionalized adsorbents. The solid lines through the data represent the fitted Langmuir curves with the parameter values quoted in Table 4.6.
 Legend: DEAE (circles); unfunctionalized (up triangles).

Table 4.6 Langmuir constants for the curves fitted in Figure 4.5

Adsorbents	Q_{\max} (mg g ⁻¹)	K_d (μM)	Initial slope, Q_{\max}/K_d (L g ⁻¹)
Magnetic anion exchanger DEAE	46.1	2.52	0.27
Unfunctionalized	6	0.43	0.20

According to Fig. 4.5 and Table 4.6, the magnetic anion exchanger exhibited much better higher adsorption towards the target protein than the unfunctionalized support, with a maximum binding capacity (Q_{\max}) of 46.1 mg g⁻¹. The unfunctionalized support

had a lower dissociation constant (K_d) of 0.43 μM , and a very low binding capacity of 6 mg g^{-1} . The tightness of protein binding (Q_{max}/K_d), which is reflected by the initial slope of the isotherm, was similar for both the functionalised and unfunctionalized supports and was calculated as 0.27 L g^{-1} and 0.2 L g^{-1} respectively. In section 4.3.1.1, a low molecular weight probe (octane) was used to determine the specific surface area of the magnetic anion exchanger and a value of 4 $\text{m}^2 \text{g}^{-1}$ was quoted. Human serum albumin is very much larger than octane and therefore the surface area that it is likely to access will be significantly less than 4 $\text{m}^2 \text{g}^{-1}$. In theory, the maximum surface concentrations for globular proteins adsorbed in side-on orientation range from approximately 1.5 to 8 mg m^{-2} depending on the precise size and shape of the molecule, but in practice, the measured plateau values for globular proteins are *ca.* 2 mg m^{-2} (Haynes and Nordes, 2004). The maximum binding capacity of 46.1 mg g^{-1} therefore equates to 5.8 monolayer equivalents of human serum albumin. Unlike affinity interactions, which require the target molecules to be in close contact with the binding sites, electrostatic interactions rely on long range forces and can act on the target molecule even when the adsorbent binding sites have been already occupied. This is a clear case of multilayer protein adsorption and has also been noted by other investigators using similar magnetic ion exchanger supports (Heebøll-Nielsen, 2002; Brown, 2009).

After one time of equilibration buffer wash for removal of very weakly interacted

protein, the elution studies of human serum albumin were investigated by incubation these protein loaded adsorbents in a strong salt concentration buffer with 1 M NaCl followed with stripping any retained protein with 1 M NaOH. Figure 4.6 shows a comparison of elution data for human serum albumin from two types of adsorbents, one magnetic anion exchanger DEAE, and another with control.

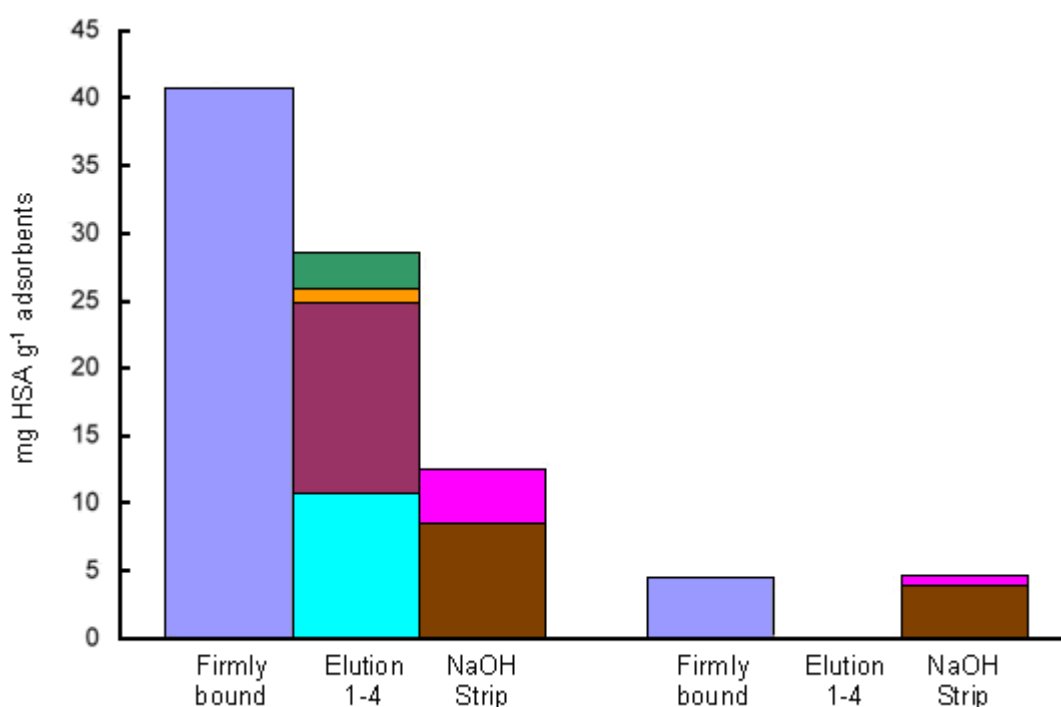


Figure 4.6 Comparison of human serum albumin elution data from magnetic anion exchange DEAE and unfunctionalized supports (columns 1-3: magnetic DEAE supports; columns 4-6: unfunctionalized supports).

Legend: Firmly bound (blue); Elution steps 1-4 (cyan, maroon, orange and green); NaOH strip steps 1 and 2 (brown and pink).

After the wash step, 40.65 mg and 4.43 mg of protein were still firmly bound to the magnetic anion exchanger and unfunctionalized support respectively; however, no

protein was eluted from the unfunctionalized support compared to 28.56 mg from the magnetic DEAE adsorbent. During the final stripping step, 12.59 mg and 4.73 mg of protein were recovered from the functionalized and unfunctionalized magnetic particles respectively. These results indicate that the main mode of protein binding to the anion exchanger is of electrostatic nature. However, subsequent deformation of the HSA, promoted additional hydrophobic interactions between the hydrophobic groups on the protein and the support surface, resulting in only 70.3% of the target molecule being eluted during four sequential elution steps. The low amount of protein bound to the unfunctionalized particles was most likely due to hydrophobic interactions, and as a consequence no protein was recovered during elution. For both supports, the HSA recovery was more than 100% (101.2% for magnetic DEAE and 106.7% for unfunctionalized particles) which can be attributed mainly to the experimental error during absorption measurements at 280 nm. The deformation of protein changed protein's shape, and subsequently influenced its adsorption at 280 nm of UV light. In addition, some adsorbents surface materials which also adsorb UV light at 280 nm wavelength were peeling off with protein when adsorbents were treated with 1 M NaOH solution. Therefore, both types of magnetic adsorbents are both obtained more than 100% of total HSA recovery rate.

4.4.2 'One-pot' synthesis of magnetic cation exchange adsorbents

4.4.2.1 Synthesis of magnetic cation exchange adsorbents with PMAA coated

ferrofluid

Magnetic cation exchange adsorbents were synthesized via the 'one-pot' manufacturing procedure, in which 2-acrylamido-2-methyl-1-propanesulfonic acid (SP) and acrylic acid (AA) respectively substituted AM as functional monomers in two different batches and formed composite adsorbents in the presence of EBA as cross-linker. PMAA coated ferrofluid formed the magnetic core in these preparations. As can be seen from Fig. 4.7, a substantial quantity of magnetite crystals remained firmly attached to the inside wall of the reactor in both preparations and the polymerization reaction failed to proceed as no polymeric beads were recovered from the reactor.

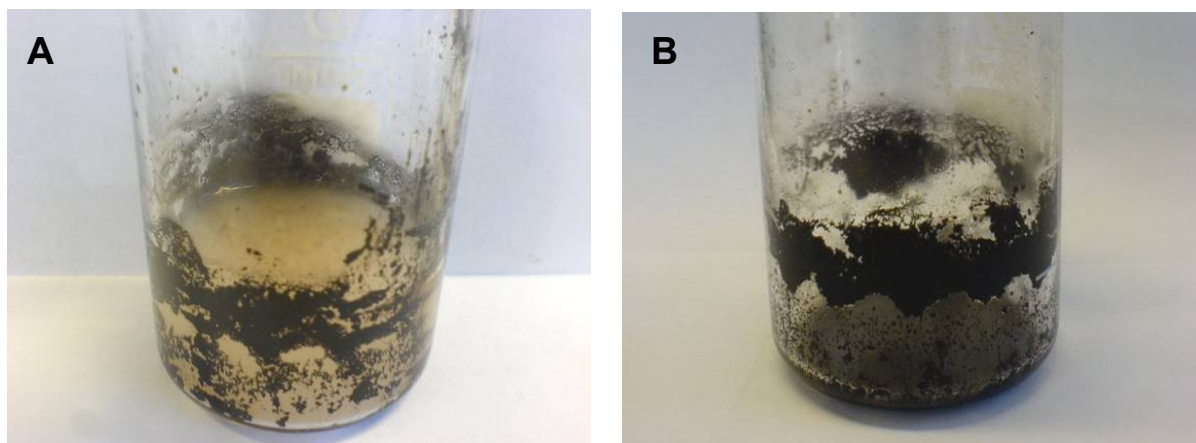


Figure 4.7 Photographs of magnetic crystals excluded from monomer droplets during the preparation of magnetic cation exchange adsorbents (A: the preparation with functional monomer AA; B: the preparation with functional monomer SP).

Both functional monomers used, namely AA and SP, are strong acids and in aqueous

solution they can be de-protonated and exist as COO^- and SO_3^- . As a result, the negatively charged monomer ions strongly repulsed the negatively charged magnetite crystals and caused their exclusion from the monomer droplets. Furthermore, the hydrophilic magnetite crystals could not be mixed with the hydrophobic continuous phase and they remained attached to the glass walls of the reactor. Clearly, negatively charged PMAA coated ferrofluid cannot be employed as is in the preparation of magnetic cation exchange adsorbents, but instead will need to be stabilized through the incorporation of positively charged materials, such as quaternary ammonium compounds.

In addition, in acidic monomer solution, the initiation of the radical polymerization reaction is usually inhibited by the protonation of activated initiator radicals. Thus, successful polymerization using acidic monomers must be carried out under neutral conditions or with monomers in saline form (Kriwet *et al.*, 1988; Wiechers and Schmidt-Naake, 2008).

4.4.2.2 Synthesis of magnetic cation exchange adsorbents with TMAOH coated ferrofluid

In further attempts to create magnetic cation exchangers, TMAOH coated ferrofluid was employed instead of PMAA. In this type of ferrofluid, the magnetite crystals are surrounded by hydroxide anions, and tetramethylammonium cations to create

electrostatic inter-particle repulsion in an aqueous environment (Berger *et al.*, 1999).

Two batches of magnetic cation exchange adsorbents were synthesized via the 'one-pot' manufacturing procedure, in which AA and SP were respectively employed as functional monomers. The monomer solutions were neutralized with 8M NaOH prior to ferrofluid addition and mixed with the continuous phase.

Following polymerization and six wash steps (see Table 4.2), the two magnetic cation exchangers, namely MCEX-AA and MCEX-SP, could not to be magnetically separated when transferred into double distilled water (see Fig. 4.8) and therefore were recovered via centrifugation.

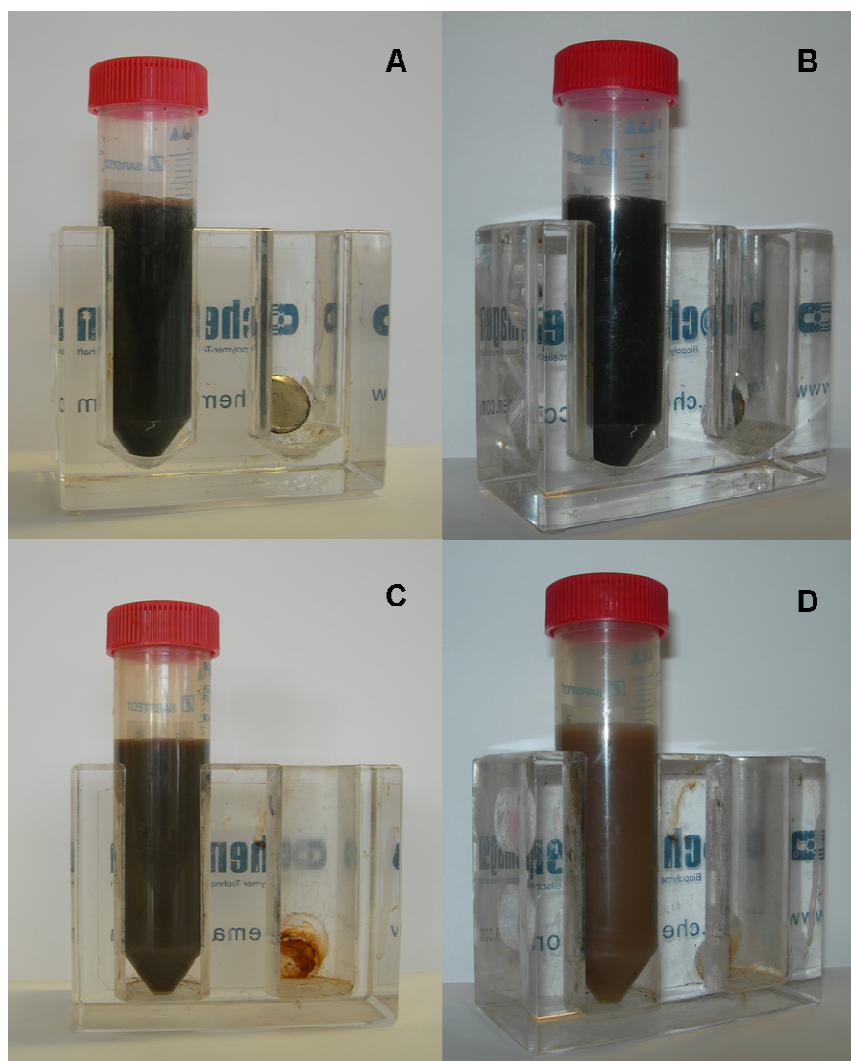


Figure 4.8 Magnetic collection of magnetic cation exchange adsorbents (A: start of magnetic collection of MCEX-AA; B: after 2 hours of application of an external magnetic field; C: start of magnetic collection of MCEX-SP; D: after 2 hours of application of an external magnetic field).

4.4.2.2.1 Particle morphology

The resulting cation exchange adsorbents were further analyzed with SEM at 5 kV and their images are presented in Fig. 4.9. Although both preparations resulted in spherical particles, loose magnetite crystals were visualized on the support surfaces

indicating partial encapsulation failure.

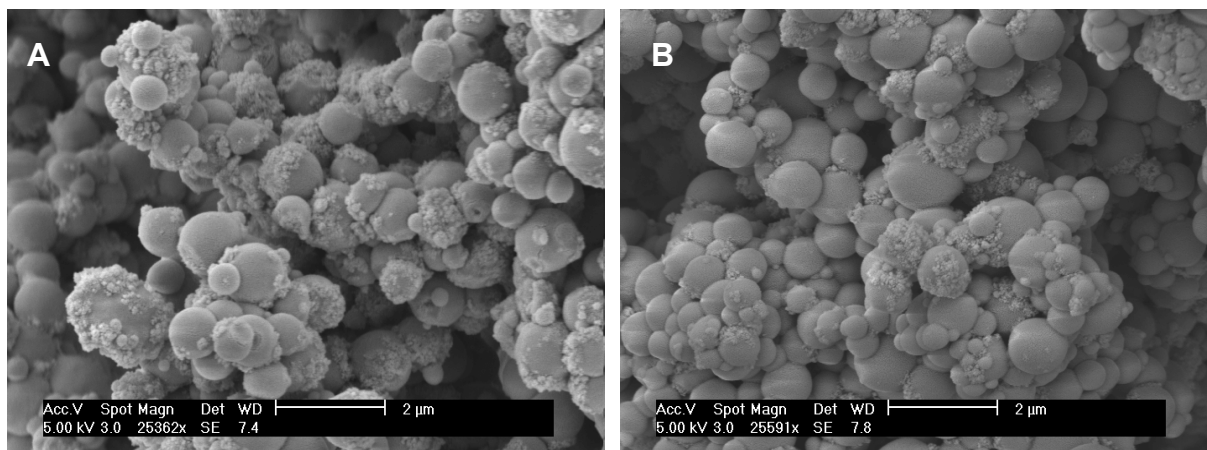


Figure 4.9 SEM images of cation exchange adsorbents after sputter coating the samples with platinum (A: MCEX-AA; B: MCEX-SP).

4.4.2.2.2 Magnetic properties

A completed hysteresis loop (see Fig. 4.10) was recorded for both magnetic cation exchangers by sweeping the external magnetic field between ± 2.0 Tesla at room temperature. The following saturation magnetization (M_s) values were determined for MCEX-SP and MCEX-AA respectively: $11.9 \text{ A m}^2 \text{ kg}^{-1}$ and $12.5 \text{ A m}^2 \text{ kg}^{-1}$, and even though both numbers are in the normal range, they are mostly due to the loose magnetite crystals, present on the support surface and therefore, the adsorbents do not actually exhibit sufficient magnetic susceptibility.

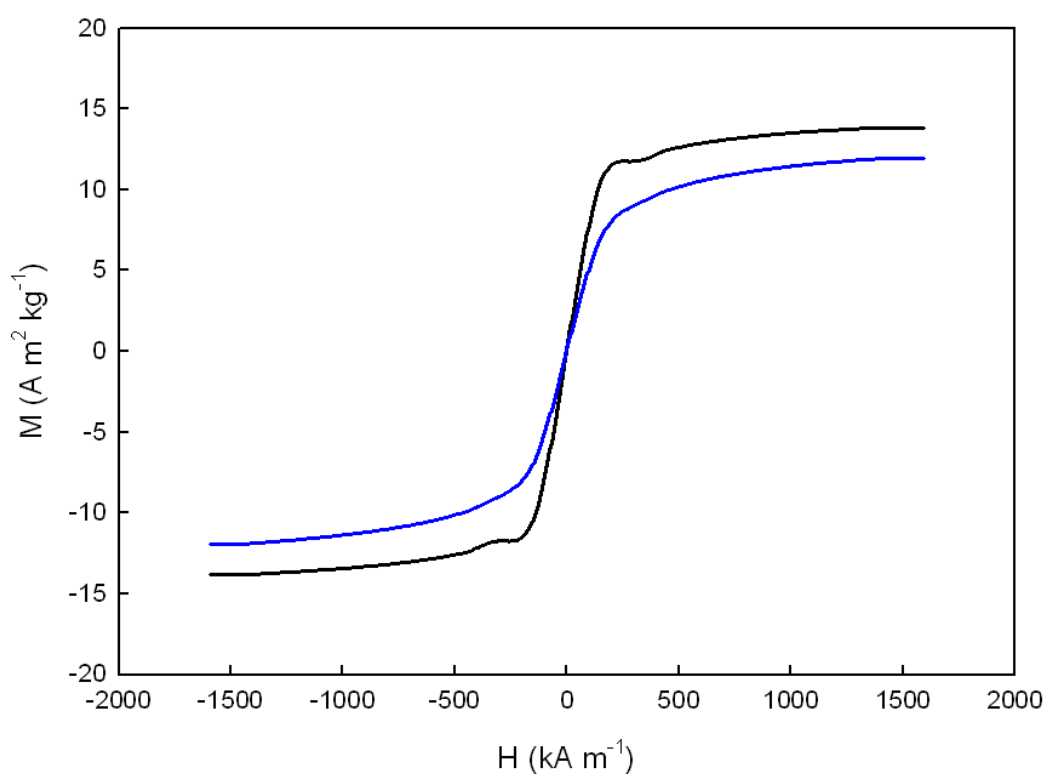


Figure 4.10 Hysteresis curves of cation exchange adsorbents (black curve: MCEX-AA; blue curve: MCEX-SP).

4.4.2.2.3 Characterization of tetramethylammonium hydroxide (TMAOH) coated ferrofluid

As can be seen from Fig. 4.11, a large quantity of the TMAOH coated magnetite crystals has settled at the bottom of the containers, indicating that they have not been properly stabilized.



Figure 4.11 Image of observation of TMAOH coated ferrofluid.

A classic superparamagnetic hysteresis loop (see Fig. 4.12A) was recorded by sweeping the external magnetic field between ± 2.0 Tesla at room temperature and resulted in $70.54 \text{ A m}^2 \text{ kg}^{-1}$ of saturation magnetization. The saturation magnetization of pure magnetite nano-sized crystals has been attested as $76.6 \text{ A m}^2 \text{ kg}^{-1}$ (see section 3.4.3), thus the magnetic content of this TMAOH coated ferrofluid can be calculated as 92.08%, or, in another words, only 7.92% (w/w) of this ferrofluid is TMAOH. Furthermore, the particle size distribution of the ferrofluid was measured as 450 nm, which is substantially larger than the stabilized magnetite crystal size (about 30 nm). In addition, big clusters of particles were observed in the TEM image instead of individual magnetite crystals (see Fig. 4.12B). It was therefore concluded that the

magnetite crystals in the ferrofluid used were not successfully stabilized with tetramethylammonium cations rendering this TMAOH coated ferrofluid preparation unsuitable for the synthesis of magnetic cation exchange adsorbents via the ‘one-pot’ manufacturing procedure.

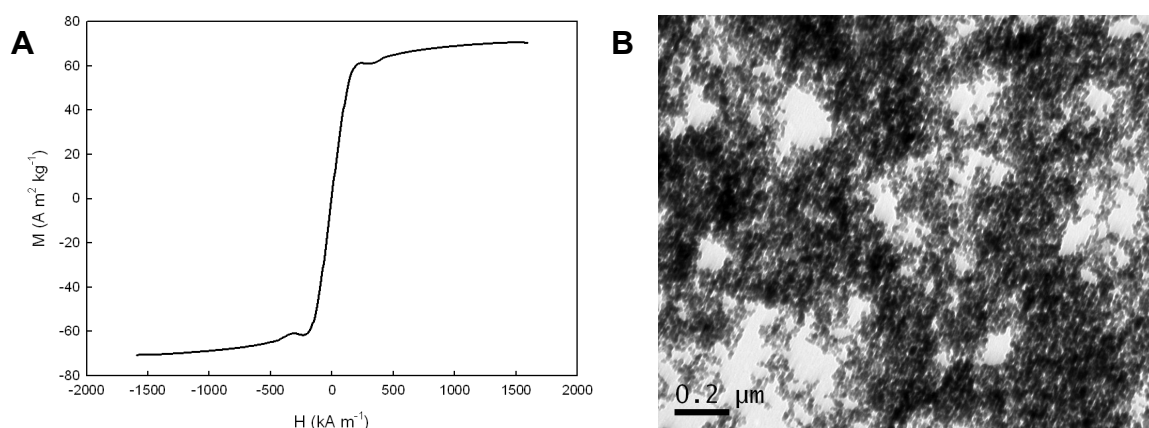


Figure 4.12 A: hysteresis curve of TMAOH coated ferrofluid; B: TEM image of TMAOH coated ferrofluid at 80 kV.

4.5 Conclusions

This chapter introduced a simple, fast and scaleable ‘one-pot’ manufacturing route to cheap magnetic adsorbents for bioprocessing, which involves incorporating coated ferrofluids into inverse emulsion polymerization reactions performed under high shear stress. Anion exchanger (DEAE) and two types of cation exchangers (COO^- and SO_3^-) were synthesized and characterized in terms of physical properties (i.e. particle size, specific surface area, magnetic properties and morphology), as well as ionic capacity and protein binding and elution performance.

The anion exchange supports were with a mean particle size of 3 μm and a specific surface area of 4 m^2g^{-1} , exhibited superparamagnetic behaviour (M_s : 13.8 $\text{A m}^{-2}\text{kg}^{-1}$; magnetic content: 18% w/w), and had an ionic capacity of 34 $\mu\text{mol Cl}^{-}\text{g}^{-1}$. Using human serum albumin as a model binding species, the adsorbents displayed multilayer binding ($Q_{\text{max}} = 46\text{ mg g}^{-1}$ adsorbent and $K_d = 2.52\text{ }\mu\text{M}$) and all of the protein was recovered during elution. However, the HSA binding capacity was 2.4-fold lower compared to the protein binding capacity of DEAE derivatized magnetic adsorbents using bovine serum albumin as a model binding species ($Q_{\text{max}} = 111\text{ mg g}^{-1}$ and $K_d = 0.49\text{ }\mu\text{M}$; Heebøll-Nielsen *et al.*, 2004). The lower binding capacity and interaction strength observed for the magnetic DEAE based anion exchanger in this work most likely reflects the much lower available surface area for capture possibly combined with a reduced ligand density of surface compared to the much rougher surfaced magnetic anion exchanger described by Heebøll-Nielsen and coworkers (2004).

In the preparation of magnetic cation exchange adsorbents, PMAA coated ferrofluid could not be dispersed into monomer droplets, because of the electrostatic repulsion between the negatively charged magnetite crystals and the functional monomer. The strong acidic nature of both types of cationic functional monomers used in this work resulted in protonation of initiator radicals, and consequently inhibited the development of the polymerization reaction. Thus, the monomers need to be

neutralized before the start of the reaction, or used in their saline form. Finally, even though positively charged tetramethylammonium hydroxide (TMAOH) coated ferrofluid was also employed for the manufacture of magnetic cation exchangers, the unstable nature of this particular ferrofluid preparation resulted in poor magnetic particle encapsulation and thereby the final adsorbents created suffered from insufficient magnetic susceptibility.

5. Concluding remarks

At the present rate of progress it is realistic to envisage commercial High-Gradient Magnetic Fishing, Magnetically Enhanced Press Filtration and Magnetically Enhanced Centrifugation systems arising within the next 10 years. Recognition of the potential of and recent progress in magnetic field assisted techniques within the bioprocessing arena has created the need to manufacture low cost 'suitable' magnetic adsorbents in process-scale quantities. However, thus far most methods for manufacturing commercially available magnetic adsorbents rely on the use of overly complex and costly techniques and protocols, which are only capable of delivering very small quantities of appropriate support materials. Against this background, the development of a simple, cheap, fast and scaleable 'one-pot' manufacturing route for production of magnetic supports appropriate for the purification of biological macromolecules, is seen as mandatory and urgent.

The feasibility of a 'one-pot' manufacturing route was initially investigated in the absence of magnetic material (Chapter 2) using an inverse liquid-liquid two phase polymerization method employing 'ammonium persulphate/ N,N,N',N'-tetramethylethylenediamine' as the initiator/accelerator system and 'Arlacel[®] 83/Isopar M' as the continuous phase. The particle size of the non-magnetic beaded poly(acrylamide-co-ethylenebisacrylamide) supports produced was shown to be readily controlled by adjusting the agitation speed during emulsification. The

rotor-stator type high shear mixing equipment employed in this work was selected because of its commercial availability in a wide range of working capacities; thus linear scale up of agitation/mixing conditions from bench to industrial scales should be relatively straightforward.

Subsequently various different magnetic core materials (naked fine particle magnetite and three different coated ferrofluids) were incorporated in 'one-pot' support manufacturing reactions employing two different initiator and continuous phase combinations (Chapter 3). Based on uniformity of dispersion of magnetic elements within molten monomer droplets (and resulting solidified support beads), and magnetic properties, the best magnetic support materials were made in 'one-pot' reactions performed with a poly(methacrylic acid) coated ferrofluid, 1,1'-azobis(cyclohexanecarbonitrile) as initiator, and Arlcel[®] 83/cyclohexane as the continuous phase.

Optimal conditions identified in Chapter 3 for 'one pot' manufacture of magnetic beaded poly(acrylamide-co-ethylenebisacrylamide) supports were finally adapted to the production of magnetic ion exchange adsorbents (Chapter 4), by replacing the neutral acrylamide monomer with different functional monomers, namely: 2-(diethylamino)ethyl methacrylate (DEAE); acrylic acid (AA) and 2-acrylamido-2-methyl-1-propanesulfonic acid (SP). In the case of both magnetic

cation exchangers (COO^- and SO_3^-), incompatibility issues were encountered, which prevented the 'one-pot' manufacture of effective magnetic cation exchangers within the available time. No such problems we experienced with the DEAE linked magnetic adsorbent beads. The protein binding and elution behavior of these materials was examined using human serum albumin as a model target. Modest binding performance was found ($Q_{\text{max}} = 46 \text{ mg g}^{-1}$; $K_d = 2.5 \text{ }\mu\text{M}$) in keeping with the low surface area ($4 \text{ m}^2 \text{ g}^{-1}$) available for capture, and >70% of the target could be eluted with 1 M NaCl.

Future work on improving 'one-pot' manufacturing procedures for non-porous magnetic supports should be initially addressed at increasing their specific surface area, specifically by extending the agitation time before triggering polymerization; and employing more powerful mixing equipment; both measures designed to reduce the mean particle size of the magnetic adsorbents, and increase surface area. Once sufficiently high specific surface area is created research into the following would be merited:

- (i) 'one-pot' manufacture of immobilized metal affinity magnetic adsorbents (by replacing anionic functional monomer with e.g. 1-Vinylimidazole);
- (ii) 'one-pot' manufacture of molecularly imprinted supports;
- (iii) 'one-pot' manufacture of magnetic cation exchange adsorbents. This would most likely require changes to the initiator, the continuous phase and the

coated ferrofluid, to ensure mutual compatibility during both dispersion of coated ferrofluid crystals within negatively charged monomer droplets, and the polymerization reaction itself.

6. Appendix

6.1 A preliminary work toward surface molecularly imprinted adsorbents

6.1.1 Introduction

Molecular imprinting is defined as “The construction of ligands selective recognition sites in synthetic polymers, where a template (i.e. atom, ion, molecule, complex or a molecular, ionic or macromolecular assembly, including microorganisms) is employed in order to facilitate recognition site formation during the covalent assembly of the bulk phase by a polymerization, with subsequent removal of some or all of the template being necessary for recognition to occur in the spaces vacated by the templating species” (Alexander *et al.*, 2006; see Fig. 6.1).

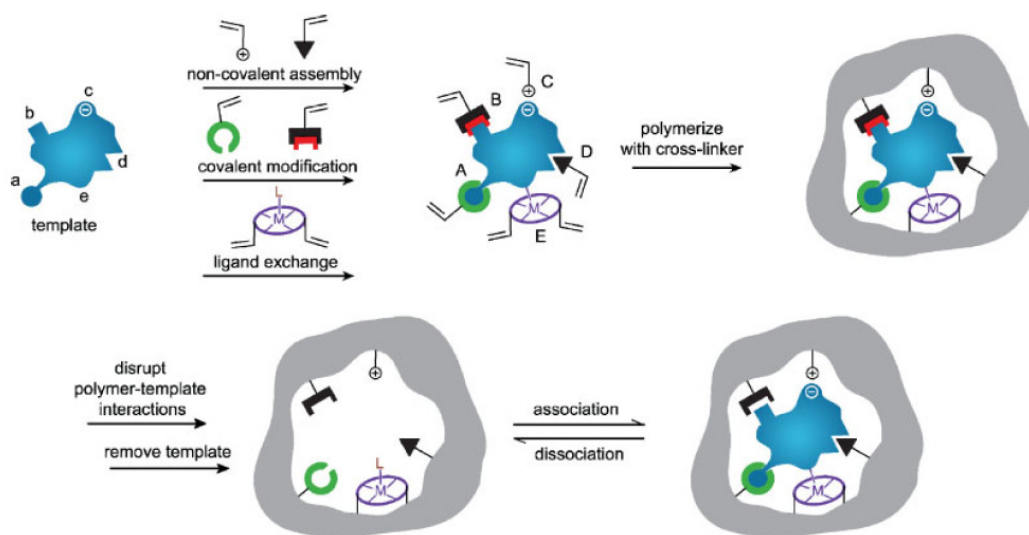


Figure 6.1 Schematic illustration of molecular imprinting process (A: reversible covalent interaction, B: semi-covalent method, C: electrostatic interaction, D: hydrophobic or van de Waals interactions, E: metal affinity interaction; taken from

Alexander *et al.*, 2006).

There are many important factors for producing molecularly imprinted adsorbents, namely, the template, functional monomers, matrix, cross-linking agents and the polymerization method. In which, the properties of the template molecule is most important as it decides the selection of functional monomer, cross-linking agents and the feasibility of the polymerization method (Cormack and Elorza, 2004). Mayes and Whitcombe (2005) introduced a large number of functional monomer and cross-linking agents which had been employed in molecular imprinting; and the polymerization methods of producing molecularly imprinted adsorbents were also systemically reviewed in literature (Pérez-Moral and Mayes; 2004).

Molecular imprinting has been shown to be very effective when targeting small molecules, such as oligopeptide (Hart and Shea, 2002), whereas there are intrinsic obstacles and limitations in the scale ability of traditional molecular imprinting from small biomolecules to biological macromolecules, and in particular proteins (Turner *et al.*, 2006; Bossi *et al.*, 2007). Molecular imprinting of proteins is a very challenging task. The reason for this could be found in several factors, which related to the properties of the protein templates. Firstly, proteins are water-soluble compounds that are not always compatible with mainstream molecular imprinting technology, which relies on using organic solvents for the polymer preparation. In addition, proteins have a flexible structure and conformation, which can be easily affected with environmental

condition (i.e. temperature or pH). These will result on selectivity loss in the imprinted selective binding cavities. In addition, the biggest obstacle is the high molecular size of protein leading to permanent entrapment. As a macromolecular, protein is difficult to reach (or leave) any formed binding site in cross-linked adsorbent matrix.

The first attempt to imprint protein by using a sequence-recognition approach was introduced by Kempe and co-workers (1995). Silica particle surface was derivatized with 3-(trimethoxysilyl)-propylmethacrylate, thus introducing double bonds, which were then used as anchorage points for the imprinting of template complex. The template protein, RNase A, was mixed with metal ions (Cu^{2+}) and with the functional monomer N-(4-vinyl-benzyl)-iminodiacetic acid (VBIDA) prior to imprinting. Imidazole groups (Im) of the two histidines exposed on the surface of the RNase A formed complexes with the metal coordination functional monomers, and subsequently creating complementary binding pockets for the recognition of the target protein after polymerization (see Fig. 6.2).

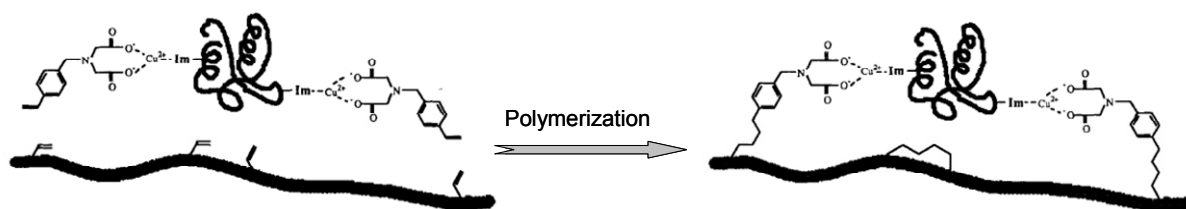


Figure 6.2 Schematic illustration of RNase A imprinting on silica surface derivatized with methacrylate groups (reproduced from Kempe *et al.*, 1995).

In order to familiar surface protein imprinting techniques toward manufacturing magnetic molecularly imprinted adsorbents, Kempe's surface metal coordination imprinting approach was firstly practiced with template molecule myoglobin from equine. Myoglobin from equine heart (see Fig. 6.3 A&B) has five surface exposed histidines, which can anchor with 4 transition metal ion ligands (2 closely spaced histidines, position 113 and 116, anchor with one transition metal ion legend; Wuenschell; 1990). Compared with 2 ligands bound RNase A, 4 ligands bound myoglobin template can form more firm binding, thus it could create highly selective binding pockets. Bovine pancreas α -chymotrypsinogen (see Fig. 6.3 C) with one surface exposed histidines was used as control.

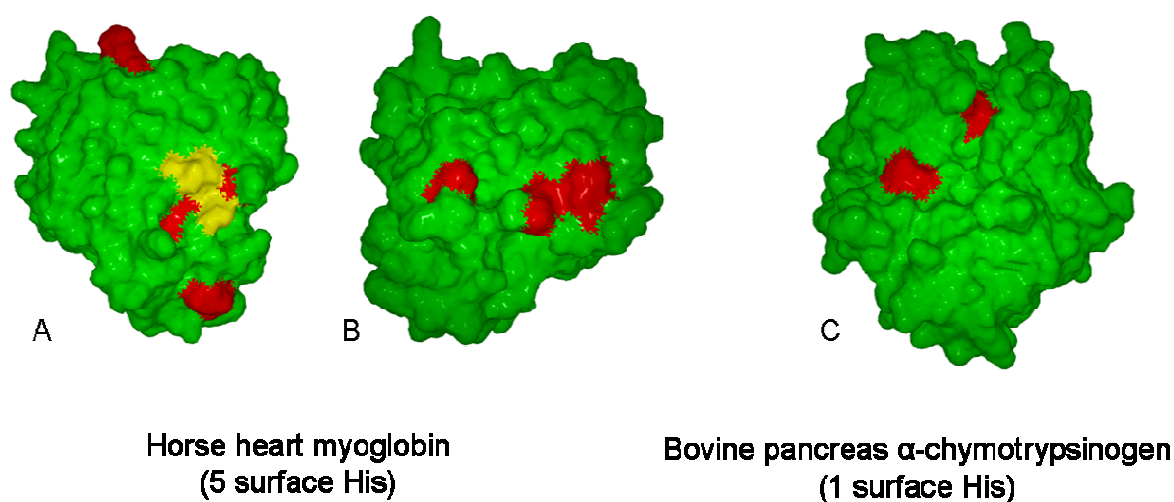


Figure 6.3 PDB Deepview surface images of myoglobin from equine heart and bovine pancreas α -chymotrypsinogen. The prosthetic group is marked in yellow while the surface His residues are highlighted in red. (A and B: front and back view of myoglobin from equine heart, C: bovine pancreas α -chymotrypsinogen).

6.1.2 Materials

Table 6.1 List of chemicals involved in this chapter

Chemical Name	Abbr.	Supplier	Description
Nucleosil 1000 Å	N.A.	Hichrom	Spherical silica particles, 10µm
3-(trimethoxysilyl)propyl methacrylate	N.A.	Sigma-Aldrich	Surface modification reagent
Ammonium persulfate	APS	Sigma-Aldrich	Initiator
N,N,N',N'-tetramethylethylenediamine	TEMED	Sigma-Aldrich	Accelerator
HEPES	N.A.	Sigma-Aldrich	Binding buffer reagent
4-vinylbenzyl chloride	N.A.	Sigma-Aldrich	N.A.
Iminodiacetic acid	N.A.	Sigma-Aldrich	N.A.
N,N-dimethylformamide	DMF	Sigma-Aldrich	Buffer
Copper ^{II} sulphate	N.A.	Sigma-Aldrich	N.A.
Diethyl ether	N.A.	Sigma-Aldrich	Extraction reagent
Ethylenediaminetetraacetic acid	EDTA	Sigma-Aldrich	Metal chelating agent
Hydrochloric acid	N.A.	Sigma-Aldrich	pH adjuster
Myoglobin from equine heart	Mb	Sigma-Aldrich	Binding modeling protein
α-chymotrypsinogen A from bovine pancreas	Chym	Sigma-Aldrich	Binding modeling protein

The double distilled water (CAS: 7732-18-5) used in this work was generated from a Hamilton water boiler (Hamilton Laboratory glass Ltd., Margate, UK). Nitrogen (CAS: 7727-37-9) was supplied by the BOC Group (Dudley, UK).

6.1.3 Experimental methods

6.1.3.1 Synthesis of N-(4-vinyl)-benzyl iminodiacetic acid (VBIDA)

Functional monomer N-(4-vinyl)-benzyl iminodiacetic acid was synthesized according to a protocol described by Morris *et al.* (1959). Routinely, 10.64 g of iminodiacetic acid and 5.28 g of NaOH were dissolved into 160 mL of water/ methanol mixture (1:1; v/v) in a 250 mL round bottom flask. The reactants were mixed by an axial stirrer in a water bath at 60°C. During the first 0.5 h, 5.72 g of 4-(vinylbenzyl) chloride was added

dropwise, whilst in the following 0.5 h another 5.72 g of 4-(Vinylbenzyl) chloride and 40 mL of 3.3 M NaOH were added dropwise. The product was subjected to vacuum evaporation of half of its volume in a rotavapor. The volume left was extracted twice with diethyl ether and the water phase was collected and adjusted to pH 2 with 37% HCl. After standing overnight, the white precipitations were washed by acidified water (pH 2) prior to be re-crystallised and dried in a desiccator. The structure of the synthesized VBIDA was confirmed by NMR (see 6.1.3.5.1).

6.1.3.2 Preparation of methacrylate-silica supports

The Nucleosil 1000Å was grafted with methacrylate groups according to the method described by Norrlof *et al.* (1984). Briefly, 0.4 g of 3-(trimethoxysilyl)propyl methacrylate was added into 40 mL of double distilled water, this mixture was then stirred (250 rpm) for 4 hours at room temperature to acquire a clear solution. This clear solution was added to 2 g of Nucleosil 1000Å particles in a round-bottomed flask and degassed under vacuum with ultrasound treatment for 5 minutes. The silanization was performed during 20 hours in a shaker water bath (160 rpm) at 50 °C. The final product was completely washed on paper filter and allowed to dry in a vacuum desiccator over night. The amount of methacrylate groups per gram of methacrylate silica supports was analyzed with Elemental Analysis technique (see 5.3.5.2).

6.1.3.3 Preparation of molecularly imprinted adsorbents

Molecularly imprinted adsorbents (MIPs) as well as non imprinted control particles

(NIPs) were produced following the protocol described by Kempe *et al.* (1995). Routinely, 4.4 mg of VBIDA, 2.8 mg of CuSO₄ and 1 g of methacrylate-silica supports were added to 4.7 mL of water/ DMF (7:3; v/v) in a round-bottomed flask. The solution was then purged by nitrogen for 30 minutes and followed with sonication for 600 s. Template molecule solution (40 mg of myoglobin in 2 mL of water/ DMF or 40 mg of α -chymotrypsinogen A in 2 mL of water/ DMF) was added into above solution. The solution was incubated at room temperature with magnetic stirring (150 rpm). After one hour, 0.1 mL of APS 10% (w/v) and 0.1 mL of TEMED 10% (v/v) were added, and the polymerization was carried with a stream of N₂ bubbling and magnetic stirring for 15 minutes. After incubation overnight at 4 °C with magnetic stirring, the imprinted adsorbents was washed by suspension, sedimentation and filtration (twice with each of the following solutions: water, 0.5M NaCl, water, 0.1M EDTA and finally water).

6.1.3.4 Batch protein binding and elution study

Preparation standard curve: Starting from a stock solution of 733 μg of myoglobin per millilitre of water/ DMF (7:3; v/v), a series of dilutions was made to give the following concentrations: 733 $\mu\text{g mL}^{-1}$, 366.5 $\mu\text{g mL}^{-1}$, 146.5 $\mu\text{g mL}^{-1}$, 73.3 $\mu\text{g mL}^{-1}$, 36.65 $\mu\text{g mL}^{-1}$, 14.66 $\mu\text{g mL}^{-1}$ and 7.33 $\mu\text{g mL}^{-1}$. A calibration curve was contrasted by measuring the absorbance of each concentration of myoglobin with UV spectrophotometry technique (see 5.3.5.3). A standard curve of α -chymotrypsinogen A was constructed in the same manner.

Batch protein binding and elution: Twenty milligram of each MIPs (myoglobin imprinted and α -chymotrypsinogen A imprinted adsorbents) and NIPs were charged with Cu^{2+} ions by suspending them in 1.5 mL of 50 mM CuSO_4 solution. The solution was incubated with shaking using an orbital shaker (IKA[®]-Werke GmbH, Staufen, Germany) at 1800 rpm for 0.25 h, and the procedure was repeated again. The supports were then equilibrated and washed from any unbound Cu^{2+} ions with 1.5 mL of water/ DMF (7:3; v/v) for 0.25 h twice. The Cu^{2+} charged MIPs and NIPs were respectively re-suspended with 1.5 mL of the lowest concentration myoglobin binding solution ($7.33 \mu\text{g mL}^{-1}$), and then mixed and incubated on the shaking plate at room temperature. After 0.5 h, the supernatant was centrifugally removed from the support and the concentration of the unbound protein was determined by using UV spectrophotometry technique (see 5.3.5.3). The above procedure was repeated sequentially by adding myoglobin solution of higher concentrations (till $733 \mu\text{g mL}^{-1}$). At the end of the protein binding procedure, the supports were washed with 1.5 mL of water/ DMF (7:3; v/v) for 0.25 h. The protein loaded supports were then washed with 1.5 mL of elution buffer composed of 20 mM HEPES, 0.5 M NaCl and 0.1 M EDTA in water/DMF. The supports were incubated for 0.5 h and then centrifugally separated. The elution procedure was repeated once. The concentrations of myoglobin in each elution were measured with UV spectrophotometry technique (see 5.3.5.3). The protein binding isotherm of each support was fitted to the Langmuir model (see

equation 4.2). Above binding and elution study was performed in the same manner by using α -chymotrypsinogen A as a model binding specie.

6.1.3.5 Analytical analysis

6.1.3.5.1 Molecule structure analysis of the synthesized VBIDA with NMR

A small amount of VBIDA was added into d_4 -methanol, and then 2 drops of NaOD D_2O solution were added into the above mixture to adjust the pH and help the VBIDA to dissolve. NMR analysis was carried out by Nuclear Magnetic Resonance DRX500 (Bruker Biospin GmbH, Germany).

6.1.3.5.2 Elemental analysis

Methacrylate group functionalized silica supports (1.5 mg) were measured and loaded in a small tin cylinder. The tin cylinder was squashed into a tiny globe to drive unnecessary air away. The sample contained small globe was then transferred into sample chamber and analyzed its elements with Elemental Analyser EA1110 (Carlo Erba Reagenti, Italy) at 1000°C.

6.1.3.5.3 UV spectrophotometry

The protein concentration was analyzed by measuring the absorbance of solutions at 525 nm (for myoglobin) or 280 nm (for α -chymotrypsinogen A) using an Uvikon 922 Spectrophotometer (Kontron Instruments, Bletchley, UK).

6.1.4 Result and discussion

6.1.4.1 Synthesis of N-(4-vinyl)-benzyl iminodiacetic acid (VBIDA)

Synthetic N-(4-vinyl)-benzyl iminodiacetic acid was analyzed its molecule structure with NMR. In the chemical shift, d_4 -methanol gets a signal at 3.3 ppm as reference. The NMR analysis result (see Fig. 5.4) is as follows: (4H, m, $-C_6H_4-$) δ 7.26-7.38; (1H_c, d, =H-) δ 6.68-6.74; (1H_b, d, CH₂-) δ 5.72-5.77; (1H_a, d, CH₂-) δ 5.2-5.22; (N-(CO₂Na)₂) δ 3.0, (2H, s, N-CH₂-) δ 3.62. Therefore, the synthesized monomer is the exactly same structure with VBIDA .

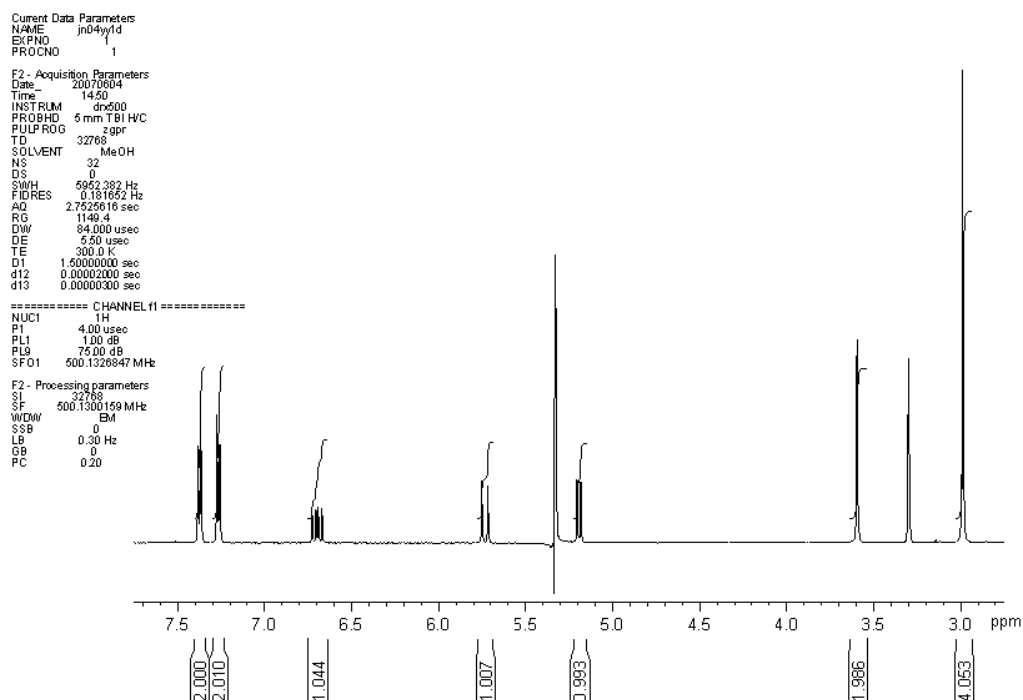


Figure 6.4 400-MHZ NMR spectrum of N-(4-vinyl)-benzyl iminodiacetic acid.

6.1.4.2 Elemental analysis

The molecule weight of methacrylate group ($C_7H_{11}O_2$) is 127 g mol^{-1} ; hence equivalent carbon element is 84 g mol^{-1} methacrylate group. The result of element analysis respectively detected 1.49% of carbon and 0.07% of hydrogen elements in the sample tested. Therefore, the concentration of methacrylate group per gram supports can be calculated as following:

$$\frac{84 \text{ g mol}^{-1}}{127 \text{ g mol}^{-1}} = \frac{1 \text{ g} \times 1.49\%}{X} \Rightarrow X = 0.023 \text{ gram methacrylate group per gram of supports};$$
$$\frac{0.023 \text{ g g}^{-1}}{127 \text{ g mol}^{-1}} \Rightarrow 177.38 \text{ } \mu\text{mol methacrylate group per gram of supports}$$

6.1.4.3 Protein batch binding

The binding isotherms of myoglobin and α -Chymotrypsinogen A onto MIPs and NIPs adsorbents in the presence and absence of Cu^{2+} were fitted to the Longmuir model using the Sigma Plot 11.0 software (Systat Software Inc, CA, USA; see Fig. 6.5-6.7.). The result shows that there is not a large difference in the binding behaviours between myoglobin, α -Chymotrypsinogen A imprinted support and NIP. Even in the absence of copper, all supports gave high binding. According to the above result, the binding behavior must be mainly attributed to non-specific interactions. In the absence of copper, the functional monomer VBIDA will expose two ionized carboxyl groups, which bring negative charge. The pH of binding buffer water/ DMF is about 6.03. If

considering the isoelectric point (pI) for the proteins, we can find that myoglobin has a pI of 7.2 and α -Chymotrypsinogen A has a pI of 9.1. Both of them are positively charged in the binding buffer (especially α -Chymotrypsinogen A has strong positive charge). Hence, the monomer VBIDA can strongly attract positive charged proteins. Therefore, the binding force is metal affinity in the presence of copper ions and electrostatic interactions in the absence of copper ions.

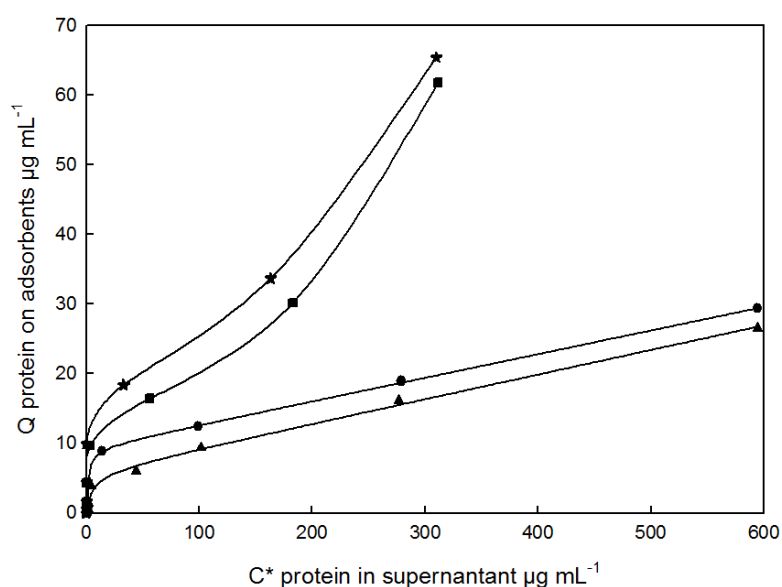


Figure 6.5 Protein binding isotherm on myoglobin imprinted adsorbents. Legend: Mb+Cu (Circle), Mb-Cu (Triangle), Chym+Cu (Square), Chym-Cu (Star) ¹¹.

¹¹Abbreviations: using myoglobin as binding specie (Mb), using α -Chymotrypsinogen A as binding specie (Chym); adsorbents was charged with Cu^{2+} ions (+Cu); adsorbents were not charged with Cu^{2+} ions (-Cu)

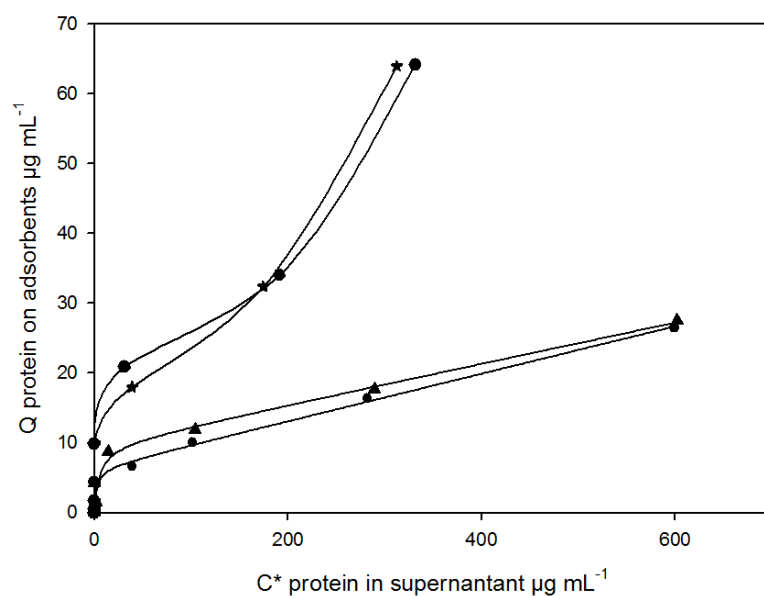


Figure 6.6 Protein binding isotherm on α -Chymotrypsinogen A imprinted adsorbents. Legend: Mb+Cu (Triangle), Mb-Cu (Diamond), Chym+Cu (Square), Chym-Cu (Star).

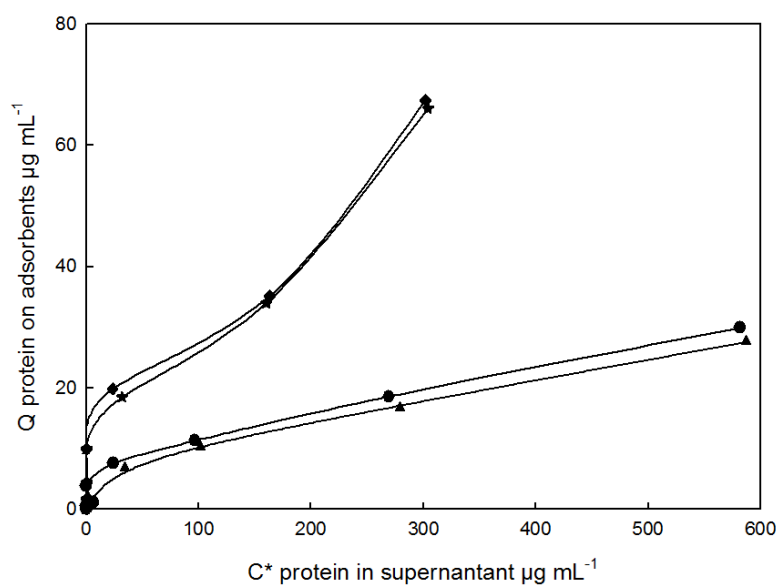


Figure 6.7 Protein binding isotherm on non imprinted (NIPs) adsorbents. Legend: Mb+Cu (Circle), Mb-Cu (Triangle), Chym+Cu (Diamond), Chym-Cu (Star)

6.1.5 Conclusions

In the report of Kempe *et al.* (1995), RNase (with a high isoelectric point of 9.4) was used during binding studies against BSA, which has low pI of 4.7. At the same time, authors selected low salt binding conditions (water/ DMF) to carry out their experiments, thus most interactions were of ionic character, as explained above. Therefore, the findings of Kempe *et al.* (1995) regarding surface molecular imprinting to selective binding is most likely an artefact and the observed effects can be explained by ion exchange and affinity interactions.

6.2 Chloride ions standard curve for calculation of ionic exchange capacity of magnetic anion exchanger

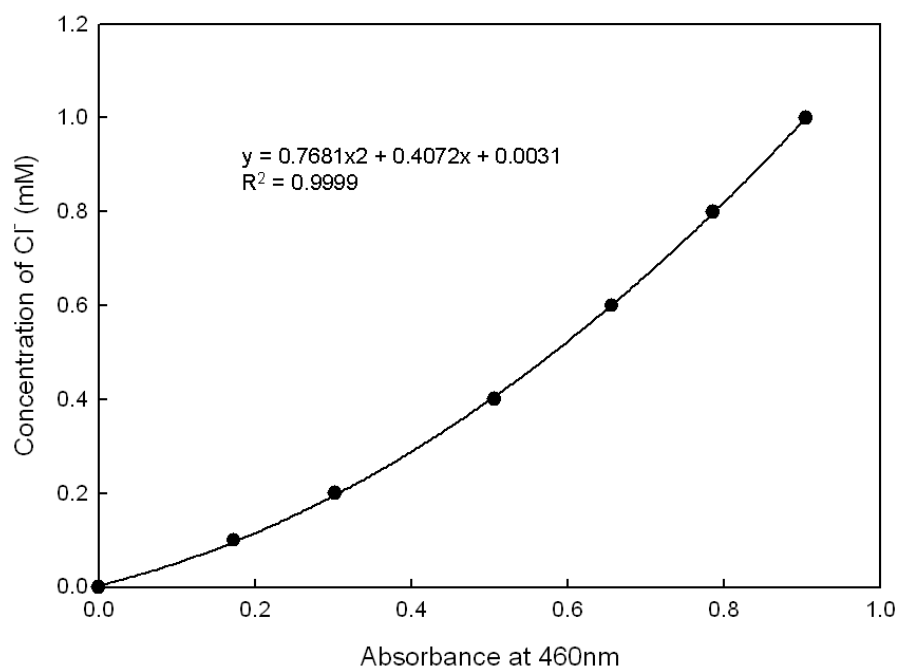


Figure 6.8 Standard curve used for calculation of chloride ions concentration after measurement of solution absorbance at 460 nm.

6.3 Protein Calibration curves for protein binding studies

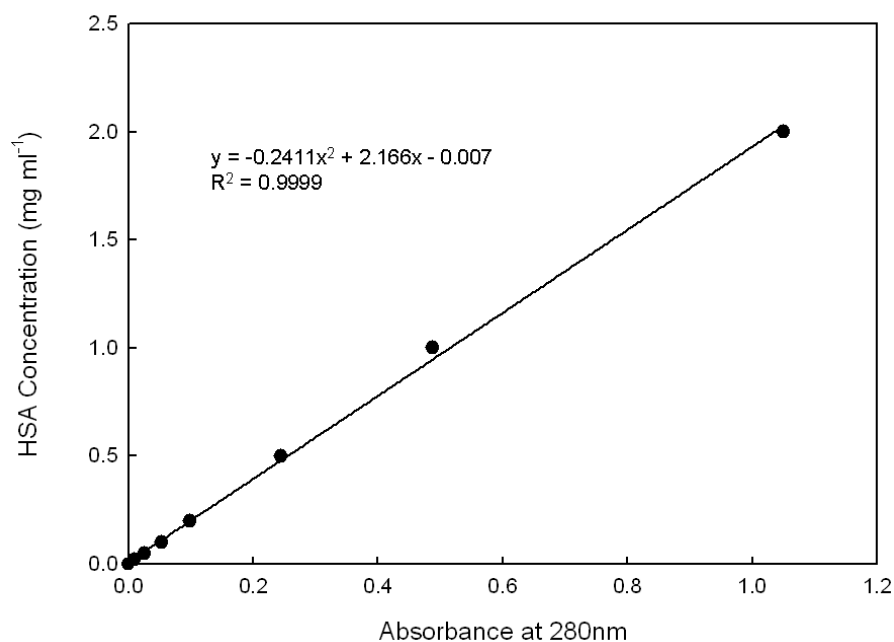


Figure 6.9 Calibration curve used for calculation of human serum albumin (HSA) concentration after measurement of solution absorbance at 280 nm.

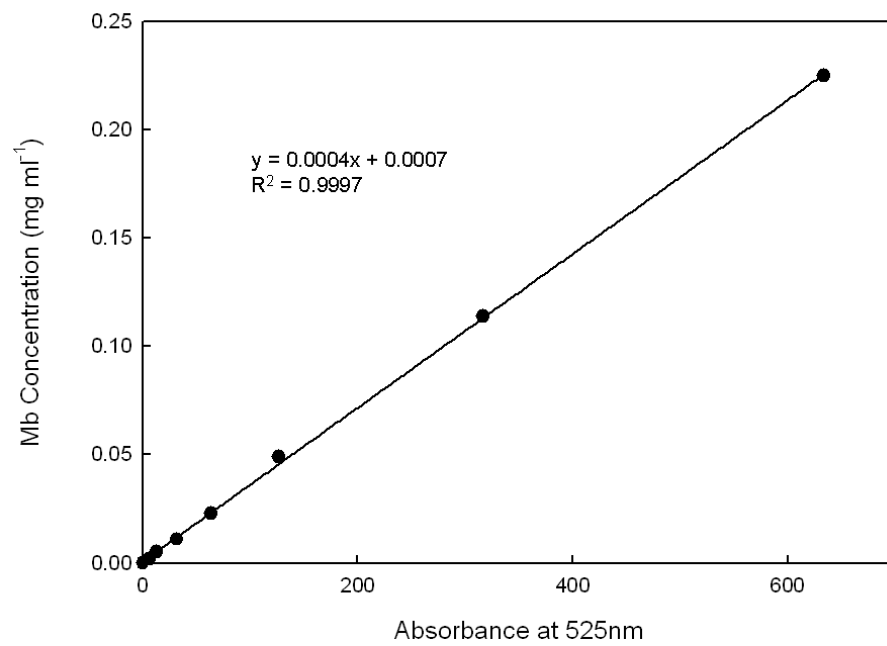


Figure 6.10 Calibration curve used for calculation of myoglobin (Mb) concentration after measurement of solution absorbance at 525 nm.

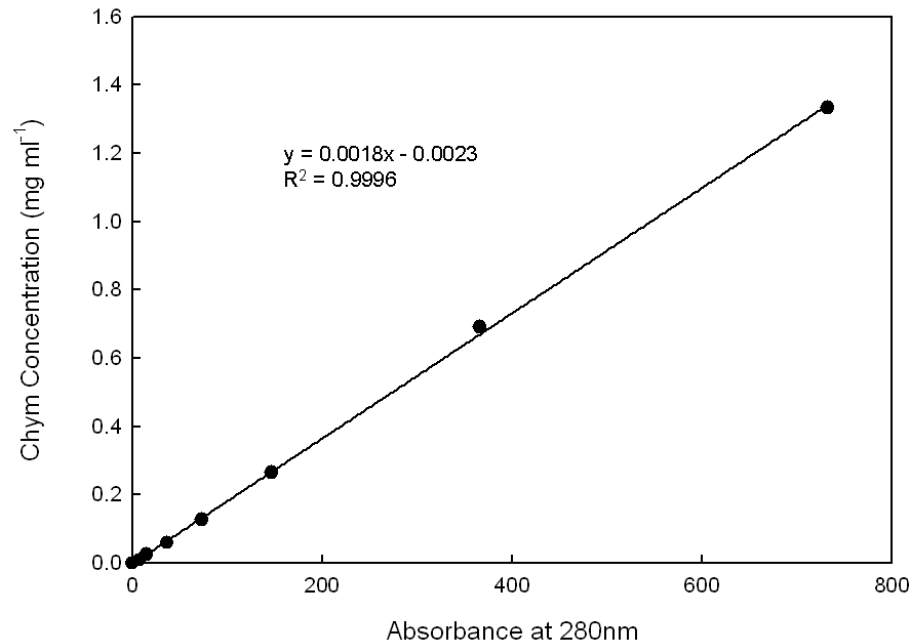


Figure 6.11 Calibration curve used for calculation of α -Chymotrypsinogen A (Chym) concentration after measurement of solution absorbance at 280 nm.

References

Al-Sabagh, A.M. 2002. The relevance HLB of surfactants on the stability of asphalt emulsion. *Colloids and Surfaces A: Physicochemical and Engineering Aspects*, 204, (1-3) 73-83.

Alexander, C., Andersson, H.S., Andersson, L.I., Ansell, R.J., Kirsch, N., Nicholls, I.A., O'Mahony, J., & Whitcombe, M.J. 2006. Molecular imprinting science and technology: a survey of the literature for the years up to and including 2003. *Journal of Molecular Recognition*, 19, (2) 106-180.

Ansell, J. & Mosbach, K. 1998. Magnetic molecularly imprinted polymer beads for drug radioligand binding assay. *Analyst*, 123, (7) 1611-1616.

Anton, N., Benoit, J.P., & Saulnier, P. 2008. Design and production of nanoparticles formulated from nano-emulsion templates--A review. *Journal of Controlled Release*, 128, (3) 185-199.

Asua, J.M. 2002. Miniemulsion polymerization. *Progress in Polymer Science*, 27, (7) 1283-1346.

Barrett, K.E. 1975. *Dispersion polymerization in organic media* London, UK, Wiley-Interscience.

Berger P., Adelman N.B., Beckman K.J., Campbell D.J., Ellis A.B., & Lisensky G.C. 1999. Preparation and Properties of an Aqueous Ferrofluid. *Journal of Chemical*

Education, 76, (7) 943-948.

Bicak, N., Acikkaya, N., & Koza, G. 1997. Controlled conversion of polyacrylamide into polyacrylic acid. *Polymer Bulletin*, 39, (4) 459-464.

Bolle, J. (bolle@mit.edu). 2009. *Magnetic fluid*.

Bondy, C. & Sollner, K. 1935. On the mechanism of emulsification by ultrasonic waves. *Transactions of the Faraday Society*, 31, 835-843.

Bossi, A., Bonini, F., Turner, A., & Piletsky, S.A. 2007. Molecularly imprinted polymers for the recognition of proteins: The state of the art. *Biosensors and Bioelectronics*, 22, 1131-1137.

Brown, G.B. 2008. *Advances in magnetic particle based bioprocessing*. PhD (Thesis). University of Birmingham.

Caruso, F., Susa, A.S., Giersig, M., & Mohwald, H. 1999. Magnetic Core-Shell Particles: Preparation of Magnetite Multilayers on Polymer Latex Microspheres. *Advanced Materials*, 11, 950-953.

Cocker, T.M., Fee, C.J., & Evans, R.A. 1997. Preparation of Magnetically Susceptible Polyacrylamide/Magnetite Beads for Use in Magnetically Stabilized Fluidized Bed Chromatography. *Biotechnology and Bioengineering*, 53, (1) 79-87.

Cormack, P.A.G. & Elorza, A.Z. 2004. Molecularly imprinted polymers: synthesis and

characterisation. *Journal of Chromatography B*, 804, (1) 173-182.

Cornell R.M. & Schwertmann U. 1996. *The Iron Oxides: Structure, Properties, Reactions Occurrence and Uses* Weinheim, Federal Republic of Germany, VCH Verlagsgesellschaft mbH.

Csetneki, I., Faix, M.K., Szilágyi, A., Kovács, A.L., Németh, Z., & Zrinyi, M. 2004. Preparation of magnetic polystyrene latex via the miniemulsion polymerization technique. *Journal of Polymer Science Part A: Polymer Chemistry*, 42, (19) 4802-4808.

Cullity B.D. & Graham C.D. 2009, "Ferromagnetism," *In Introduction to magnetic materials*, 2 ed. New Jersey: John Wiley and Sons Inc., pp. 115-150.

Dainiak, M.B., Galaev, I.Y., & Mattiasson, B. 2002. Polyelectrolyte-Coated Ion Exchangers for Cell-Resistant Expanded Bed Adsorption. *Biotechnology Progress*, 18, (4) 815-820.

Dave S.R. & Gao X.H. 2009. Monodisperse magnetic nanoparticles for biodetection, imaging, and drug delivery: a versatile and evolving technology. *Nanomedicine and nanobiotechnology*, 1, (6) 583-609.

Davies, J.T. 1957. A quantitative kinetic theory of emulsion type, I. Physical chemistry of the emulsifying agent. *In Proceedings of the International Congress of Surface Activity*, pp. 426-438.

- Deng Y., Wang L., Yang W., Fu S., & Elaissari A. 2003. Preparation of magnetic polymeric particles via inverse microemulsion polymerization process. *Journal of Magnetism and Magnetic Materials*, 257, 69-78.
- Denkbas, E.B., Kilitay, E., Birlikseven, C., & Öztürk, E. 2002. Magnetic chitosan microspheres: preparation and characterization. *Reactive and Functional Polymers*, 50, (3) 225-232.
- Dery, J.P., Borra, E.F., & Ritcey, A.M. 2008. Ethylene glycol based ferrofluid for the fabrication of magnetically deformable liquid mirrors. *Chemistry of Materials*, 20, 6420-6426.
- Desnoyer, C., Masbernard, O., & Gourdon, C. 2003. Experimental study of drop size distributions at high phase ratio in liquid-liquid dispersions. *Chemical Engineering Science*, 58, (7) 1353-1363.
- Ditsch, A., Yin, J., Laibinis, P., Wang, D.I.C., & Hatton, T.A. 2006. Ion-exchange purification of proteins using magnetic nanoclusters. *Biotechnology Progress*, 22, 1153-1162.
- Dunlop, E.H., Feiler, W.A., & Mattione, M.J. 1984. Magnetic separation in biotechnology. *Biotechnology advances*, 2, 63-74.
- Dunnill, P. & Lilly, M.D. 1974. Purification of enzymes using magnetic bio-affinity materials. *Biotechnology and Bioengineering*, 16, (7) 987-990.

Durdureanu-Angheluta, A., Ardeleanua R., Pintealaa M., Harabagiua V., Chiriacc H., & Simionescua B.C. 2008. Silane covered magnetite particles: Preparation and characterisation. *Digest Journal of Nanomaterials and Biostructures*, 3, (1) 33-40.

Elbert, D.L. 2011. Liquid-liquid two-phase systems for the production of porous hydrogels and hydrogel microspheres for biomedical applications: A tutorial review. *Acta Biomaterialia*, 7, (1) 31-56.

Fang, L.Z. 1993. *The Devil Valley Master*. Beijing,China, Bibliography and Document Publishing House.

Fernandez-Lahore, H.M., Kleef, R., Kula, M.R., & Thommes, J. 1999. The influence of complex biological feedstock on the fluidization and bed stability in expanded bed adsorption. *Biotechnology and Bioengineering*, 64, (4) 484-496.

Flory, P.J. 1942. Thermodynamics of High Polymer Solutions. *The Journal of Chemical Physics*, 10, (1) 51-61.

Foner, S. 1956. Vibrating Sample Magnetometer. *Review of Scientific Instruments*, 27, (7) 548-548.

Fowler, M. Historical Beginnings of Theories of Electricity and Magnetism. 1997. University of Virginia, Virginia, USA 11-16-2010.

http://galileoandstein.physics.virginia.edu/more_stuff/E&M_Hist.html

- Franzreb, M., Siemann-Herzberg, M., Hobley, T.J., & Thomas, O.R.T. 2006. Protein purification using magnetic adsorbent particles. *Applied Microbiology and Biotechnology*, 70, 505-516.
- Gerber, R. & Birss, R.R. 1983. *High gradient magnetic separation* Chichester, UK, Research Studies Press Div. of John Wiley & Sons, Ltd.
- Getzlaff M. 2008. *Fundamentals of Magnetism*. Heidelberg, Germany. Springer Science+Business Media.
- Goetz, V., Remaud, M., & Graves, D.J. 1991. A novel magnetic silica support for use in chromatographic and enzymatic bioprocessing. *Biotechnology and Bioengineering*, 37, (7) 614-626.
- Griffin, W.C. 1949. *Classification of Surface-Active Agents by HLB*. *Journal of the Society of Cosmetic Chemists*, 1, 311-326.
- Guardia, P., Batlle-Brugal, B., Roca, A.G., Iglesias, O., Morales, M.P., Serna, C.J., Labarta, A., & Batlle, X. 2006. Surfactant effects in magnetite nanoparticles of controlled size. *Journal of Magnetism and Magnetic Materials*, 3, (2) 756-759.
- Guesdon, J.L. & Avrameas, S. 1977. Magnetic solid phase enzyme immunoassay. *Immunochemistry*, 14, 443-447.
- Gupta, A.K. & Gupta, M. 2005. Synthesis and surface engineering of iron oxide nanoparticles for biomedical applications. *Biomaterials*, 26, 3995-4021.

Halling, P.J. & Dunnill, P. 1979. Improved nonporous magnetic supports for immobilized enzymes. *Biotechnology and Bioengineering*, 21, (3) 393-416.

Halling, P.J. & Dunnill, P. 1980. Magnetic supports for immobilized enzymes and bioaffinity adsorbents. *Enzyme and Microbial Technology*, 2, 2-10.

Harris, E.L.V. & Angal, S. 1989. *Protein purification methods : a practical approach* Oxford, UK, IRL Press.

Harris, L.A., Goff, J.D., Carmichael, A.Y., Riffle, J.S., Harburn, J.J., St.Pierre, T.G., & Saunders, M. 2003. Magnetite Nanoparticle Dispersions Stabilized with Triblock Copolymers. *Chemistry of Materials*, 15, (6) 1367-1377.

Hart, B.R. & Shea, K.J. 2002. Molecular imprinting for the recognition of N-terminal histidine peptides in aqueous solution. *Macromolecules*, 35, 6192-6201.

Hatch, G.P. & Stelter, R.E. 2001. Magnetic design considerations for devices and particles used for biological high-gradient magnetic separation (HGMS) systems. *Journal of Magnetism and Magnetic Materials*, 225, (1-2) 262-276.

Haynes, C.A. & Nordes, W. 2004. Globular proteins at solid/ liquid interfaces. *Colloids and Surfaces B, Biointerfaces*, 2, 517-566.

Heebøll-Nielsen, A. 2002. *High gradient magnetic fishing; support functionalisation and application for protein recovery from unclarified bioprocess liquors*. PhD (Thesis). Technical University of Denmark.

Heebøll-Nielsen, A., Justesen, S.F.L., & Thomas, O.R.T. 2004. Fractionation of whey proteins with high-capacity superparamagnetic ion-exchangers. *Journal of Biotechnology*, 113, 247-262.

Heebøll-Nielsen, A., Dalkiaer, M., Hubbuch, J.J., & Thomas, O.R.T. 2004. Superparamagnetic adsorbents for high-gradient magnetic fishing of lectins out of legume extracts. *Biotechnology and Bioengineering*, 87, (3) 311-323.

Helpdesk of Malvern Instruments Ltd. (helpdesk@malvern.com). 28-10-2008. *Refractive index*.

Hickstein, B. & Peuker, U.A. 2008. Characterization of protein capacity of nanocation exchanger particles as filling material for functional magnetic beads for bioseparation purposes. *Biotechnology Progress*, 24, 409-416.

Hirschbein B.L. & Whitesides G.M. 1982. Affinity separation of enzymes from mixtures containing suspended solids. Comparisons of magnetic and nonmagnetic techniques. *Applied Biochemistry and Biotechnology*, 7, 157-176.

Hu, Y., Liu, R., Zhang, Y., & Li, G. 2009. Improvement of extraction capability of magnetic molecularly imprinted polymer beads in aqueous media via dual-phase solvent system. *Talanta*, 79, (3) 576-582.

Huang, C., Lynch, C. C., & Strikovsky, A. 2006, *Inverse emulsion method of making polymer imprint beads*, 7105289B2, Aspira Biosystems Inc., (US patent).

Huang, C. S. & Mateo, A. 2002, *Compositions and methods for surface imprinting*, 20020110901A1, Aspria biosystems Inc., (US patent).

Hubbuch, J.J. 2000. *Development of adsorptive separation system for recovery of protein from curde bioprocess liquors*. PhD (Thesis). Technical University of Denmark.

Hubbuch, J.J., Matthiesen, D.B., Hobley, T.J., & Thomas, O.R.T. 2001. High gradient magnetic separation versus expanded bed adsorption: a first principle comparison. *Bioseparation*, 10, (1) 99-112.

Hubbuch, J.J. & Thomas, O.R.T. 2002. High-gradient magnetic affinity separation of trypsin from porcine pancreatin. *Biotechnology and Bioengineering*, 79, (3) 301-313.

Jiles, D. 1991. *Introduction to magnetism and magnetic materials* London, Chapman and Hall.

Käppler, T.E., Hickstein, B., Peuker, U.A., & Posten, C. 2008. Characterization of magnetic ion-exchange composites for protein separation from biosuspensions. *Journal of bioscience and bioengineering*, 105, (6) 579-585.

Kartsev V.P. 1975. *Thousand years of magnets* Moscow, Russia. Mir Publishers.

Kempe, M. & Mosbach, K. 1995. Separation of amino acids, peptides and proteins on molecularly imprinted stationary phases. *Journal of Chromatography A*, 691, 317-323

Khalafalla, S. & Reimers, G. 1980. Preparation of dilution-stable aqueous magnetic

fluids. *Magnetics, IEEE Transactions on*, 16, (2) 178-183.

Kippax, P. 2008. Measuring particle size using modern laser diffraction techniques, *China Paint & Coatings Industry magazine*, 1,30-36.

Kondo, A., Kamura, H., & Higashitani, K. 1994. Development and application of thermo-sensitive magnetic immunomicrosphere for antibody purification. *Apply microbiology biotechnology*, 41, 99-105.

Kraume, M., Gabler, A., & Schulze, K. 2004. Influence of Physical Properties on Drop Size Distribution of Stirred Liquid-Liquid Dispersions. *Chemical Engineering & Technology*, 27, (3) 330-334.

Krishnan, K., Pakhomov, A., Bao, Y., Blomqvist, P., Chun, Y., Gonzales, M., Griffin, K., Ji, X., & Roberts, B. 2006. Nanomagnetism and spin electronics: materials, microstructure and novel properties. *Journal of Materials Science*, 41, (3) 793-815.

Kriwet, B., Walter, E., & Kissel, T. 1998. Synthesis of bioadhesive poly(acrylic acid) nano- and microparticles using an inverse emulsion polymerization method for the entrapment of hydrophilic drug candidates. *Journal of Controlled Release*, 5, 149-158.

Kurt Gottlob 1915, *Caoutchouc substance and process of making same*, 1149577 (US patent).

LaMer, V.K. & Dinegar, R.H. 1950. Theory, Production and Mechanism of Formation of Monodispersed Hydrosols. *Journal of the American Chemical Society*, 72, (11)

4847-4854.

Lee, Y., Rho, J., & Jung, B. 2003. Preparation of magnetic ion-exchange resins by the suspension polymerization of styrene with magnetite. *Journal of Applied Polymer Science*, 89, (8) 2058-2067.

Levison, P.R., Badger, S.E., Dennis, J., Hathi, P., Davies, M.J., Bruce, I.J., & Schimkat, D. 1998. Recent developments of magnetic beads for use in nucleic acid purification. *Journal of Chromatography A*, 816, (1) 107-111.

Liao, M.H. & Chen, D.H. 2002. Preparation and characterization of a novel magnetic nano-adsorbent. *Journal of Materials Chemistry*, 12, (12) 3654-3659.

Lin, C.L., Lee, C.F., & Chiu, W.Y. 2005. Preparation and properties of poly(acrylic acid) oligomer stabilized superparamagnetic ferrofluid. *Journal of Colloid and Interface Science*, 291, (2) 411-420.

Lindner, J., Wagner, K., Eichholz, C., & Nirschl, H. 2010. Efficiency Optimization and Prediction in High-Gradient Magnetic Centrifugation. *Chemical Engineering & Technology*, 33, (8) 1315-1320.

Liu, H., Wang C., Gao, Q., & Tong, Z. 2010. Magnetic hydrogels with supracolloidal structures prepared by suspension polymerization stabilized by Fe₂O₃ nanoparticles. *Acta Biomaterialia*, 6, 275-281.

Liu, X., Guan, Y., Liu, H., Ma, Z., Yang, Y., & Wu, X. 2005. Preparation and

characterization of magnetic polymer nanospheres with high protein binding capacity.

Journal of Magnetism and Magnetic Materials, 293, (1) 111-118.

Lovell, P.A. & El-Aasser, M.S. 1997. *Emulsion polymerization and emulsion polymers* Chichester, UK, John Wiley.

Ma Z. & Liu H. 2007. *Synthesis and surface modification of magnetic particles for application in biotechnology and biomedicine. China Particuology*, 5, 1-10.

Ma, Z.Y., Guan, Y.P., Liu, X.Q., & Liu, H.Z. 2005. Preparation and characterization of non-porous superparamagnetic polymer microspheres with epoxy groups by dispersion polymerization. *Chinese Journal of Chemical Engineering*, 16, 239-243.

Mahadevan, S., Gnanaprakash, G., Philip, J., Rao, B.P.C., & Jayakumar, T. 2007. X-ray diffraction-based characterization of magnetite nanoparticles in presence of goethite and correlation with magnetic properties. *Physica E: Low-dimensional Systems and Nanostructures*, 39, (1) 20-25.

Mayes, A.G. & Whitcombe, M.J. 2005. Synthetic strategies for the generation of molecularly imprinted organic polymers. *Advanced Drug Delivery Reviews*, 57, (12) 1742-1778.

McCurrie, R.A. 1994. *Ferromagnetic materials: structure and properties* London, UK, Academic Ltd.

Mendenhall, G.D., GENG, Y., & HWANG, J. 1996. Optimization of long-term stability of

magnetic fluids from magnetite and synthetic polyelectrolytes. *Journal of Colloid and Interface Science*, 184, 519-526.

Moffat, G., Williams, R.A., Webb, C., & Stirling, R. 1994. Selective separations in environmental and industrial processes using magnetic carrier technology. *Minerals Engineering*, 7, (8) 1039-1056.

Moralesy M.P., Sernaz C.J., Bødkerx F., & Mørupx S. 1997. Spin canting due to structural disorder in maghemite. *Journal of Physics: Condensed Matter*, 9, 5461-5467.

Mori, Y. & Kawaguchi, H. 2007. Impact of initiators in preparing magnetic polymer particles by miniemulsion polymerization. *Colloids and Surfaces B: Biointerfaces*, 56, 246-254.

Morris, L.R., Mock, R.A., Marshall, C.A., & Howe, J.H. 1959. Synthesis of some amino acid derivatives of styrene. *Journal of the American Chemical Society*, 81, 377-382.

Mosbach, K. & Andersson, L. 1977. Magnetic ferrofluids for preparation of magnetic polymers and their application in affinity chromatography. *Nature*, 270, 259-261.

Muller-Schulte, D. & Schmitz-Rode, T. 2006. Thermosensitive magnetic polymer particles as contactless controllable drug carriers. *Journal of Magnetism and Magnetic Materials*, 302, (1) 267-271.

Munro, P.A., Dunnill, P., & Lilly, M.D. 1977. Nonporous magnetic materials as enzyme

supports: Studies with immobilized chymotrypsin. *Biotechnology and Bioengineering*, 19, (1) 101-124.

Nayak, N.C. & Shin, K. 2008. Human serum albumin mediated self-assembly of gold nanoparticles into hollow spheres. *Nanotechnology*, 19, (26) 1-4.

Norrlow, O., Glad, M., & Mosbach, K. 1984. Acrylic polymer preparations containing recognition sites obtained by imprinting with substrates. *Journal of Chromatography*, 299, 29-41.

O'Brien, S.M., Sloane, R.P., Thomas, O.R.T., & Dunnill, P. 1997. Characterisation of non-porous magnetic chelator supports and their use to recover polyhistidine-tailed T4 lysozyme from a crude E. coli extract. *Journal of Biotechnology*, 54, (1) 53-67.

O'Brien, S.M., Thomas, O.R.T., & Dunnill, P. 1996. Non-porous magnetic chelator supports for protein recovery by immobilised metal affinity adsorption. *Journal of Biotechnology*, 50, (1) 13-25.

O'Connor, E. (evelyn.oconnor@camida.com). 24-11-2008. *Inquiry about AIBN*. (yxy571@bham.ac.uk).

Oberteuffer, J. 1973. High gradient magnetic separation. *Magnetics, IEEE Transactions on*, 9, (3) 303-306.

Oberteuffer, J. 1974. Magnetic separation: A review of principles, devices, and applications. *Magnetics, IEEE Transactions on*, 10, (2) 223-238.

Odenbach S. 2002A. *Ferrofluid: Magnetically Controllable Fluid and their Application* Heidelberg, Germany, Springer.

Odenbach, S. 2002B. *Magnetoviscous effects in ferrofluids* Heidelberg, Germany, Springer.

Odian, G. 1970. *Principles of polymerization* London, UK, McGraw-Hill Book Company.

Oladosu, S. (Seun.Oladosu@sial.com). 25-10-2007. *Inquire about AIBN.* (yxy571@bham.ac.uk)

Ortega-Vinuesa, J.L., Tengvall, P., & Lundström, I. 1998. Molecular packing of HSA, IgG, and fibrinogen adsorbed on silicon by AFM imaging. *Thin Solid Films*, 324, (1-2) 257-273.

Parker, M.R. 1977. Physics of magnetic separation. *Contemporary physics*, 18, (3) 279-306.

Perez-Moral, N. & Mayes, A.G. 2004. Comparative study of imprinted polymer particles prepared by different polymerisation methods. *Analytica Chimica Acta*, 504, (1) 15-21.

Pettersson, L. 1999, *Certificate of analysis of StreamlineTM QXL*, Amersham Pharmacia Biotech, Uppsala, Sweden, 277891.

Philippova, O., Barabanova, A., Molchanov, V., & Khokhlov, A. 2010. Magnetic polymer beads: recent trends and developments in synthetic design and applications.

European Polymer Journal, 47, 542-559.

Pich, A., Bhattacharya, S., Ghosh, A., & Adler, H.J.P. 2005. Composite magnetic particles: 2. Encapsulation of iron oxide by surfactant-free emulsion polymerization.

Polymer, 46, (13) 4596-4603.

Pitfield, I.D. 1992. *Perfluorocarbon chromatographic supports*. PhD (Thesis).

University of Cambridge.

Pollak, A., Blumenfeld, H., Wax, M., Baughn, R., & Whitesides, G. 1980. Enzyme immobilization by condensation copolymerization into cross-linked polyacrylamide gels. *Journal of American Chemistry Society*, 102, 6324-6336.

Polyanskiy, M. Refractive Index Database. 2011. [Accessed August 5th, 2011].

<http://refractiveindex.info>.

Pross, A., Platkowski, K., & Reichert, K.H. 1998. The inverse emulsion polymerization of acrylamide with pentaerythritolmyristate as emulsifier. 1. Experimental studies.

Polymer International, 45, (1) 22-26.

Quorum Technologies Ltd. Critical Point Drying Technical Brief. 2009. Quorum Technologies Ltd. Kent, UK 02-02-2011.

http://www.quorumtech.com/pdf/criticalPointDrying/CPD_technical_brief.pdf

Raacuciu M., Creang D.E., & Airinei A. 2006. Citric-acid-coated magnetite nanoparticles for biological applications. *The European Physical Journal E*, 21, (2) 117-121.

Rachkov, A. & Minoura, N. 2001. Towards molecularly imprinted polymers selective to peptides and proteins. The epitope approach. *Biochimica et Biophysica Acta*, 1544, 255-266.

Ramirez, L.P. & Landfester, K. 2003. Magnetic Polystyrene Nanoparticles with a High Magnetite Content Obtained by Miniemulsion Processes. *Macromolecular Chemistry and Physics*, 204, (1) 22-31.

Rawle, A. Basic principles of particle analysis. 2011. Malvern instrument Ltd., Worcestershire, UK (Pamphlet).

Razzaghi, K. & Shahraki, F. 2010. On the effect of phase fraction on drop size distribution of liquid-liquid dispersions in agitated vessels. *Chemical Engineering Research and Design*, 88, (7) 803-808.

Robinson, P.J., Dunnill, P., & Lilly, M.D. 1973. The Properties of Magnetic. Supports in Relation to Immobilized Enzyme Reactors. *Biotechnology and Bioengineering*, 15, (3) 603-606.

Roche Diagnostics GmbH 2000, *Magnetic glass particles, method for their preparation and uses thereof*, EP1154443 (patent).

Rosen, M.J. 1989. *Surfactants and Interfacial Phenomena*, 2nd ed. Chichester, UK, John Wiley & Sons.

Rosensweig R.E. 1985. *Ferrohydrodynamics* Cambridge, UK, Cambridge University Press.

Safarik I. & Safarikova M. 2004. Magnetic techniques for the isolation and purification of proteins and peptides . *BioMagnetic Research and Technology*, 2, 1-17

Safarik, I. & Safarikova, M. 1993. Batch isolation of hen egg white lysozyme with magnetic chitin. *Journal of Biochemical and Biophysical Methods*, 27, (4) 327-330

Saravanan, M., Bhaskar, K., Maharajan, G., & Pillai, K.S. 2004. Ultrasonically controlled release and targeted delivery of diclofenac sodium via gelatin magnetic microspheres. *International Journal of Pharmaceutics*, 283, (1-2) 71-82

Sauter, J. (1926) 'Die Grössenbestimmung der in Gemischnebeln von Verbrennungskraftmaschinen vorhandenen Brennstoffteilchen', VDI-Forschungsheft Nr. 279.

Sauter, J. (1928) 'Die Grössenbestimmung der in Gemischnebeln von Verbrennungskraftmaschinen vorhandenen Brennstoffteilchen', VDI-Forschungsheft Nr. 312.

Schildknecht, C.E. 1956. *Polymer processes : chemical technology of plastics, resins, rubbers, adhesives and fibers* London, UK, Interscience Publishers.

Shen, L., Laibinis, P.E., & Hatton, T.A. 1998. Bilayer surfactant stabilized magnetic fluids: Synthesis and interactions at interfaces. *Langmuir*, 15, (2) 447-453

Shinoda, K. & Saito, H. 1968. The effect of temperature on the phase equilibria and the types of dispersions of the ternary system composed of water, cyclohexane, and nonionic surfactant. *Journal of Colloid and Interface Science*, 26, (1) 70-74

Shinoda, K. & Saito, H. 1969. The stability of O/W type emulsions as functions of temperature and HLB of emulsifiers: The emulsification by PIT-method. *The Journal of Colloid and Interface Science*, 30, (2) 258-263.

Silverson Machines Ltd. Model L5 Series Laboratory Mixers Technical Information. 2010. Silverson Machines Ltd., Chesham ,UK 12-24-2010.

<http://www.silverson.com/us/lab-mixer-technical-information.html>

Spaldin N.A. 2003, "Review of basic magnetostatics," *In Magnetic Materials*, 1 ed. Cambridge: The Press Syndicate of The University of Cambridge.

Steitz, B., Salaklang, J., Finka, A., O'Neil, C., Hofmann, H., & Petri-Fink, A. 2007. Fixed Bed Reactor for Solid-Phase Surface Derivatization of Superparamagnetic Nanoparticles. *Bioconjugate Chemistry*, 18, (5) 1684-1690.

Stolarski, M., Fuchs, B., Kassa, S.B., Eichholz, C., Keller, K., & Nirschl, H. 2006. Magnetic field enhanced press-filtration. *Chemical Engineering Science*, 61, (19) 6395-6403

Svoboda, J. 1987. *Magnetic Methods for the Treatment of Minerals* Amsterdam, Netherlands, Elsevier Science Publishers.

Svoboda, J. & Fujita, T. 2003. Recent developments in magnetic methods of material separation. *Minerals Engineering*, 16, (9) 785-792.

Tamayo, F.G., Turiel, E., & Martin-Esteban, A. 2007. Molecularly imprinted polymers for solid-phase extraction and solid-phase microextraction: Recent developments and future trends. *Journal of Chromatography A*, 1152, 32-40

TCI America. Silane Coupling Agents. 2010. Protland, USA 12-10-2010.

<http://www.tciamerica.com/product/materials-chem/F014.shtml>

Tepper, T., Ilievski, F., Ross, C.A., Zaman, T.R., Ram, R.J., Sung, S.Y., & Stadler, B.J.H. 2003. Magneto-optical properties of iron oxide films. *Journal of applied physics*, 93, (10) 6948-6950

Theodossiou, I. & Thomas, O.R.T. 2002. DNA-induced inter-particle cross-linking during expanded bed adsorption chromatography: Impact on future support design. *Journal of Chromatography A*, 971, 73-86

Thomas, O.R.T., Matts, P.J., & White, G.F. 1988. Localization by electron microscopy of alkylsulphatase in bacterial cells. *Journal of general microbiology*, 134, 1229-1236

Tong, X.D., Xue, B., & Sun, Y. 2001. A Novel Magnetic Affinity Support for Protein Adsorption and Purification. *Biotechnology Progress*, 17, (1) 134-139

Turner, N.W., Jeans, C.W., Brain, K.R., Allender, C.J., & Britt, D.W. 2006. From 3D to 2D: A review of molecular imprinting of proteins. *Biotechnology Progress*, 22, 1474-1489

Ugelstad, J., Ellingsen, T., Berge, A., & Helgee, B. 1983, *Magnetic polymer particles and process for the preparation thereof*, 83/03920 (US patent).

Urbain, O. M. & Steman, W. R. 1941, *Process for treating liquids*, 2232294 (US patent).

Varanda L.C., Jafelicci M., Tartaj P., & O'Grady K. 2002. Structural and magnetic transformation of monodispersed iron oxide particles in a reducing atmosphere. *Journal of applied physics*, 92, (4) 2079-2085.

Viloria-Cols, M.E., Hatti-Kaul, R., & Mattiasson, B. 2004. Agarose-coated anion exchanger prevents cell-adsorbent interactions. *Journal of Chromatography A*, 1043, (2) 195-200.

Vogel, A.I. 1989. *Vogel's Textbook of Quantitative Chemical Analysis*, 5th ed. Harlow, UK, Longman Scientific & Technical.

Waters, K.E., Rowson, N.A., Greenwood, R.W., & Williams, A.J. 2007. Characterising the effect of microwave radiation on the magnetic properties of pyrite. *Separation and Purification Technology*, 56, (1) 9-17.

Watson J. 1973. Magnetic filtration. *Journal of applied physics*, 44, (9) 4209-4213.

Watson, J. 1975. Theory of capture of particles in magnetic high-intensity filters. *Magnetics, IEEE Transactions on*, 11, (5) 1597-1599.

Whitby, G.S. & Katz, M. 1933. Synthetic Rubber. *Industrial & Engineering Chemistry*, 25, (12) 1338-1348.

White, G.F. & Thomas, O.R.T. 1990. Immobilization of the surfactantdegrading bacterium *Pseudomonas C12B* in polyacrylamide gel beads: I. Effect of immobilization on the primary and ultimate biodegradation of SDS, and redistribution of bacteria within beads during use. *Enzyme and Microbial Technology*, 12, 697-705.

Wiechers, S. & Schmidt-Naake, G. 2008. Copolymerization of 2-acrylamido-2-methyl-1-propanesulfonic acid and 1-vinylimidazole in inverse miniemulsion. *Macomolecular reaction engineering*, 2, 126-134.

Wohlfarth, E.P. 1980. *Ferromagnetic materials: : a handbook on the properties of magnetically ordered substances* Amsterdam, Netherland, North-Holland Publishing Co.

Wooding A., Kilner M., & Lambrick D.B. 1991. Studies of the double surfactant layer stabilization of water-based magnetic fluids. *Journal of Colloid and Interface Science*, 144, (1) 236-242.

Wooding, A., Kilner, M., & Lambrick, D.B. 1992. "Stripped" magnetic particles. Applications of the double surfactant layer principle in the preparation of water-based

- magnetic fluids. *Journal of Colloid and Interface Science*, 149, (1) 98-104.
- Wormuth K. 2001. Superparamagnetic Latex via Inverse Emulsion Polymerization. *Journal of Colloid and Interface Science*, 241, 366-377.
- Wuenschell, G.E., Naranjo, E., & Arnold, F.H. 1990. Aqueous two-phase metal affinity extraction of heme proteins. *Bioprocess Engineering*, 5, 199-202.
- Xie G., Zhang Q., Luo, Z.P., Wu M., & Li T. 2003. Preparation and characterization of monodisperse magnetic poly(styrene butyl acrylate methacrylic acid) microspheres in the presence of a polar solvent. *Journal of Applied Polymer Science*, 87, (11) 1733-1738.
- Xu, Z.Z., Wang, C.C., Yang, W.L., Deng, Y.H., & Fu, S.K. 2004. Encapsulation of nanosized magnetic iron oxide by polyacrylamide via inverse miniemulsion polymerization. *Journal of Magnetism and Magnetic Materials*, 277, (1) 136-143.
- Xue, B. & Sun, Y. 2002. Fabrication and characterization of a rigid magnetic matrix for protein adsorption. *Journal of Chromatography A*, 947, (2) 185-193.
- Yavuz, C.T., Prakash, A., Mayo, J.T., & Colvin, V.L. 2009. Magnetic separations: From steel plants to biotechnology. *Chemical Engineering Science*, 64, (10) 2510-2521.
- Zhang, Q., Zhang, H., Xie, G., & Zhang, J. 2007. Effect of surface treatment of magnetic particles on the preparation of magnetic polymer microspheres by miniemulsion polymerization. *Journal of Magnetism and Magnetic Materials*, 311, (1)

140-144.

Zhu, Y., Da, H., Yang, X., & Hu, Y. 2003. Preparation and characterization of core-shell monodispersed magnetic silica microspheres. *Colloids and Surfaces A: Physicochemical and Engineering Aspects*, 231, (1-3) 123-129.

Zulqarnain, K. 1999. *Scale-up of affinity based separation based on magnetic support particles*. PhD (Thesis). University Collage London.